Library

EFFECTS OF FOREST-FIRE DEVEGETATION ON WATERSHED GEOMORPHOLOGY IN BANDELIER NATIONAL MONUMENT, NEW MEXICO

BY

WILLIAM DENNIS WHITE

B.S., University of New Mexico, 1977

THESIS

Submitted in Partial Fulfillment of the
Requirements for the Degree of

Master of Science in Geology

The University of New Mexico
Albuquerque, New Mexico

July, 1981

William Dennis White
Candidate

Geology
Department

This thesis is approved, and it is acceptable in quality and form for publication on microfilm:

Approved by the Thesis Committee:

Stephen G. Wells, Chairperson

Raymond V. Ingersoll

Roger Y. Anderson

Accepted:

Dean, Graduate School

Date

ACKNOWLEDGMENTS

The author wishes to express his sincere appreciation for the critical and timely review of this manuscript provided by committee members Dr. Steve G. Wells, Dr. Raymond V. Ingersoll and Dr. Roger Anderson. The initial funding was provided to Dr. S. G. Wells by Grant No. PX7029-7-0809 of the National Park Service (Southwest Region Office, U. S. Department of the Interior). Additional support has been provided through Department of Geology scholarships (1978, 1979). Special thanks are given to Rick Dingus for his photographic contributions during the first year of the project and to Sandy Anderson for her aid in field instrumentation. The author further wishes to express his appreciation for all the help provided in the field and in the office by my friends Rick Schmidt, Devon Rose, Larry Smith, Jerry Schultz, Cliff McNary, Dave Wilson, Susan Hunter, and my typist, Frances Hale. A very special thanks is given to all the very helpful personnel at the United States Geological Survey Water Resources Division: Richard Lepp and Dave Funderburg,

Lead Hydrological Technicians; Linda Beal, Computer Technician; Louis P. Denis and William Dean, Supervisory Hydrologists; and Richard Thomas, Hydrologist. Thanks are also given to Chris Judson and John Lissoway, NPS, for making their slide libraries available. And finally, without the continued emotional and logistical support of all my family, including Anne, the completion of this project would never have been possible.

EFFECTS OF FOREST-FIRE DEVEGETATION ON WATERSHED GEOMORPHOLOGY IN BANDELIER NATIONAL MONUMENT, NEW MEXICO

BY

William Dennis White

ABSTRACT OF THESIS

Submitted in Partial Fulfillment of the
Requirements for the Degree of

Master of Science in Geology

The University of New Mexico
Albuquerque, New Mexico

July, 1981

ABSTRACT

In 1977 the La Mesa fire burned forested portions of the Pajarito Plateau in the Jemez Mountains, north-central New Mexico. Six small drainage basins within the Frijoles Canyon watershed, Bandelier National Monument, were instrumented to measure the geomorphic adjustments of the watershed in response to devegetation. Three drainage basins representing a qualitative estimate of devegetation (i.e., intense, moderate and light burns) were instrumented at an elevation of approximately 2530 m; three basins were instrumented at a lower elevation of 2195 m. The amount of sediment derived from devegetated hillslopes is influenced by: (1) the amount of fire-induced devegetation and organic ash formation, (2) seasonal variations in weathering and runoff, (3) sediment production from burrowing animals, and (4) protective post-fire forest litter. Increased rilling in the headwaters, and channel cutting and filling at the basin mouths make these portions of the study basins most responsive to de-vegetation. Rapid revegetation in the upper-elevation study area reduced sediment production within two years

after the La Mesa fire. Lower-elevation mesas have been identified as the landscapes most susceptible to fire-induced erosion. Morphometric analysis defined a greater number of first-order streams developed on the lower mesas than on the upper mesas. The greater number of first-order streams permits rapid sediment removal from devegetated headwater hillslopes to the trunk ephemeral drainages. Post-fire sedimentation occurs as bar deposits along third-, fourth-, and fifth-order ephemeral drainages and as over-bank deposits on the floodplain of the deeply incised, perennial Rito de los Frijoles. Post-fire hydrographs of the Rito de los Frijoles exhibit sharp runoff peaks with steep limbs indicating an increase in flashy flow behavior. Undercutting of the banks of the Rito de los Frijoles is a result of the increased bedload the perennial channel is carrying after the La Mesa fire.

TABLE OF CONTENTS

	Page
List of Figures	xii
List of Tables	xviii
List of Plates	xix
Introduction	1
Geologic Setting of Study Area	4
Previous Work	7
Techniques of Investigation	10
Drainage Basin Selection	10
Field Instrumentation	15
Laboratory Procedures	20
Study Basin Geomorphology and Instrumention	23
Burnt Mesa Study Basins	29
Apache Springs Study Basins	30
Results	42
Textural Properties of Surficial Material	42
Infiltration Properties of Surficial Material	45
Hillslope Instrumentation	53
Erosion-Pin Studies	53
Erosion-Grid Studies	73
Channel Instrumentation, Morphology, and Stratigraphy	79
Precipitation	92
Geomorphic Mapping	94
Morphometric Analysis	96

Page

Discussion. 102
Pre-Brun Geomorphic Conditions. 102
Hillslope Processes in Devegetated Drainage Basins. 104
Relationship of Weathering and Forest-Fire Devegetation 104
Types and Distribution of Hillslope Erosion Related to Forest-Fire Devegetation. 108
Erosion Rates and Distribution in Devegetated Drainage Basins. 117
Comparison of Drainage Basins in Differing Climatic and Topographic Settings. 120
Comparison of Drainage Basins of Differing Burn Intensity. 129
Seasonality of Erosion Rates 135
Channel Processes and Morphologic Adjustments in Devegetated Watersheds. 148
Ephemeral Channels in Mesa-Top Catchment Areas. 148
Perennial Channel - Rito de los Frijoles. . . 154
Streamflow Behavior of the Rito de los Frijoles as affected by the La Mesa Fire 159
Morphometry and Forest-Fire Devegetation. 167
Process-Response Model in Forest-Fire Devegetated Watersheds 171
Summary and Inferences. 174

Conclusions 181

Appendices. 182

Appendix I Grain-Size Distribution for all Study Basins, except BMINT. 182

Figure IA Grain-Size Distributions of Hillslope and Channel Samples Taken from BMMOD. 183

Figure IB Grain-Size Distributions of Hillslope and Channel Samples Taken from BMLIGHT and BMARCH 184

Figure IC Grain-Size Distributions of Hillslope and Channel Samples Taken from ASINT. 185

Page

Figure ID Grain-Size Distributions of Hillslope and Channel Samples taken from ASMOD. 186

Figure IE Grain-Size Distributions of Hillslope and Channel Samples taken from ASLIGHT. 187

Appendix II Erosion-Pin Measurements for all Sites. 188

Table IIA Summary of Erosion-Pin Data for the BMINT Basin 191

Table IIB Summary of Erosion-Pin Data for the BMMOD Basin 193

Table IIC Summary of Erosion-Pin Data for the BMLIGHT Basin 195

Table IID Summary of Erosion-Pin Data for the BMARCH Site 197

Table IIE Summary of Erosion-Pin Data for the ASINT Basin 198

Table IIF Summary of Erosion-Pin Data for the ASMOD Basin 200

Table IIG Summary of Erosion-Pin Data for the ASLIGHT Basin 201

Appendix III Erosion-Grid Measurements for all Sites 202

Table IIIA Summary of Erosion-Grid Data, Stations A and B BMINT. 204

Table IIIB Summary of Erosion-Grid Data for Stations C, BMMOD, and D, BMLIGHT.. 205

References 206

LIST OF FIGURES

Figure		Page
1	Location Map of Bandelier National Monument, Northcentral New Mexico	2
2	Geology and Topography of the Frijoles Canyon Watershed, Bandelier National Monument . .	5
3	Photograph Illustrating the Effects and Qualities Defining an Intense Burn.	11
4	Photograph Illustrating the Effects and Qualities Defining a Moderate Burn.	12
5	Photograph Illustrating the Effects and Qualities Defining a Light Burn	13
6	Photograph of Erosion-Grid Instrumentation Technique	17
7	Locations of Instrumented Basins in the Burnt Mesa Study.	26
8	Geomorphic Map of the Intense-Burn Study Basin, Burnt Mesa	27
9	Topographic Map of the Intense-Burn Study Basin, Burnt Mesa	28
10	Longitudinal Profiles from Basin Divide to Basin Mouth of the Burnt Mesa Study Basins. . . .	31
11	Geomorphic Map of the Moderate-Burn Study Basin, Burnt Mesa.	32
12	Geomorphic Map of the Light-Burn Study Basin, Burnt Mesa.	33
13	Locations of Instrumented Basins in the Apache Springs Study Area	34

Figure Page

14 Geomorphic Map of the Intense-Burn Study Basin, Apache Springs. 36

15 Longitudinal Profiles from Basin Divide to Basin Mouth of the Apache Springs Study Basins 37

16 Geomorphic Map of the Moderate-Burn Study Basin, Apache Springs. 38

17 Geomorphic Map of the Light-Burn Study Basin, Apache Springs 39

18 Grain-Size Distributions of Hillslope and Channel Samples Taken from BMINT 43

19 Topographic Profile and Change in Ground-Surface Elevation for Final Measurement of Erosion-Pin Transect A, BMINT. 54

20 Topographic Profile and Change in Ground-Surface Elevation for Final Measurement of Erosion-Pin Transect B, BMINT. 55

21 Topographic Profile and Change in Ground-Surface Elevation for Final Measurement of Erosion-Pin Transect C, BMINT. 56

22 Topographic Profile and Change in Ground-Surface Elevation for Final Measurement of Erosion-Pin Transect A, BMMOD. 57

23 Topographic Profile and Change in Ground-Surface Elevation for Final Measurement of Erosion-Pin Transect B, BMMOD. 58

24 Topographic Profile and Change in Ground-Surface Elevation for Final Measurement of Erosion-Pin Transect C, BMMOD. 59

25 Topographic Profile and Change in Ground-Surface Elevation for Final Measurement of Erosion-Pin Transect A, BMLIGHT. 60

26 Topographic Profile and Change in Ground-Surface Elevation for Final Measurement of Erosion-Pin Transect B, BMLIGHT. 61

Figure Page

27 Topographic Profile and Change in Ground-Surface Elevation for Final Measurement of Erosion-Pin Transect C, BMLIGHT. 62

28 Topographic Profile and Change in Ground-Surface Elevation for Final Measurement of Erosion-Pin Transect A, ASINT. 63

29 Topographic Profile and Change in Ground-Surface Elevation for Final Measurement of Erosion-Pin Transect B, ASINT. 64

30 Topographic Profile and Change in Ground-Surface Elevation for Final Measurement of Erosion-Pin Transect C, ASINT. 65

31 Topographic Profile and Change in Ground-Surface Elevation for Final Measurement of Erosion-Pin Transect A, ASMOD. 66

32 Topographic Profile and Change in Ground-Surface Elevation for Final Measurement of Erosion-Pin Transect B, ASMOD. 67

33 Topographic Profile and Change in Ground-Surface Elevation for Final Measurement of Erosion-Pin Transect C, ASMOD. 68

34 Topographic Profile and Change in Ground-Surface Elevation for Final Measurement of Erosion-Pin Transect B, ASLIGHT. 69

35 Net Change in Ground-Surface Elevation at Grid Station B, BMINT, April 1980 74

36 Net Change in Ground-Surface Elevation at Grid Station C, BMMOD, April 1980 75

37 Net Change in Ground-Surface Elevation at Grid Station D, BMLIGHT, April 1980 76

38 Changes in Channel Bed Elevation by Cutting and Filling, BMINT, July 1978. 80

39 Changes in Channel Bed Elevation by Cutting and Filling, BMINT, September 1980 81

40 Changes in Channel Bed Elevation by Cutting and Filling, ASINT.. 82

Figure		Page
41	Net Change in Ground-Surface Elevation at Grid Station A, BMINT, April 1980.	83
42	Changes in Channel Bed Elevation by Cutting and Filling, ASINT	85
43	Post-Burn Channel Aggradation in the Axial Drainage Below BMMOD and BMINT Study Basins.	86
44	Sketches of Channel Fill Deposits and Channel Cross Sections	87
45	Three Cross-Sectional Profiles of Trunk, Mesa-Top Ephemeral Canyon Showing the Probable Maximum Flood	89
46	Monthly Precipitation Records Within Bandelier National Monument at Those Recording Stations Operative Following the La Mesa Fire	93
47	Physiographic Areas of the Frijoles Canyon Watershed, Bandelier National Monument	97
48	Semi-Log Plots of Stream Order Versus Log Number of Streams and Log Mean Stream Length for the Rito de los Frijoles	100
49	Effects of Frost Heave on Devegetated Ground-Surface.	106
50	Rill Development (Photo A = November 1977) and Obliteration (Photo B = April 1980) on a Valley-Side Slope within BMINT	113
51	Relationship Between Runoff and Forest-Fire Devegetation for Two Precipitation Events, Burnt Mesa	118
52	Sediment Yield Versus Burn Intensity Relationships for the Apache Springs Study Basins and the Burnt Mesa Study Basins.	122
53	Densely Vegetated, Axial Drainage Below ASINT. . . .	125
54	Schematic Cross Sections Illustrating the Physiographic Settings of the Study Basins within each Study Area.	126

Figure Page

55 Dense and Rapid Revegetation of the Valley-Side Slopes Between the Apache Springs Study Basins and the Upper-Elevation Axial Drainages Provides Storage of Fire-Associated Sediment. . . . 128

56 Needle Cast Covering the Ground Surface in the BMMOD Study Basin. 130

57 Mounds of Colluvium (Light Areas in Upper Half of Photograph) Burrowing of Gophers. 131

58 Headwaters of BMINT Study Basin 133

59 Seasonal Variations in Ground-Surface Elevation for the BMINT Study Basin 136

60 Seasonal Variations in Ground-Surface Elevation for the BMMOD Study Basin 137

61 Seasonal Variations in Ground-Surface Elevation for the BMLIGHT Study Basin 138

62 Seasonal Variations in Ground-Surface Elevation for the BMARCH Study Basin. 139

63 Seasonal Variations in Ground-Surface Elevation for the ASINT Study Basin 140

64 Seasonal Variations in Ground-Surface Elevation for the ASMOD Study Basin 141

65 Seasonal Variations in Ground-Surface Elevation for the ASLIGHT 142

66 Seasonal Variations in Ground-Surface Elevation for the Erosion-Grid Stations within the BMINT Study Basin 143

67 Seasonal Variations in Ground-Surface Elevation for the Erosion-Grid Stations within the BMMOD Study Basin 144

68 Seasonal Variations in Ground-Surface Elevation for the Erosion-Grid Stations within the BMLIGHT Study Basin 145

69 Lower-Elevation Mesas have a Thinner Colluvial Cover than the Upper Mesas. 149

Figure		Page
70	Bedrock Constrictions in a Major Ephemeral Channel.	150
71	Wide Channel Reaches of High-Order Drainages Provide Storage for Fire-Associated Sediment	152
72	Plunge Pools Provide Storage of Fire-Derived Sediment	153
73	Overbank Deposits of Fire-Derived Sediment on the Floodplain of the Rito de los Frijoles. . .	155
74	Undercutting of the Banks of the Rito de los Frijoles in Response to an Increased Bed Load Following the La Mesa Fire.	157
75	Hydrographs of Pre- and Post-Burn Streamflow for the Rito de los Frijoles, Bandelier National Monument.	160
76	Mean Monthly Discharge for the Pre-Burn Record of the Rito de los Frijoles, Bandelier National Maonument	162
77	Mean Monthly Discharge for the Post-Burn Record of the Rito de los Fijoles, Bandelier National Monument.	163
78	Flow Duration Curves for the Pre- and Post-Records of the Rito de los Frijoles, Bandelier National Monument.	165
79	Process-Response Model of Devegetated Fluvial Systems.	172
80	Geomorphic Response to Precipitation Events Following the Devegetation by Forest Fire.	175

LIST OF TABLES

Table		Page
1	Geomorphic Characteristics of Study Basins in Bandelier National Monument, New Mexico. . .	25
2	Summary of Instrumentation of each Study Basin, Bandelier National Monument, New Mexico	41
3	Summary of Ground-Surface and Soil-Core Descriptions, Infiltration Rates, and Bulk Densities for Samples Tested and Collected at Infiltration Test Sites within the Study Basins.	47
4	Average Annual Change in Ground-Surface Elevation ($\bar{\Delta}$/yr) per Transect for all Study Basins	72
5	Average Annual Change in Ground-Surface Elevation ($\bar{\Delta}$/yr) per Grid Station for the Burnt Mesa Area	78
6	Discharge Calculations of Runoff Events by the Slope-Area Method, Burnt Mesa Study Area. .	91
7	Summary of Linear Parameters of Morphometric Analysis of the Rito de los Frijoles Watershed System.	98
8	Mean Length of Overland Flow on Interfluves for the Study Basins in the Apache Springs and Burnt Mesa Area	111
9	Summary of Mean Annual Surface Change and Sediment Yield for Each Study Basin.	118
10	Drainage Density and Bifurcation Ratios for the Physiographic-Areas of the Frijoles Canyon Watershed	168

LIST OF PLATES

Plate 1. Geomorphic Map of the Lower Frijoles Canyon Watershed, Bandelier National Monument, Los Alamos and Sandoval Counties, New Mexico. . . . . In Pocket

INTRODUCTION

The effects of vegetational change on hydrologic and geologic systems have been investigated for durations of geologic time (Schumm, 1968) and for shorter historic periods (Dodge, 1902; Rich 1911; Anderson and Trobitz, 1941; Storey and others, 1964; Dryness, 1965; Harris, 1977). These previous studies deal primarily with sediment yield and runoff changes in response to devegetation by land-use changes, such as logging or mining (Brater, 1939; Harris, 1977).

In June 1977, the La Mesa fire burned approximately 60 km^2 of forested land on the Pajarito Plateau, of the Jemez Mountains, north-central New Mexico (Fig. 1). Of the 60 km^2 burned, approximately 42 km^2 were within the Bandelier National Monument. The Rito de Los Frijoles watershed, the northernmost portion of the Bandelier National Monument, experienced the greatest areal extent of devegetation by the La Mesa Fire.

The purpose of this study is to delineate the impact of devegetation by the La Mesa forest fire on geomorphic processes in selected portions of the Rito

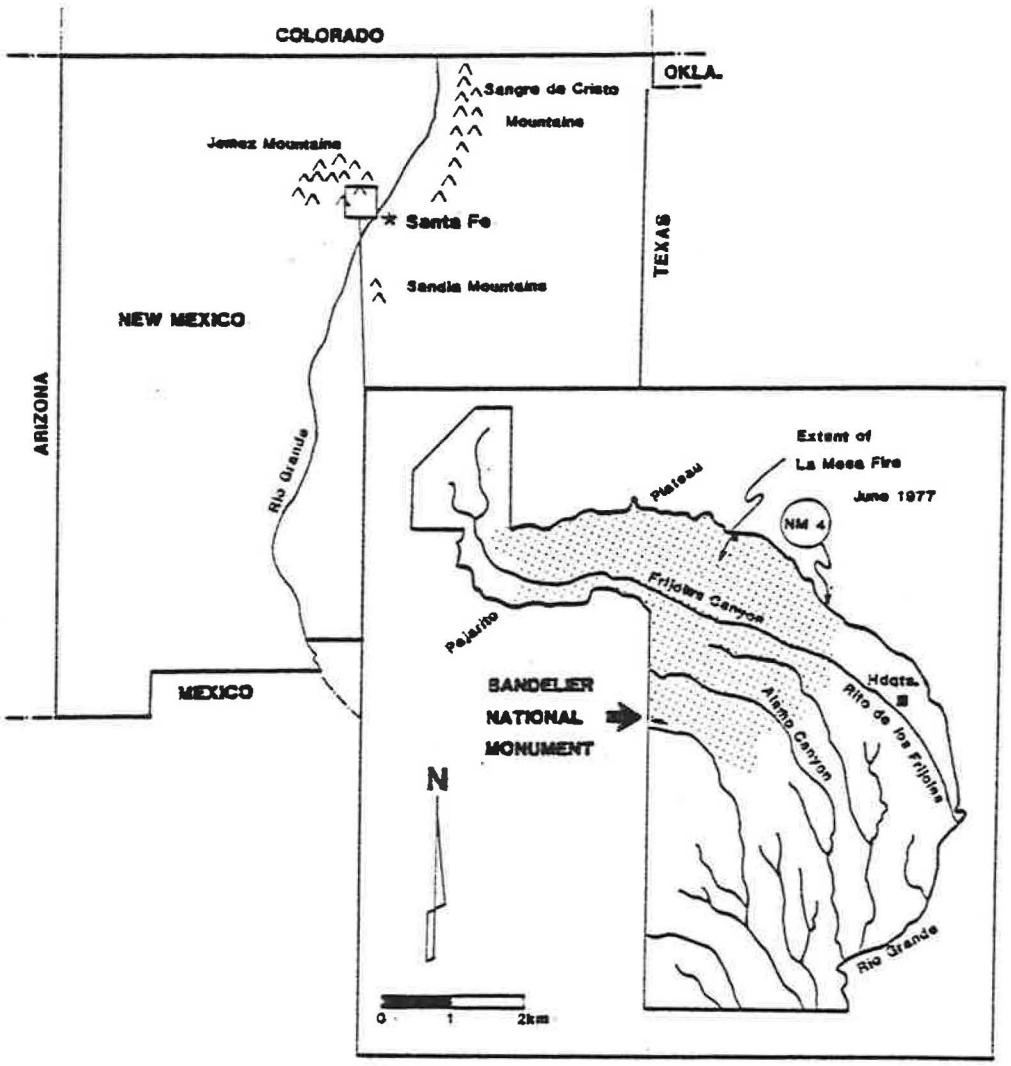


Figure 1: Location Map of Bandelier National Monument, Northcentral New Mexico. Stippled Pattern Represents the Extent of the La Mesa Fire within the Monument.

de los Frijoles watershed. Those geomorphic processes of interest include hillslope erosion, channel sedimentation, and concomitant modification of landforms. To assess the the impact of the La Mesa fire, this study addresses four main points: (1) identification of sediment source areas, (2) determination of rates and controls of sediment production, (erosion rates), (3) characterization of the adjustments of the ephemeral channels to increased sediment supply, and (4) characterization of the morphologic adjustments of the perennial, master stream (Rito de los Frijoles) to increased runoff and sediment supply. This study evaluates the geomorphic processes and adjustments to devegetated conditions for a three-year period. Thus, results discussed herein are restricted to time periods of short duration (e.g., several years) rather than time periods involving tens of years. A morphometric analysis of the Frijoles Canyon watershed provides baseline information on the spatial arrangement of hillslopes and channels. The geomorphic responses of noninstrumented, devegetated watersheds developed on the volcanic plateaus surrounding the Jemez Caldera may be predicted based upon a synthesis of field studies, morphometric analysis, and geomorphic mapping performed in this study.

Geologic Setting of Study Area

The Frijoles Canyon watershed is developed on a portion of the southeastern flanks of the Pleistocene Valles Caldera volcanic complex (Fig. 2). Bedrock geology of the study watershed includes the Bandelier Tuff, unnamed basalt flows, the Tshicoma Formation, and the Paliza Canyon Formation (Smith and others, 1970). The Bandelier Tuff comprises approximately 75 percent of the areal extent Frijoles Canyon watershed. The uppermost headwater portion of the watershed (approximately 20 percent areal extent) is comprised of two volcanic domes of the Tschicoma Formation. The lowermost portion of the Frijoles Canyon watershed consists of interfingering basalt flows and Bandelier Tuff which overlies a maar feature (Eichelberger and Heiken, unpublished report).

The mid-portion of the Frijoles Canyon watershed is cut by three north-northwest-trending, high-angle normal faults (Fig. 2). These faults offset the Bandelier Tuff with the east blocks being downthrown. Stratigraphic separation is greatest on the western-most fault. Topographic relief along the major fault-line scarp is approximately 120 m.

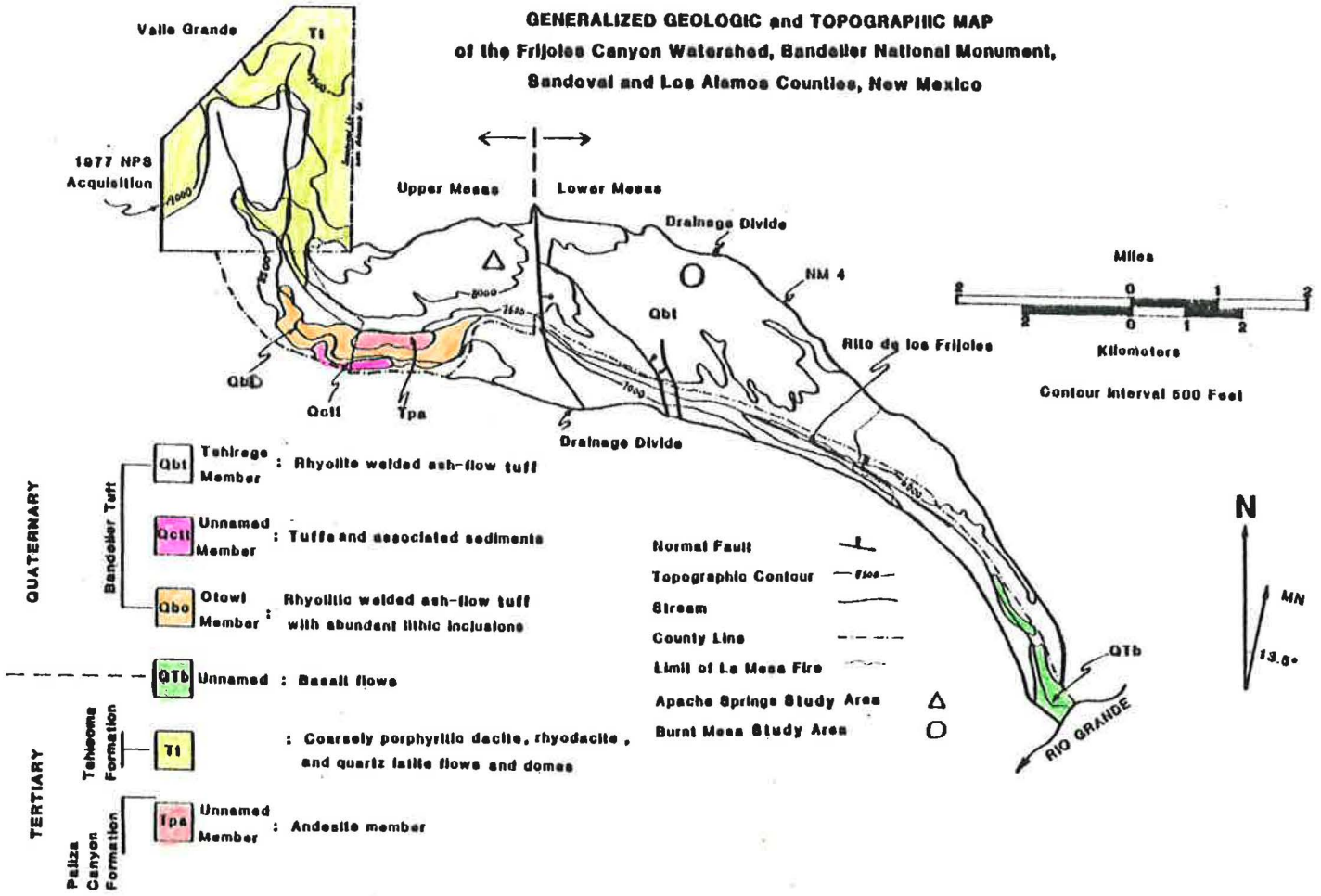


Figure 2: Geology and Topography of the Frijoles Canyon Watershed, Bandelier National Monument. Study Areas are Indicated by Δ and O.

The physiographic setting of the study area is a volcanic plateau incised by deep canyons with local relief of 60 to 240 m along these canyon walls. The mouth of the Frijoles watershed is at an elevation of 1640 m, receives 38 cm of precipitation (Earth Environmental Consultants Inc., 1978; here referred to as EECI), and has cholla and mesquite as its typical vegetation. The headwaters of the Frijoles watershed is at an elevation of 3050 m, receives 76 cm of precipitation (Earth Environmental Consultants Inc., 1978), and has a spruce-fir forest type. The largest catchment areas of the Frijoles Canyon watershed are the mesas of the Pajarito Plateau. The mesas are formed primarily on the Bandelier Tuff unit which is offset by the normal faults discussed above. The resulting fault-line scarp is the physiographic boundary separating the upper mesas from the lower mesas of the Pajarito Plateau (Fig. 2).

Previous Work

Hydraulic geometry of rivers and streams has been described and quantified by a number of researchers (e.g., Mackin, 1948; Leopold and Maddock, 1953; Schumm, 1977). Within mountainous settings, the geomorphic concepts of grade and dynamic equilibrium have been examined (e.g., Miller, 1958; Heede, 1975). Heede (1972; 1977) has demonstrated the influence of channel character and forest density on the hydraulic behavior of mountainous streams. In a detailed geomorphic study of a mountainous watershed in Virginia, Hack and Goodlett (1960) observed variations in surface particle size, vegetation type and asymmetry of hillslopes according to the type of runoff, soil moisture conditions and the exposure of the hillslope.

The effects of heating by fire on forest soils have been examined by a number of researchers. The expansion and contraction of the regolith upon heating by forest fire and subsequent cooling and produces fine-grained particles which migrate into the soil reducing soil porosity (Packer and Williams, 1974). Tarrant (1956) observed that percolation was reduced following a severe

fire due to the reduction in macroscopic pore volume of the ground surface. Campbell and others (1977) report infiltration rates of 2.6 cm/hr on severely burned ground and a 6.8 cm/hr rate on unburned ground in a limestone terrane. The combustion of the forest litter produces a water repellent ash which decreases the infiltration rates (Krammes and Debano, 1965; DeBano and others, 1970; Savage and others, 1972). With decreased infiltration, there is a corresponding increase in runoff. The increase in overland flow cuts new rills into the ground surface which leads to increased sediment production (Megehan and Molitor, 1975).

Dryness (1965) has stressed the role of forest litter in controlling erosion. Raindrop impact on a denuded ground surface will break down soil aggregates, which ultimately results in the clogging of the surface porosity (Dunford, 1954). Imerson (1977) noted that bare soil mounds, produced by burrowing animals in a forested region, are important sources of suspended sediment and are particularly susceptible to rain splash. In a burned pine forest, an important source of forest litter is the incompletely consumed forest canopy. Partially burnt needles drop to the ground following the fire and protect the recently denuded ground from rain splash and overland flow (Megehan and Moliter, 1975).

During the summers of 1974 and 1978, the EECI conducted a soil survey of the Bandelier National Monument. EECI (1978) noted that the lower mesas are eroding as indicated by pedestaling the grasses. In addition, EECI (1978) observed that the upper mesas of the Monument show strong soil profile development indicating soil formation occurred under climatic conditions more favorable than are now present.

Preceding the La Mesa fire, a biological study, conducted by L. Potter and T. Foxx, (University of New Mexico), was near completion. Their investigation was concerned with the mortality rates of trees as governed by the amount of fuel loading (dead, standing, and downed trees) in areas of recurring fire. Foxx and Potter, (1978) noted that the La Mesa fire was extremely hot and severe in places. In addition, the importance of needle fall in retarding overland flow and aiding grass seedling growth was noted (Potter and Foxx, 1979).

Within a month following the La Mesa fire, a joint effort was made by the National Forest Service, National Park Service, and the Los Alamos Scientific Laboratories to reseed the area of the La Mesa fire. The reseeding effort was done by helicopter, using grass seeds native to the Pajarito Plateau. Potter and Foxx (1979) note that the reseeding effort was most successful on the upper elevation mesas.

TECHNIQUES OF INVESTIGATION

Drainage-Basin Selection

The selection of study basins within the mesa-top catchment areas of the Frijoles watershed involved the locating of small catchment areas (thousands of square meters) which represent different burn intensities of the forest fire. A qualitative estimate of burn intensity was recommended by the National Park Service (K. Newton, personal communication, 1977). This qualitative estimate is given below:

(1) intense burn: complete destruction of all ground and tree foliage, leaving only charred trunks and branches (Fig. 3);

(2) moderate burn: destruction of ground foliage, leaving only the crowns of taller trees (Fig. 4); and

(3) light burn: destruction of the ground foliage and small shrubs; larger trees and shrubs not destroyed (Fig.5).



Figure 3: Photograph Illustrating the Effects and Qualities Defining an Intense Burn. Note the Lack of Needles on the Burned Trees, and the Denuded Ground Surface.



Figure 4: Photograph Illustrating the Effects and Qualities Defining a Moderate Burn. Note the Presence of Pine Needles on the Ground Surface.



Figure 5: Photograph Illustrating the Effects and Qualities Defining a Light Burn. Note Unburned, Small Tree Right of Center, and Other Small, Slightly Burned Trees at Right Margin.

A second selection criterion was to locate areas which differ in topographic and vegetative characteristics. Given the extent of the La Mesa fire and the geology of the plateau, it was possible to instrument different climatic settings with uniform bedrock geology. Finally, basins with similar aspects and without disturbance by roads or fire lines were selected for detailed studies.

This study at times refers to conditions present previous to the La Mesa fire and conditions present following the fire. These times are referred to as pre-burn and post-burn, respectively. The term burn is used, as opposed to fire, because this study is concerned with the burned residues (ash) left by the fire and not the fire itself. Ash is used in this study to denote burned organic debris and is not to be confused with volcanic ash (which is referred to as tuff).

Field Instrumentation

Hillslope segments and ephemeral channel reaches were instrumented in each study basin to monitor the amount, distribution, and seasonal variations in sediment contribution to the stream channel. Modifications of the ephemeral channel morphology were measured with erosion-chain transects (Leopold and others, 1966). Hillslope erosion was measured by two types of field instrumentation: (1) erosion-pin transects (Leopold and others, 1966), and (2) a portable contour-plotting frame (here called an erosion grid) which permits 25 elevation measurements over a 1 m^2 area (Campbell, 1974).

Erosion-chain transects include a series of lightweight chains installed vertically into the bed of the ephemeral channel and perpendicular to the channel banks. Scouring of the channel bed is recorded by the chains when the bed of the channel is lowered; during scour the chain falls and is laid out horizontally in the direction of flow. Filling of the channel is recorded by the depth of fill on the horizontal segment of the chain.

Erosion-pin transects are a series of pins crossing each study basin at the basin mouth, mid-basin, and basin headwater regions. An erosion pin consists of a 25 cm long spike with a washer, 4 cm in width, slipped over the shaft of the spike. The pin is installed vertically into the ground, with the pin head holding the washer flush to the ground surface. A caliper is used to measure the separation between the bottom of the nail head and the washer. As run-off events erode the ground around the pin, the washer drops along the pin shaft recording cumulative degradation. The washers are sometimes covered by sediment derived from up-slope; therefore, the washer allows measurement of both ground-surface reduction and aggradation, with the pin head being the reference point. The various inclinations the washer may assume on a given pin shaft results in a measure-ment accuracy of ± 1 mm.

The erosion grid consists of an aluminum frame that is slipped over four, permanently installed reference stakes (Fig. 6). When emplaced in the field, 25 aluminum rods are slipped through holes in the frame at 0.2 m spacing. The rods are gently placed on the ground surface and the length of the rod above the frame is measured. Changes in rod length from the datum can be interpreted as changes in ground-surface elevation. This technique allows detailed measurements over an area without affecting the surface runoff with permanently emplaced stakes.

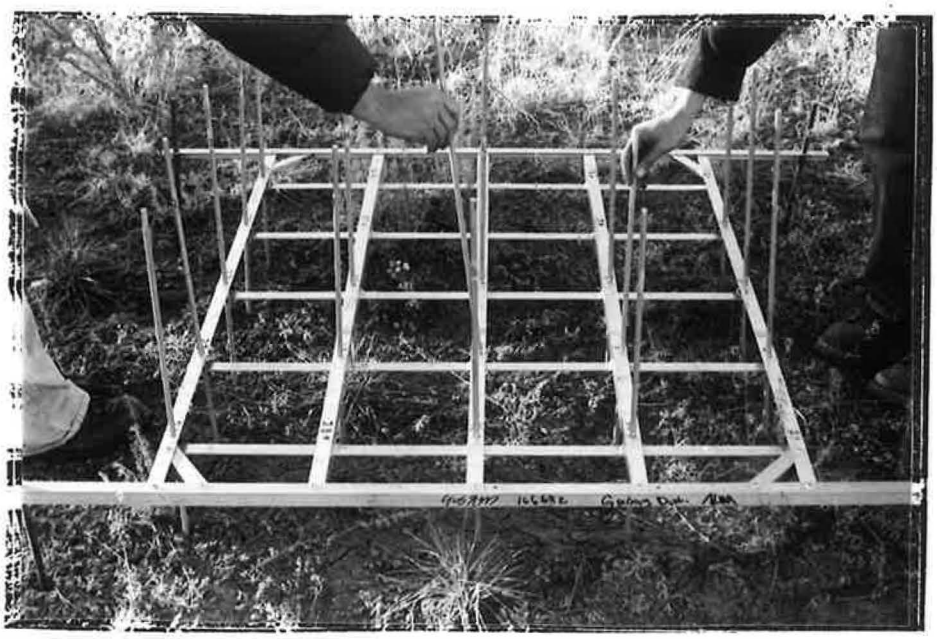


Figure 6: Photograph of Erosion-Grid Instrumentation Technique. Note the Permanent Rebar Reference Stake in the Lower Left Corner..

Topographic base maps at a scale of 1:240 were constructed for each study basin with a plane table and alidade (Higler & Watts) survey. Periodically, slope-area runoff measurements and hillslope inclination were surveyed with a Ushikata transit to document runoff events and hillslope degradation and aggradation. Longitudinal profiles for each study basin were constructed for a comparison of study basin length and relief.

Another field technique for monitoring geomorphic processes and landscape changes in the devegetated basins is repetitive terrestrial photography (Malde, 1973). In the present study, the camera is used in two ways: (1) for a portable and visual note-taking method, and (2) for repetitive photography at 4 permanent camera stations. Both procedures permit geomorphic processes to be monitored over extended time periods.

To evaluate the possible impact of the fire on soil infiltration capacity and runoff contribution, a simple infiltration study was conducted in the field. The set-up consists of an open-end cylinder gently pounded into the ground surface. A piece of cheesecloth was placed inside the cylinder to protect the ground surface from further disturbance during the application of water. One liter of water was poured into the cylinder, and the time required for the ground surface to absorb the standing water

constituted the infiltration rate. Infiltration tests were conducted both on surfaces covered by fire-associated ash and on surfaces having been stripped of the ash layer. Soil cores of most infiltration test areas were taken to describe the texture and layering in the soil.

To characterize the pre-burn and post-burn ephemeral channel morphology, trenches were cut into the channel beds. The pre-burn channel morphology usually was identified by the presence of an in situ fire-derived ash layer. If the ash layer was not preserved, the pre-burn channel morphology was determined by noting channel deposits containing grains with ash coatings versus deposits of grains without ash coatings. Each trench was described and sketched in the field.

Laboratory Procedures

Graphic presentation of erosion-pin transect measurements involved the use of a Hewlett-Packard computer with cassette tape data storage and plotter attachment. The initial relative ground-surface elevations for each transect were surveyed and stored on the data tape. Data for each measurement date were then keyed into the computer, stored on the tape, and plotted against the initial datum. Thus, a series of computer-generated plots of ground-surface elevation change were constructed for different time intervals.

Particle-size distributions were determined for scoop samples taken from hillslope and channel sections of each study basin. The purpose was to determine differences in grain-size distributions on the hillslopes as compared to the particle-size distribution present in the ephemeral channels.

Soil cores collected at the infiltration study sites were cut in half and described using a binocular microscope at 20x magnification. Additionally, bulk density of the soil layers was determined for the soil

cores taken from the infiltration sites. This measurement was done by removing a cubic centimeter of soil from the soil core, oven drying the sample, and weighing the oven-dried sample.

Aerial photographs of the Bandelier National Monument were taken following the La Mesa fire by Koogle and Pouls Engineering, Inc., (Albuquerque, New Mexico) at a scale of 1:6000. The photographs were used to describe the landscapes developed within the Frijoles watershed. Landscape units were mapped from these aerial photographs in the lower Frijoles watershed. Map units were defined according to morphologic expression, vegetation density, and the size of material comprising the slopes. The map units are basically a reflection of the erosional processes responsible for the landform expression.

Morphometric analyses of the Frijoles watershed were conducted according to methods established by Strahler (1964). These morphometric analyses include ordering of streams, measuring stream lengths, and determining drainage density, bifurcation ratio, and drainage basin area. A topographic map of the Frijoles Canyon watershed at a scale of 1:12,000 was used to measure these morphometric properties.

Streamflow data collected at the U. S. Geological Survey (U.S.G.S.) stream gaging station on the Rito de los Frijoles, Bandelier National Monument were utilized. The

gaging station was operational during the period 1963 to 1969. The station was re-opened in July 1977 (soon after the La Mesa Fire) and was operational at the conclusion of this study. Mean monthly discharges for each period were tablulated and flow duration curves were constructed for each period of record (U. S. Geological Survey, 1963-1969; 1977-1979).

STUDY BASIN GEOMORPHOLOGY AND INSTRUMENTATION

Three months following the La Mesa fire, three basins had been instrumented on the upper-elevation mesas in the Apache Springs area, and three basins on the lower-elevation mesas had been instrumented in the Brunt Mesa area. In both study areas, the three basins are small, low-order headwater drainage basins and reflect the qualitative type of burn intensity (i.e., intense, moderate, light). Stream (or basin) order is a method of denoting certain stream segments within a drainage network (Strahler, 1964). Unbranched stream segments are referred to as first-order; the confluence of the two first-order streams forms a second-order stream segment, etc. Hence, low-order basins refer to small basins drained by first-, second-, or third-order streams.

The Apache Springs study area is at an elevation of approximately 2530 m with a mixed conifer forest comprised of ponderosa pine (Pinus ponderosa), white fir (Abies concolor), Douglas-fir (Pseudotsuga menziesii) and aspen (Populus tremuloides). The Burnt Mesa study area

is at an elevation of approximately 2195 m and is characterized by a mosaic of ponderosa pine in dense stands of young trees, open park-like stands of mature trees, and open meadows of grasses. Hereon, the respective burn intensity at each elevation is referred to in abbreviated form, such that BMINT refers to the intense-burn basin within the Burnt Mesa study area; BMMOD refers to the moderate-burn basin within the Burnt Mesa area; BMLIGHT refers to the light-burn basin within the Burnt Mesa area; BMARCH refers to the pin transect along an unexcavated ruin; ASINT refers to the intense-burn watershed within the Apache Springs study area; ASMOD refers to the moderate-burn basin within the Apache Springs area; ASLIGHT refers to the light-burn basin within the Apache Springs area.

Low-order drainage basins of Burnt Mesa and Apache Springs differ in their geomorphic character (Table 1). Drainage basins within the Burnt Mesa area are typically elongate due to their development on incised mesa tops. The Apache Springs basins are characteristically circular due to their development on the valley-side slopes of wide, shallow valleys (Table 1). Drainage basins of the Apache Springs are steeper and shorter than those of Burnt Mesa. Relief in the drainage basins is similar in both areas (Table 1). Bedrock outcrops are not extensive in the drainage basins;

Basin	Area (m^2)	Aspect	Order	Relief (m)	Length (m)	Perimeter (m)	Basin Circularity	Basin Slope
Burnt Mesa								
Intense	4116.5	WNW	3rd	11.86	129.97	298.09	.582	.091
Moderate	813.8	S	1st	8.65	67.06	146.30	.478	.129
Light	1426.0	S	1st	5.57	70.84	177.39	.570	.079
Apache Springs								
Intense	1431.5	S	2nd	11.16	51.51	143.26	.876	.217
Moderate	677.7	S	1st	8.12	49.07	124.05	.553	.166
Light	380.4	ESE	1st	5.41	25.97	67.36	.776	.208

Table 1. Geomorphic Characteristics of Study Basins in Bandelier National Monument, New Mexico. Basin circularity (R_c) is defined as $R_c = 4\pi A/P^2$, where A = area and P = perimeter. Basin slope is defined as Relief/Length.

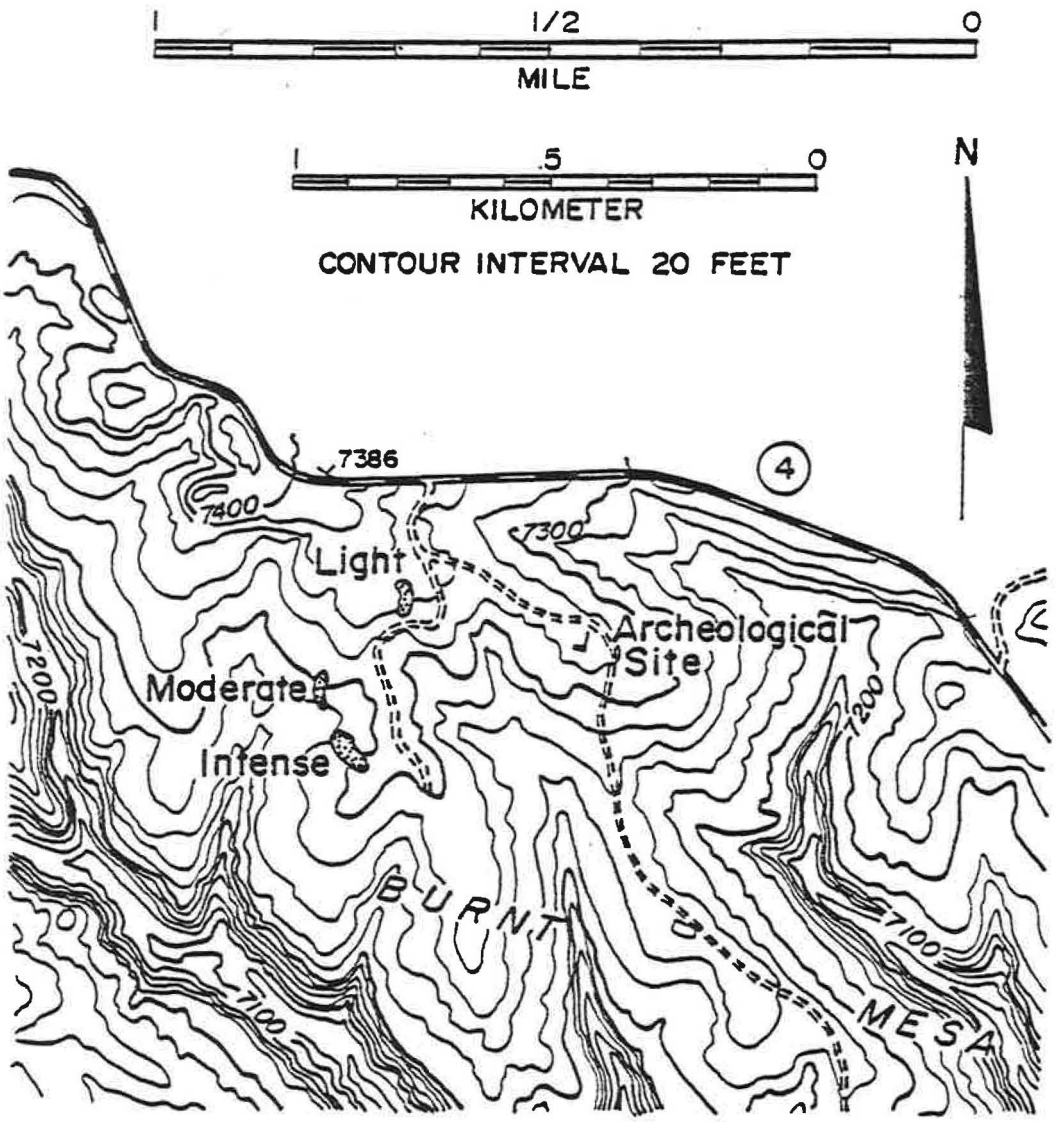


Figure 7: Locations of Instrumented Basins in the Burnt Mesa Study Area. See Figure 2 for the Location of the Area Within the Frijoles Canyon Watershed. State Road 4 Forms the Northern Boundry of the Monument.

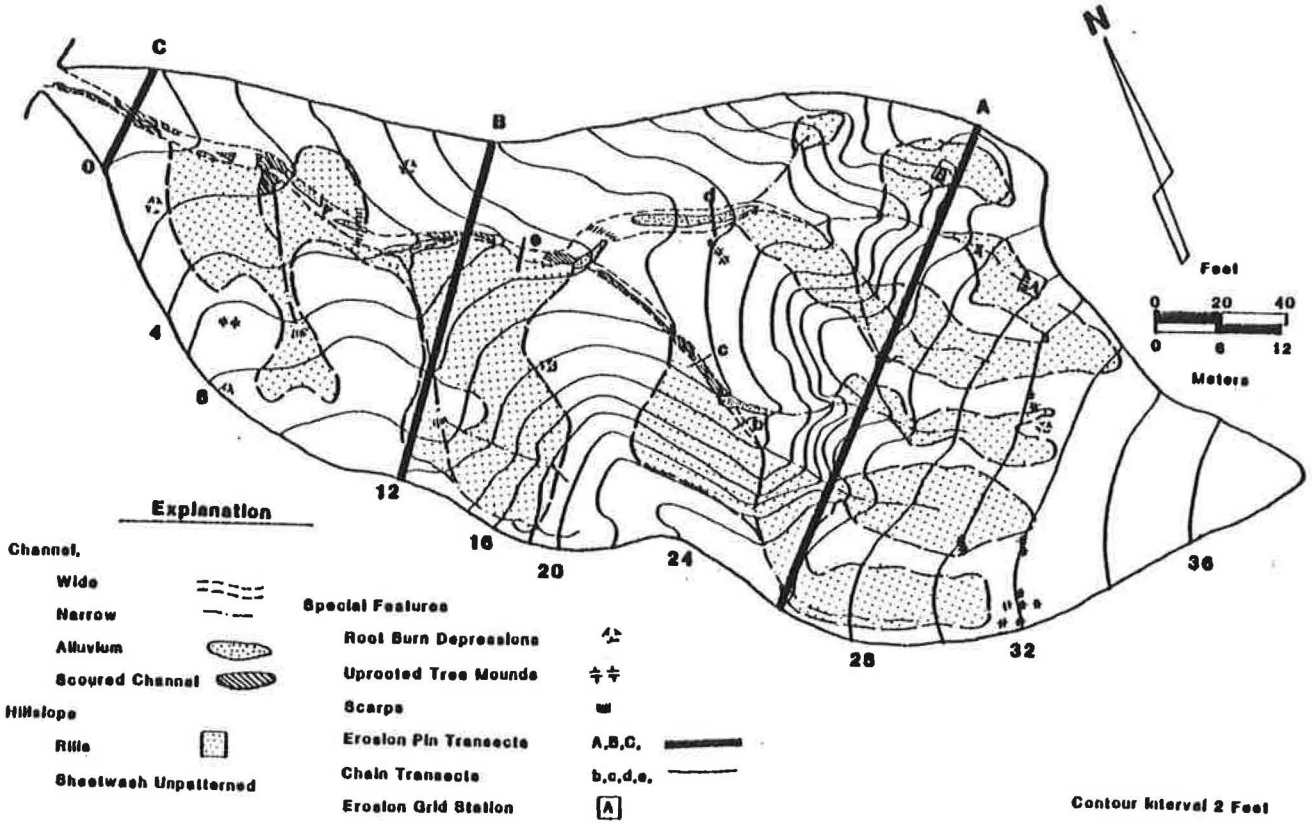


Figure 8: Geomorphic Map of the Intense-Burn Study Basin, Burnt Mesa. Instrument Locations are Indicated.

TOPOGRAPHIC MAP OF INTENSE-BURN WATERSHED, BURNT MESA

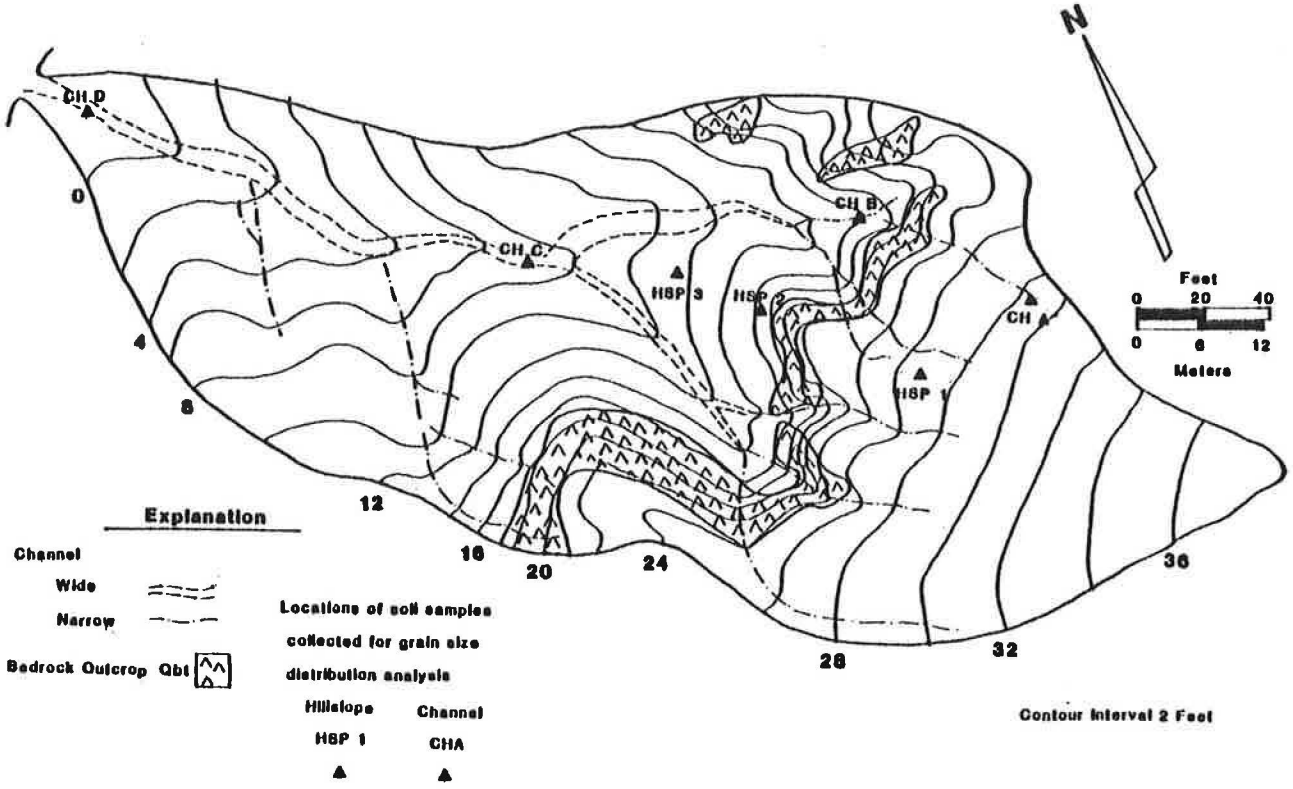


Figure 9: Topographic Map of the Intense-Burn Study Basin, Burnt Mesa. Hillslope and Channel Sample Locations are Indicated.

rather, varying thicknesses of water-worked colluvium and alluvium cover the basins.

Areas having suffered a similar degree of burn intensity will have supported similar densities of forest debris previous to a fire. This is a reflection of the relationship between amount of fuel loading and forest-fire burn intensity (Foxx and Potter, 1978). In Bandelier National Monument, a given burn intensity at the upper-elevation mesas (e.g., Apache Springs) supported a similar density of forest stand debris as did the same burn intensity at the lower-elevation mesas (e.g., Burnt Mesa).

Burnt Mesa Study Basins

The spatial relationship of the Burnt Mesa Study basins is illustrated in Figure 7. Included in the Burnt Mesa area is an erosion-pin transect installed on an unexcavated archaeological site to serve as a control area. The site is located in a meadow on the highest point of a mesa top, and is not a drainage basin. The archaeological site burned over very quickly due to the very light amount of fuel loading and revegetated soon after the fire.

BMINT is the largest basin investigated and covers 4116.5 m^2 (Figs. 8 and 9). Previous to the fire, the basin was forested with a dense, young stand of ponderosa pine. The study basin can be divided into three geomorphic

components: (1) low-relief headwater area perched above a bedrock outcrop, (2) steeper slopes of the bedrock in the upper and mid-basin, and (3) gentle slopes of the distal basin. These components are illustrated in the longitudinal profile of the basin (Fig. 10).

BMMOD is the steepest of the Burnt Mesa basins (Table 1). The hillslopes are generally uniform and bedrock crops out only in the distal portion of the basin (Fig. 11). The longitudinal profile of the basin is presented in Figure 10. This basin supported a park-like stand of mature ponderosa pine previous to the fire.

BMLIGHT is an open meadow with few pine and scrub oak trees. Bedrock does not crop out in this basin (Fig. 12). This results in a uniform longitudinal profile, as compared to the other Burnt Mesa basins (Fig. 10).

Apache Springs Study Basins

Locations of the Apache Springs study basins are given in Figure 13. The study basins are located further apart than the study basins of Burnt Mesa because basins not disturbed by human activity (i.e., road construction) were more difficult to locate.

In the Apache Springs area, ASINT is the largest and steepest basin (Table 1). This basin has an extensive outcrop of bedrock in the headwaters and has very little

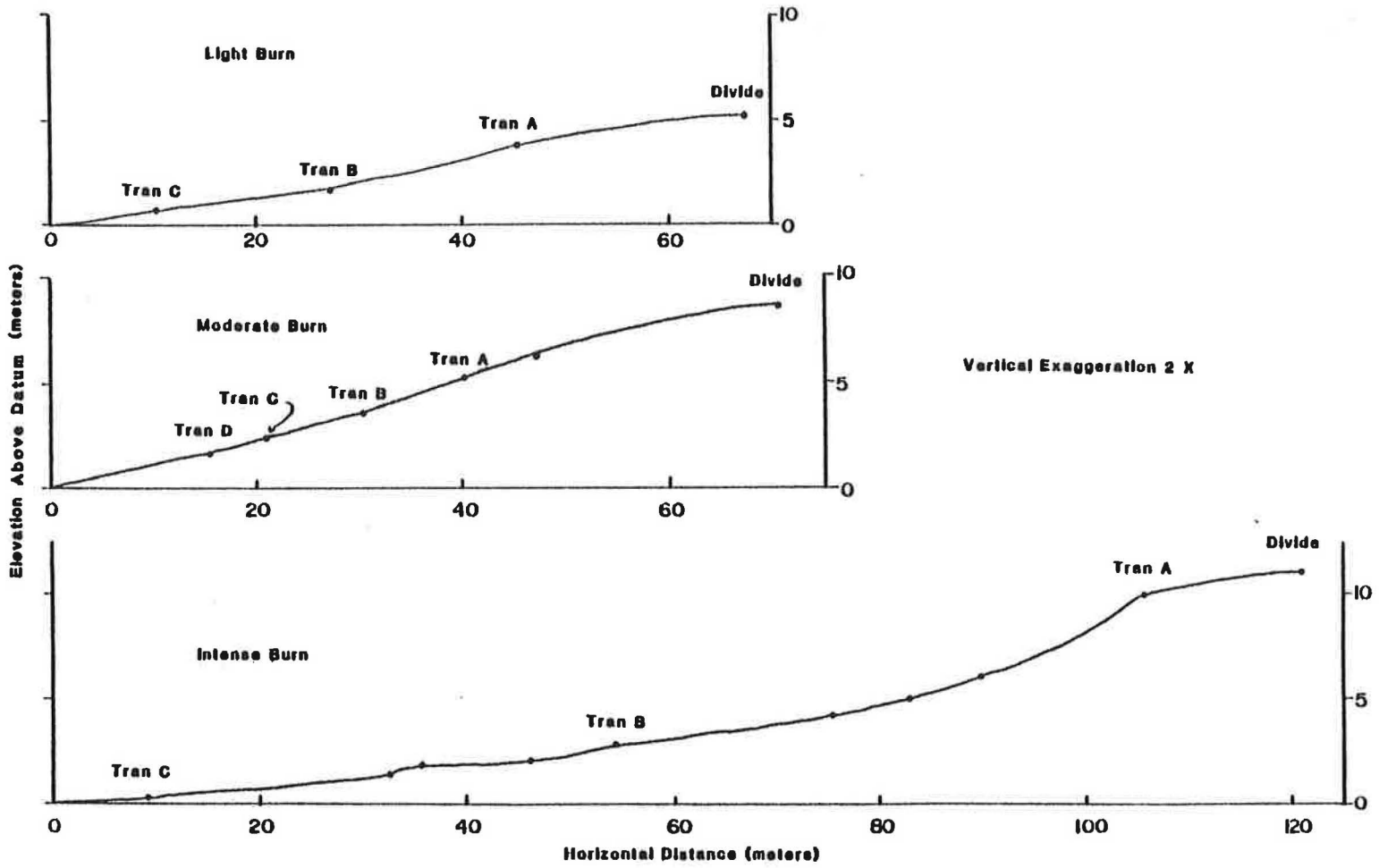
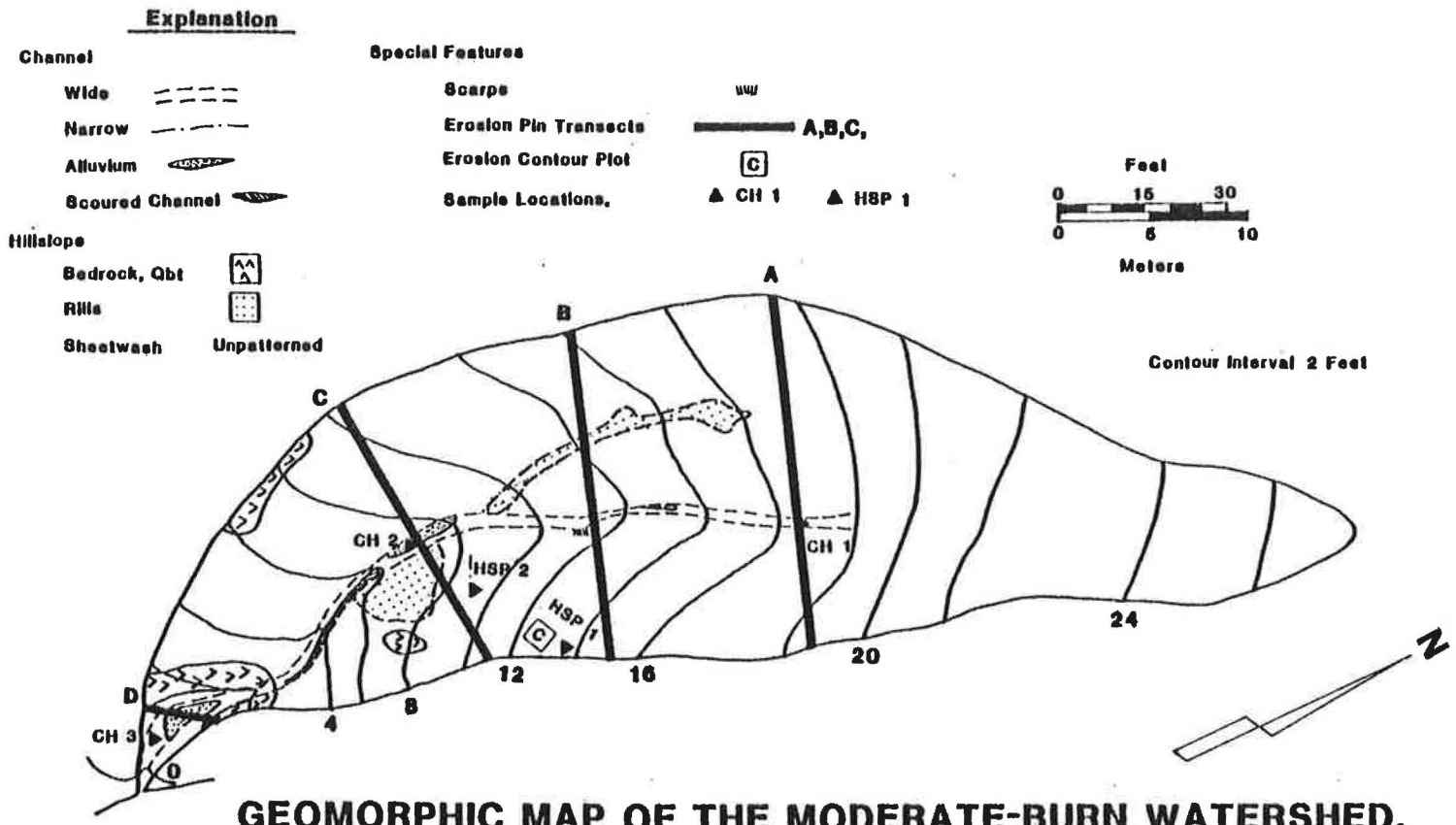


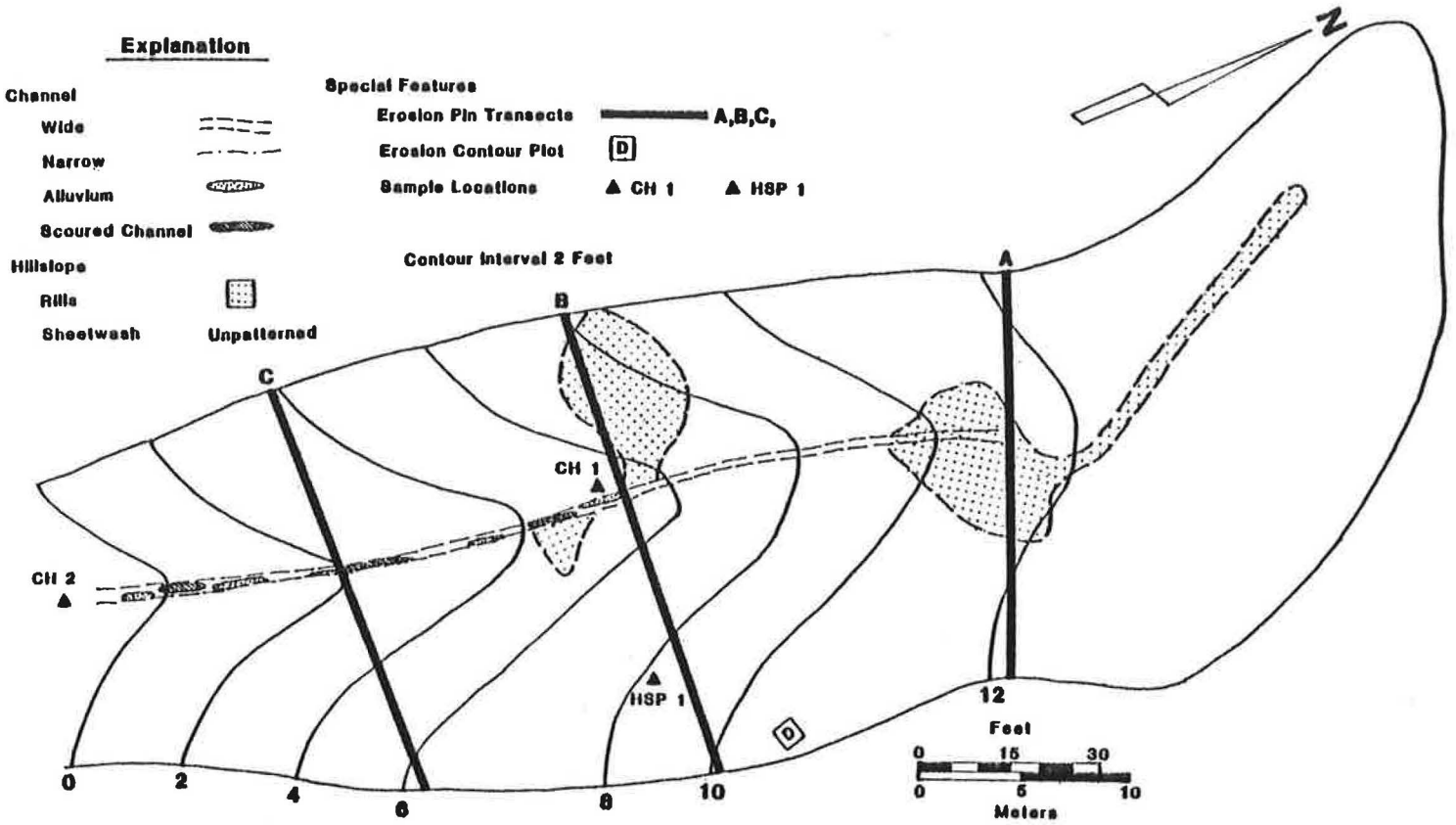
Figure 10: Longitudinal Profiles from Basin Divide to Basin Mouth of the Burnt Mesa Study Basins. Datum is the Basin Mouth. Points Where Erosion-Pin Transects Cross the Profiles are Indicated.



GEOMORPHIC MAP OF THE MODERATE-BURN WATERSHED,

BURNT MESA

Figure 11: Geomorphic Map of the Moderate-Burn Study Basin, Burnt Mesa. Instrument and Sample Locations are Indicated.



GEOMORPHIC MAP OF THE LIGHT-BURN WATERSHED, BURNT MESA

Figure 12: Geomorphic Map of the Light-Burn Study Basin, Burnt Mesa. Instrument and Sample Locations are Indicated.

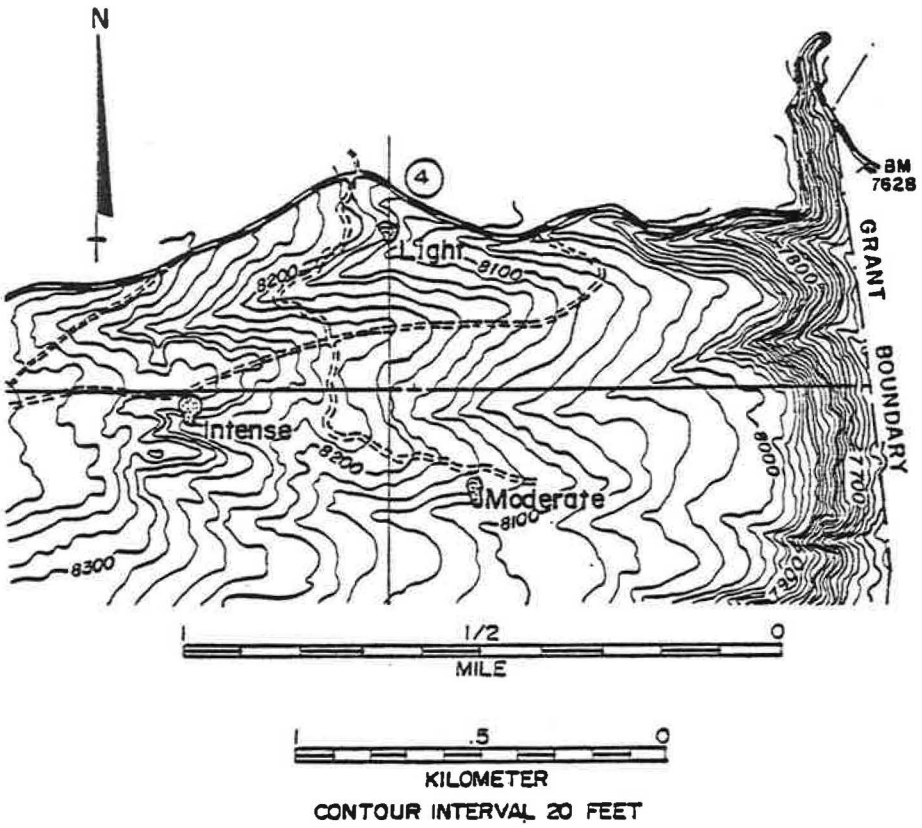


Figure 13: Locations of Instrumented Basins in the Apache Springs Study Area. See Figure 2 for the Location of the Area Within the Frijoles Canyon Watershed. Scarp on Right Hand Side of Figure is Fault-Line Scarp Separating the Upper and Lower Mesas.

catchment area above the bedrock (Fig. 14). The upper and mid-basin slopes are steep but become shallower in the distal portion of the basin (Fig. 15). This intense-burn basin supported a dense young stand of ponderosa pine, spruce, and fir.

ASMOD has an extensive headwater area above a bedrock outcrop (Fig. 16). This gives the basin an elongate morphology that is not characteristic of the Apache Springs area (Table 1). The longitudinal profile of the basin is presented in Figure 15. This basin supported an open stand of mature pines and smaller spruce and fir trees.

ASLIGHT is the smallest of all the study basins (Table 1). The basin is developed on the edge of a mesa which gives it a distintly convex longitudinal profile (Fig. 17 and 15).

Instrumentation of each study basin was completed by mid-September of 1977, except for ASLIGHT and the archaeological site on Burnt Mesa, (BMARCH). This was due to the difficulty in locating basins conforming to the conditions outlined for basin selection (see Techniques of Investigation Section). The light-burn in the Apache Springs area was finally located and instrumented in November of 1977. The archaeological site on Burnt Mesa was not instrumented until March 1978. This allowed the rapidly burned over mesa-top meadow area with the archaeological site to become revegetated.

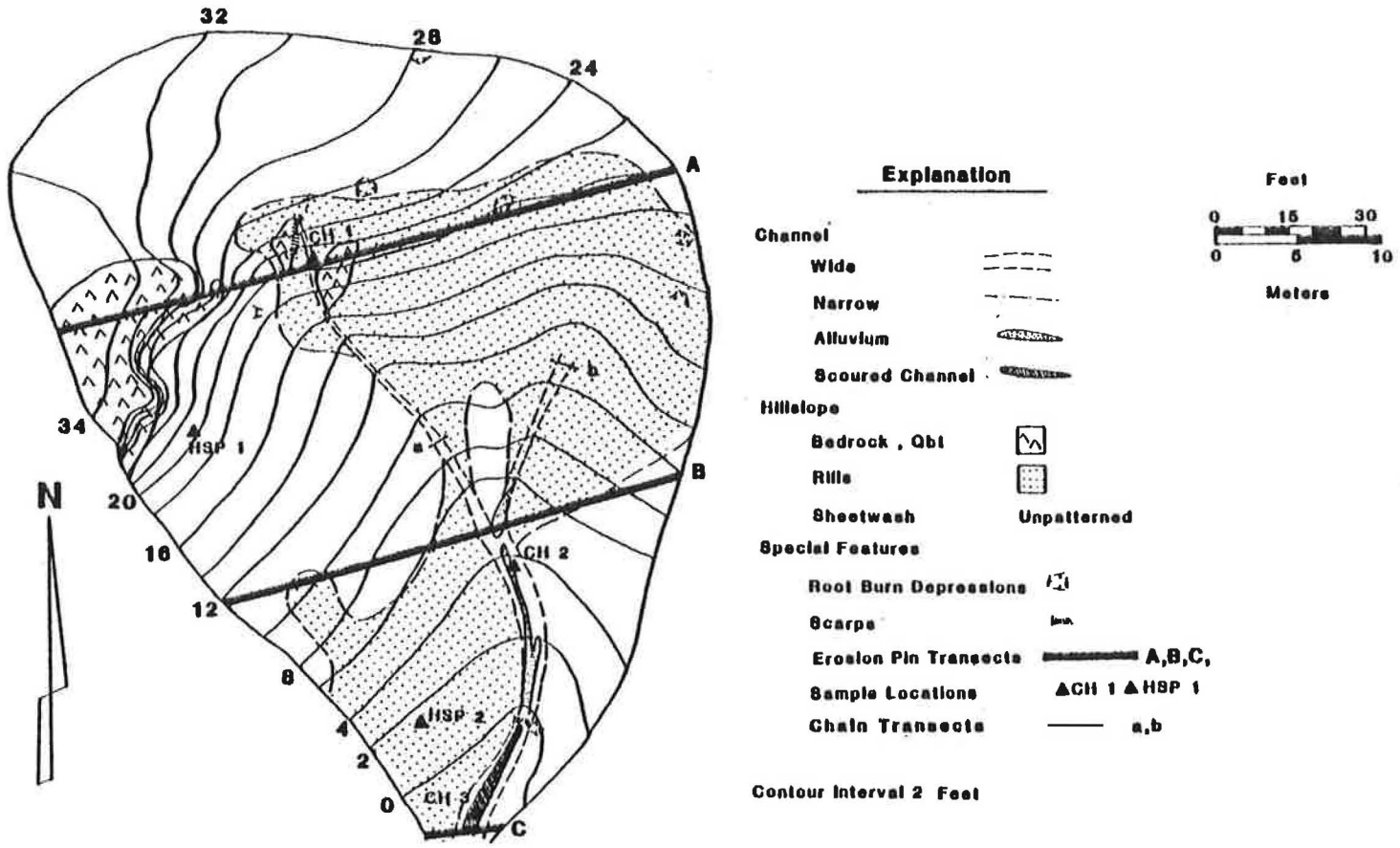


Figure 14: Geomorphic Map of the Intense-Burn Study Basin, Apache Springs. Instrument and Sample Locations are Indicated.

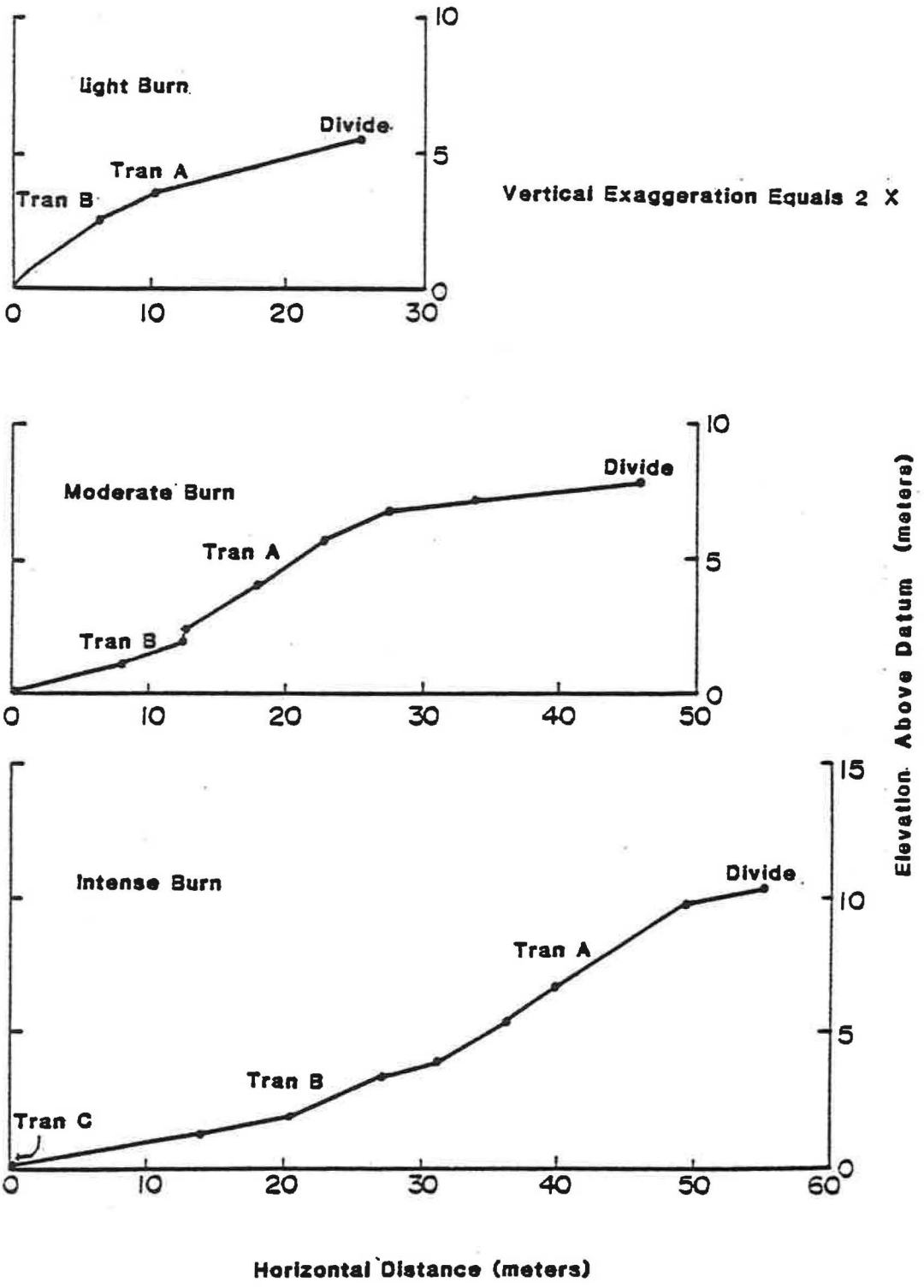


Figure 15: Longitudinal Profiles from Basin Divide to Basin Mouth of the Apache Springs Study Basins. The Points where Erosion-Pin Transects Cross the Profile are Indicated.

GEOMORPHIC MAP OF MODERATE-BURN WATERSHED, APACHE SPRINGS

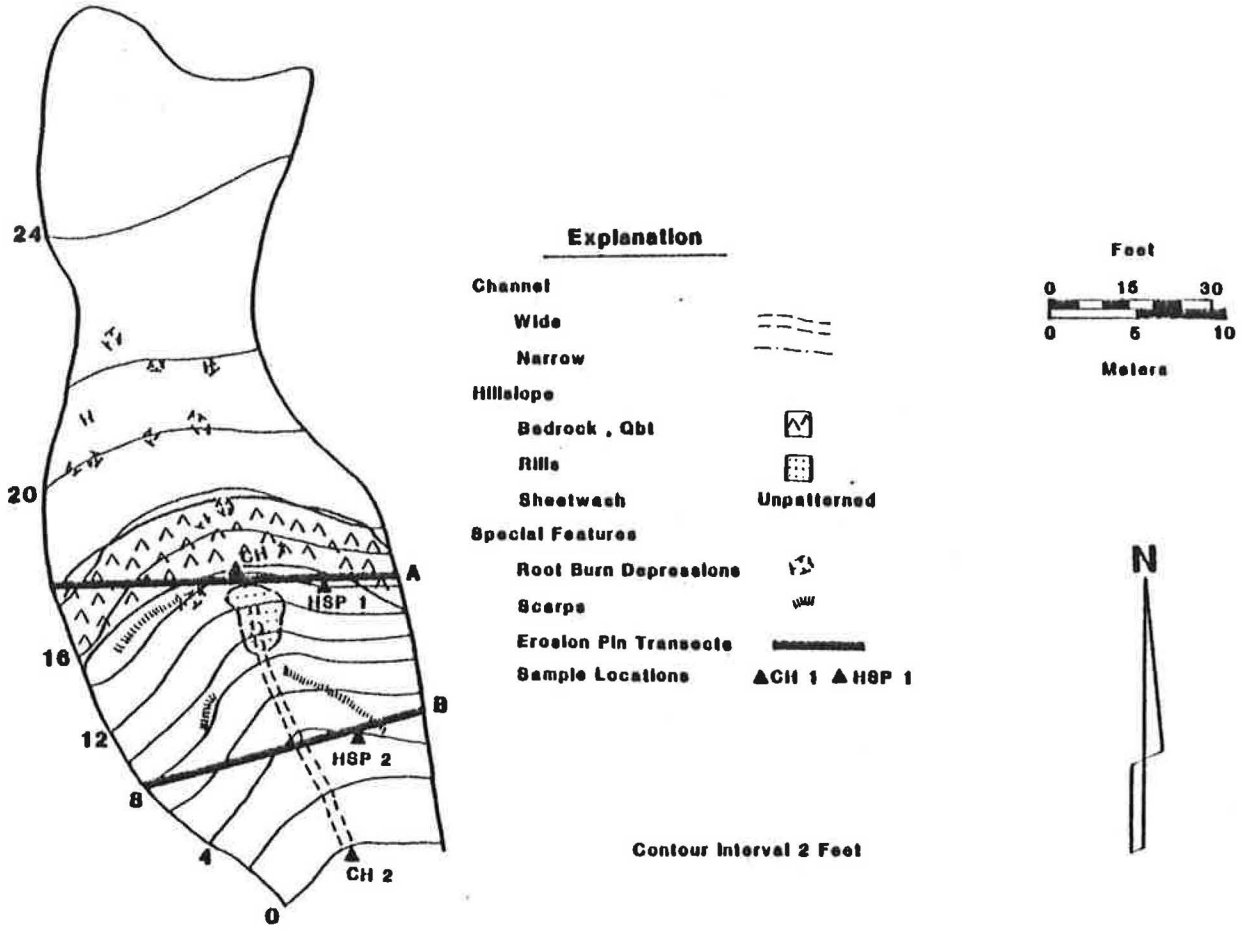


Figure 16: Geomorphic Map of the Moderate-Burn Study Basin, Apache Springs. Instrument and Sample Locations are indicated.

GEOMORPHIC MAP OF LIGHT-BURN WATERSHED , APACHE SPRINGS

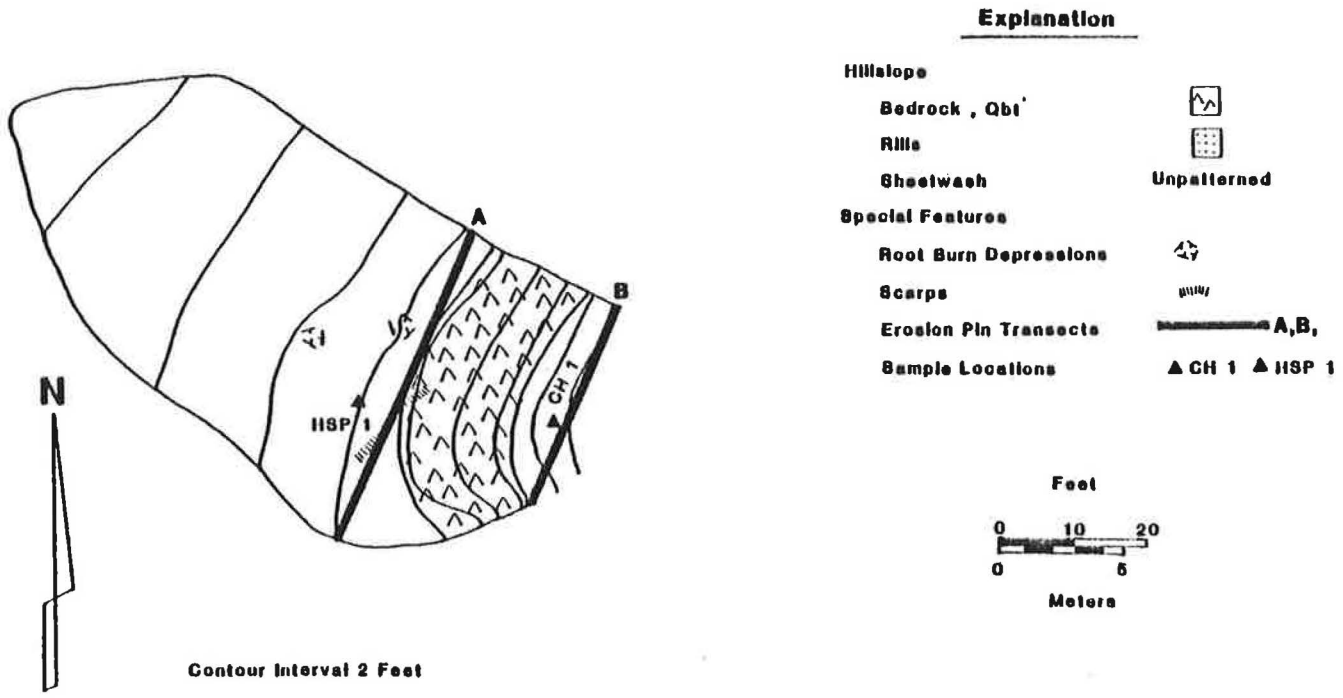


Figure 17: Geomorphic Map of the Light-Burn Study Basin, Apache Springs. Instrument and Sample Locations are Indicated.

The ASMOD and ASLIGHT study basins were instrumented with two erosion-pin transects. BMARCH was instrumented with a single pin transect. All other study basins were instrumented with three erosion-pin transects with transect A in the headwater region, transect B in the mid-basin region, and transect C across the basin mouth. BMMOD is an elongate basin and was instrumented with a fourth pin transect (transect D) across the basin mouth (Table 2).

Study Area	Basin	Channel Scour & Fill Chain Transects	Hillside Erosion-Pin Transects	Erosion-Grid Stations
BURNT MESA	INTENSE	4 transects	3 transects/100 m length 145 pins/ 0.6-0.9 m spacing	2-1 m^2 plots
	MODERATE	none	4 transects/52 m 46 pins/0.9 m spacing	1-1 m^2 plot
	LIGHT	none	3 transects/65m length 55 pins/ 1.2 m spacing	1-1 m^2 plot
APACHE SPRINGS	INTENSE	2 transects	3 transects/65 m length 86 pins/ 0.9 m spacing	none
	MODERATE	none	2 transects/33 m length 46 pins 0.9 m spacing	none
	LIGHT	none	2 transects/17 m length 37 pins/ 0.6 m spacing	none

Table 2: Summary of the Instrumentation of each Study Basin, Bandelier National Monument, New Mexico

RESULTS

Textural Properties of Surficial Material

Figure 18 illustrates representative histograms of the grain-size distributions of samples collected from hillslope and channel sections of the BMINT study basin. The histograms represent the textures of the upper 5 to 6 cm of the ground surfaces. The grain-size distributions of all study basins are included in Appendix I. In all figures, down-gradient is represented from left to right, sample number 1 being the uppermost slope or channel segment sampled. Sample locations are displayed on Figures 9, 11, 12, 14, 16, and 17.

The texture of the surficial cover is similar in the Burnt Mesa and Apache Springs study areas. The similarity is due to both study areas having been developed on the Bandelier Tuff. In general, hillslope samples exhibit a bimodal distribution; channel samples exhibit a unimodal distribution. In Figure 18, the coarse tail (> -1 phi) of the hillslope samples arises from the pebble size and larger fragments of tuff present in the ground surface. The fine tail (< 4 phi) of the hillslope samples is an

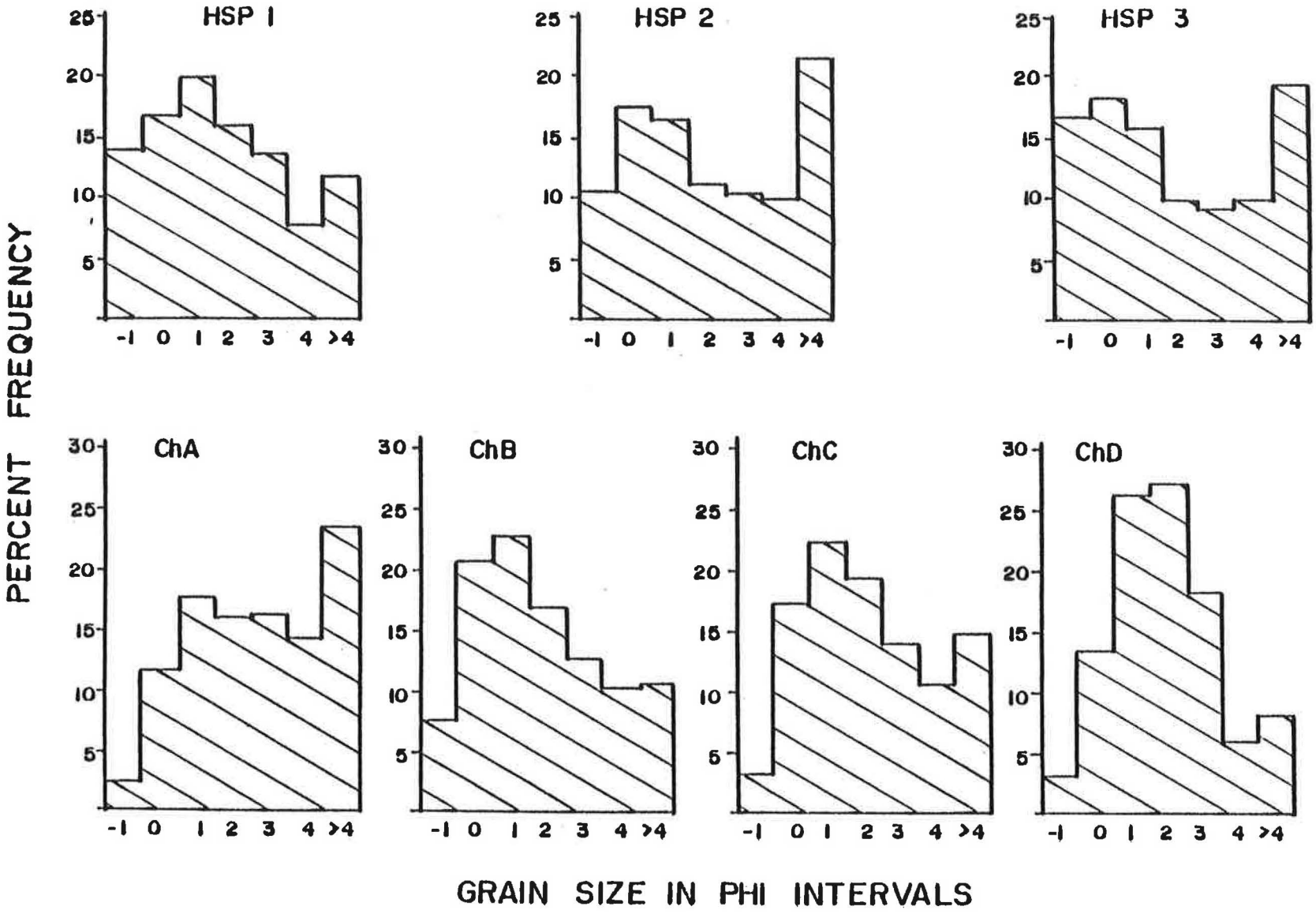


Figure 18: Grain-Size Distributions of Hillslope and Channel Samples Taken from BMINT.

indication of soil development (i.e., pedogenic clay accumulation) in the near surface. An accumulation of fine-grained debris in the downslope direction is suggested for the hillslope samples. Grain-size distributions of the ephemeral channels exhibit an unimodal trend in the downstream direction, indicating a sorting (0 to 2 phi range) of the sediment transported in these uppermost stream segments of the Frijoles Canyon watershed. The differences between hillslope and channel samples are accentuated with increasing basin area (BMINT being the largest study basin). The smaller study basins (e.g., ASLIGHT, Appendix I) exhibit the least differences between hillslope and channel samples.

Infiltration Properties of Surficial Material

Combustion of forest litter produces a fine-grained ash. The percentage of fire-derived, fine-grained debris in the near surface was not determined. However, the ashed ground surfaces were observed to have lower infiltration rates than ground surfaces without the ash layer. Table 3 is a compilation of the results of infiltration studies conducted in the Burnt Mesa and Apache Springs study areas. The tests were performed to establish the influence of an ashed ground surface on infilration rates. Eleven tests were conducted: four tests in the BMINT study basin; two in the BMMOD, BMLIGHT and ASINT study basins; and one in the ASMOD basin. Infiltration rates were found to be generally lower on fire-derived ash surfaces (mean = 30 cm/hr) than on unashed ground surfaces (mean = 42 cm/hr). The wide range of infiltration rates (7 to 61 cm/hr, ashed; 14 to 83 cm/hr, unashed) is attributable to site-specific variations in grain size and texture of the subsurface colluvial debris. For example, the BMLIGHT infiltration sample (H) contained 30 percent tuff fragments (3-10 mm mean diameter). The coarse texture of the sub-surface

allowed a high infiltration rate (82.8 cm/hr). Conversely, the BMMOD basin had a well-developed clay layer in the headwaters (Sample F). The clay impeded the downward percolation of water which resulted in a relatively low infiltration rate (28.8 cm/hr). See Table 3 for textural descriptions of the subsurface materials at the infiltration test sites. Ashed ground surfaces were found to have lower bulk densities (0.56 to 1.09 gm/cm^3) than unashed ground surfaces (1.20 to 1.43 gm/cm^3). The number of tests were not sufficient to establish any trends in infiltration rates from basin to basin.

Study Site	Core Depth cm (from surface)	Ground Surface (GS) and Core Description (CD)	Infiltration Rate cm/hr		Bulk Density	
			Ash	No Ash	depth (cm)	gm/cm^3
Burnt Mesa						
BMINT ashed headwater slope		GS: black, dry, fine grained with some charcoal fragments.	7.2			
Sample A	0-1.6	CD: burn layer; 95% <1mm, 2% 2-5 mm crystal fragments, 3% ash.			0.5-1.5	0.97
	1.6-2.0	burn discoloration fades to light brown.				
	2.0-9.5	98% <1mm fines, 1% 1-2mm crystal fragments, 1% root-lets.			3.0-4.0	1.36
	9.5-10.0	red-brown clay.				
BMINT stripped headwater slope		GS: tan, dry, fine grained.		14.4		
	0-0.07	CD: slight burn discolora-tion.			0.5-1.5	1.43
					3.0-4.0	1.36
Sample B	0.7-9.5	97% <1mm fines, 1% 1-4m crys-tal fragments, 1% rootlets.				

Table 3. Summary of Ground-Surface and Soil-Core Descriptions, Infiltration Rates, and Bulk Densities for Samples Tested and Collected at Infiltration Test Sites within the Study Basins.

Study Site	Core Depth cm (from surface)	Ground Surface (GS) and Core Description (CD)	Infiltration Rate cm/hr		Bulk Density	
			Ash	No Ash	depth (cm)	gm/cm^3
Burnt Mesa (cont'd)						
BMINT ashed side slope		GS: black, punky, fine grained with 2% pebbles (4-10mm).	21.6			
Sample C	0-3.0	CD: burn layer; black to gray color; 84% <0.5mm fines; 12% 1-2mm, 1% 2-4mm, 3% ash.			0.2-1.2	1.08
					2.8-3.8	1.06
	3.0-9.0	Tan to white color; 80% <0.5mm fines, 13% 0.5-1mm, 7% 1-5mm.			8.0-9.0	1.17

Table 3. (Cont'd) Summary of Ground-Surface and Soil-Core Descriptions, Infiltration Rates, and Bulk Densities for Samples Tested and Collected at Infiltration Test Sites within the Study Basins.

Study Site	Core Depth cm (from surface)	Ground Surface (GS) and Core Description (CD)	Infiltration Rate cm/hr		Bulk Density	
			Ash	No Ash	depth (cm)	gm/cm^3
Burnt Mesa (cont'd)						
BMINT stripped side slope Sample D	------	GS: white, cakey, fine grained with 4% pebbles (4-10m).		64.9	--------	
BMMOD ashed divide slope Sample E	------	GS: needle cover; black-brown fine grained with 10% 2-5mm crystal and tuff fragments.	36.0		--------	
BMMOD stripped headwater slope		GS: needle cover; tan fine grained with 5% 2-5 crystal and tuff fragments, plus 5% pebbles (4-10mm).		28.8		
Sample F	0-1.0	CD: burn discoloration				
	1-6.5	buff color; 76% <1mm, 3% 1-3mm, 1% pebbles.			1.0-2.0	1.47
	6.5-20.0	red-brown clay with 3% tuff fragments (4-10mm) and small rootlets.			10.5-11.5	1.62

Table 3. (Cont'd) Summary of Ground Surface and Soil-Core Descriptions, Infiltration Rates, and Bulk Densities for Samples Tested and Collected at Infiltration Test Sites within the Study Basins.

Study Site	Core Depth cm (from surface)	Ground Surface (GS) and Core Description (CD)	Infiltration Rate cm/hr		Bulk Density	
			Ash	No Ash	depth (cm)	gm/cm^3
Burnt Mesa (cont'd)						
BMLIGHT ashed divide slope		GS: black, pebbly surface; 20% 5-14 mm tuff fragments, 10% 2-6mm crystal and tuff fragments.	14.4			
Sample G	0-1.5	CD: burn discoloration;				1.09
	1.5-14.0	(gray brown) continues through pebbly sub-surface (15% 5-14 mm).			3.0-4.0 9.0-10.0	0.98
	14.0-15.0	Light brown color; fine grained			14.0-15.0	1.12
BMLIGHT stripped toe slope		GS: brownish pebbly surface		82.8		
	0-4.5	CD: brown fades with depth			0.5-1.5	1.20
		(burn discoloration), 5%			2.0-3.0	1.21
Sample H	4.5-15.0	tuff fragments (3-10mm). light brown with 30% tuff fragments.			7.0-8.0	1.17

Table 3. (Cont'd) Summary of Ground-Surface and Soil-Core Descriptions, Infiltration Rates, and Bulk Densities for Samples Tested and Collected at Infiltration Test Sites within the Study Basins.

Study Site	Core Depth cm (from surface)	Ground Surface (GS) and Core Description (CD)	Infiltration Rate cm/hr		Bulk Density	
			Ash	No Ash	depth (cm)	gm/cm^3
Apache Springs						
ASINT ashed W. divide slope		GS: black, powdered surface with 2% pebbles, 8% 2-5mm.	61.2			
	0-3.0	CD: burn layer; 25% 2-8mm,			1.3-2.3	0.56
		4% charcoal fragments, 5%			2.5-3.5	0.87
Sample I		ash, 1% pebbles, 65% < 2 mm fines.				
	3.0-12.0	buff to brown color with 5%			4.0-5.0	1.35
		unaltered tuff fragments, 25%				
		1-5 crystal and tuff fragments			10.0-11.0	1.32
		2% rootlets.				
ASINT stripped E. side slope		GS: tan-brown with 2% charcoal fragments, 1% pebbles 14% 2-5mm.		18.0		
	0-2.0	CD: burn discoloration.			1.5-2.5	1.23
Sample J	2.0-7.0	increase in coarse sand and			5.0-6.0	1.47
		tuff fragments with rootlets.				
	7.0-11.5	20% angular crystal fragments <8mm.				
	11.5-19.0	buff color, increase in fine			12.0-13.0	1.40
		grained percentage (to 85%).				

Table 3.(cont'd) Summary of Ground-Surface and Soil-Core Descriptions, Infiltration Rates, and Bulk Densities for Samples Tested and Collected at Infiltration Test Sites within the Study Basins.

Study Site	Core Depth cm (from surface)	Ground Surface (GS) and Core Description (CD)	Infiltration Rate cm/hr		Bulk Density	
			Ash	No Ash	depth (cm)	gm/cm^3
Apache Springs (Cont'd)						
ASMOD ashed headwater slope		GS: dense needle cover black, powdered surface, 8% pebbles 10% 2-5mm.	39.6			
	0.0-2.0	CD: burn layer, 3% charcoal.			0.2-1.2	0.99
	1.0-2.0	burn discoloration fades to buff.				
Sample K	2.0-4.0	10% 4-8mm tuff fragments, 3% 1-4mm crystal fragments, 2% rootlets.			2.0-3.0	0.95
	4.0	Bedrock.				

Table 3 (Cont'd) Summary of Ground-Surface and Soil-Descriptions, Infiltration Rates, and Bulk Densities for Samples Tested and Collected at Infiltration Test Sites within the Study Basins.

Hillslope Instrumentation

Erosion-Pin Studies

Three erosion-pin transects were installed in each of the study basins, with the exceptions of ASMOD and ASLIGHT (two transects each), and BMMOD (four transects). In each study basin, transect A occurs in the headwater area, transect B occurs in the mid-basin area, and transect C occurs near the basin mouth. Table 2 provides the number of erosion-pins in each study basin. Figures 19 through 34 are graphic representations of the erosion-pin transects in all the study basins. The location of the respective transect profiles are shown in Figures 8, 11, 12, 14, 16, 17.

In all profiles, the topographic positions of erosion-pins are plotted as well as changes in elevation of the washers on the pins. The original ground surface profiles (black lines) were determined by surveying pins at or near breaks in slope and extrapolating the elevations of intervening pins. The small, horizontal segments on the black line represent the relative position of a given pin; the connecting line segments approximate the ground surface.

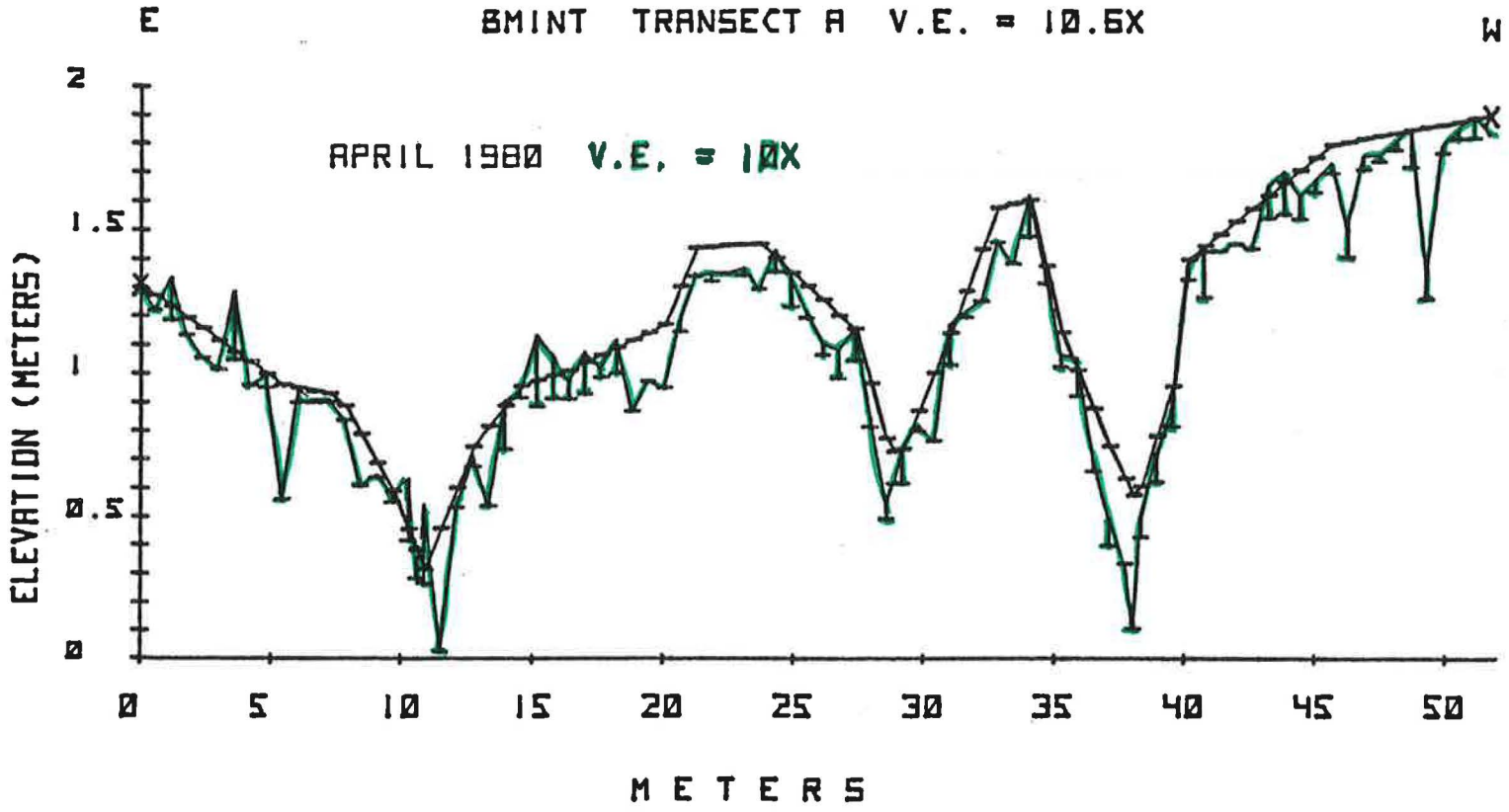


Figure 19: Topographic Profile and Change in Ground-Surface Elevation for Final Measurement of Erosion-Pin Transect A, BMINT. Original Ground Surface Indicated in Black and Change in Ground-Surface Elevation Indicated in Green. See Text for Additional Explanation.

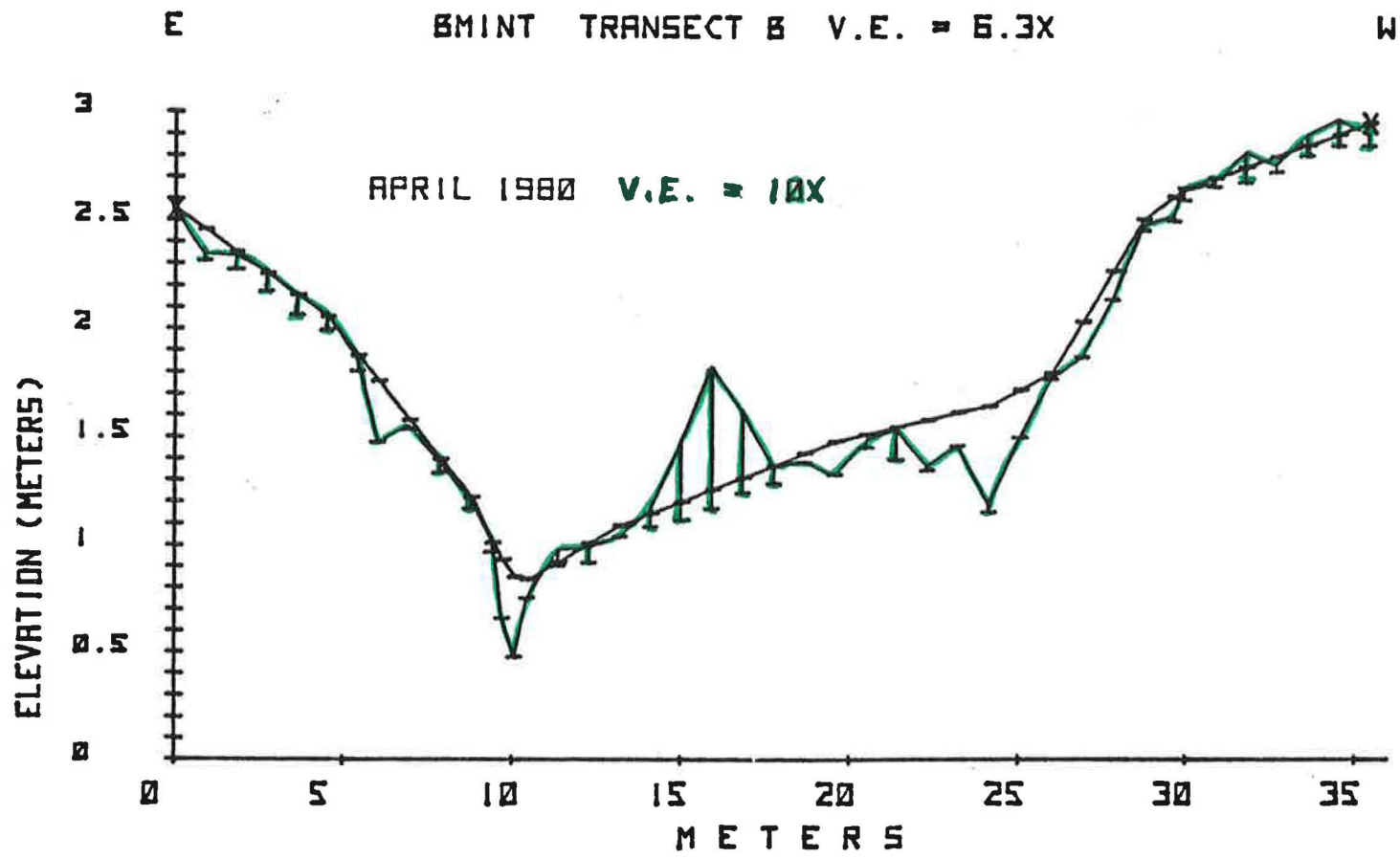


Figure 20: Topographic Profile and Change in Ground-Surface Elevation for Final Measurement of Erosion-Pin Transect B, BMINT. Original Ground Surface Indicated in Black and Change in Ground-Surface Elevation Indicated in Green. See Text for Additional Explanation.

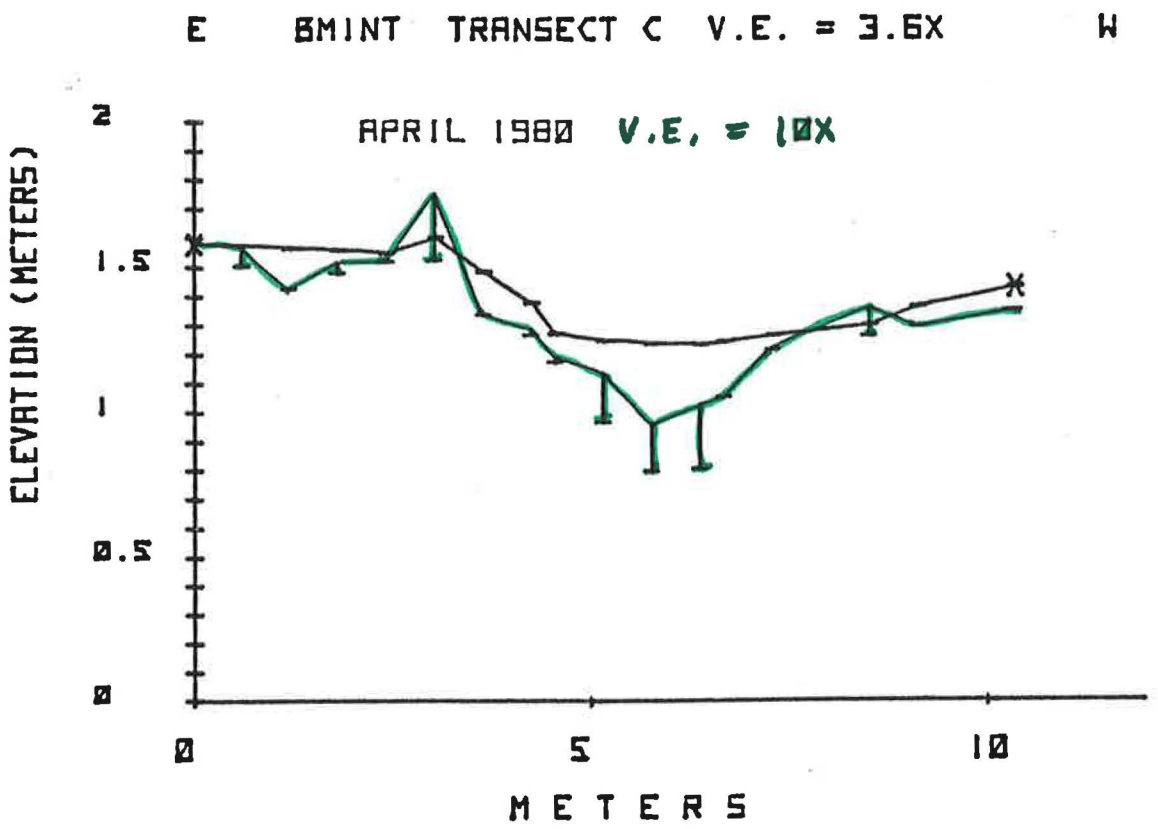


Figure 21: Topographic Profile and Change in Ground-Surface Elevation for Final Measurement of Erosion-Pin Transect C, BMINT. Original Ground Surface Indicated in Black and Change in Ground-Surface Elevation Indicated in Green. See Text for Additional Explanation.

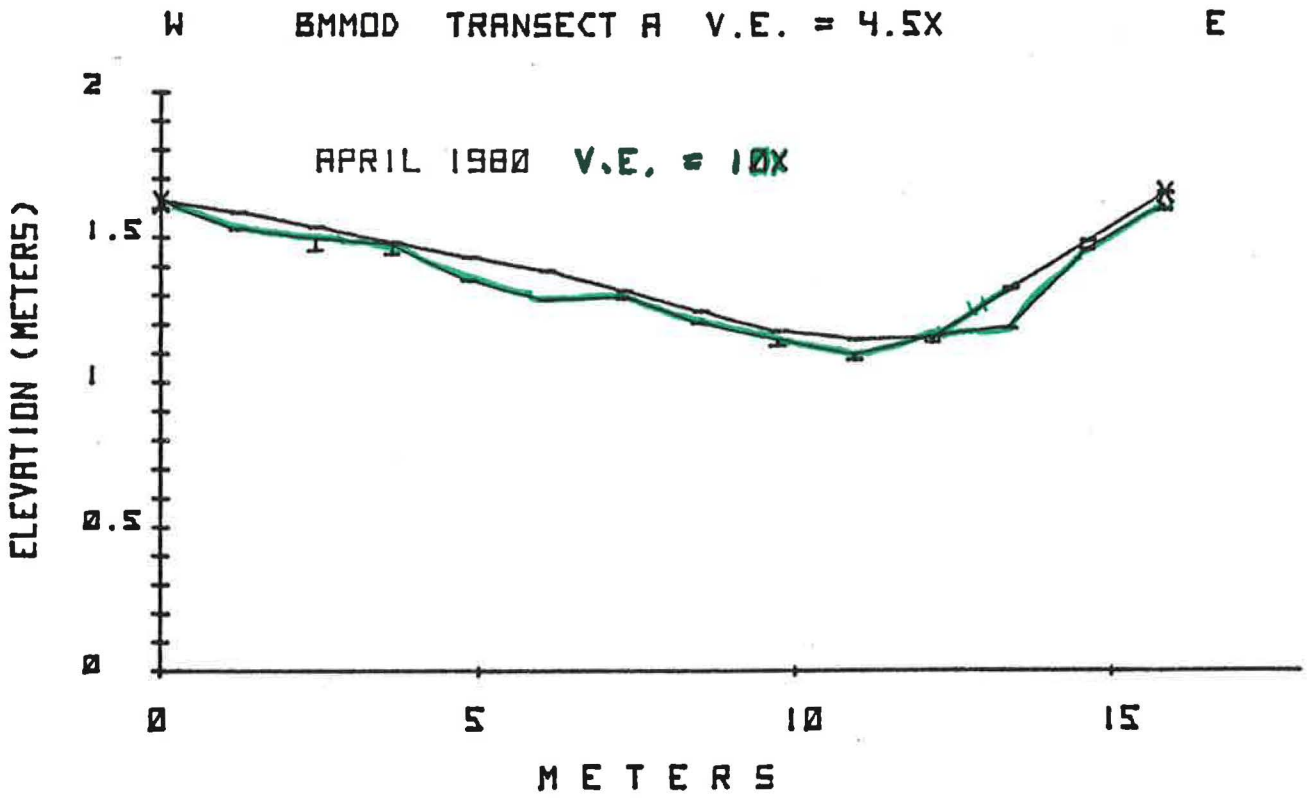


Figure 22: Topographic Profile and Change in Ground-Surface Elevation for Final Measurement of Erosion-Pin Transect A, BMMOD. Original Ground Surface Indicated in Black and Change in Ground-Surface Elevation Indicated in Green. See Text for Additional Explanation.

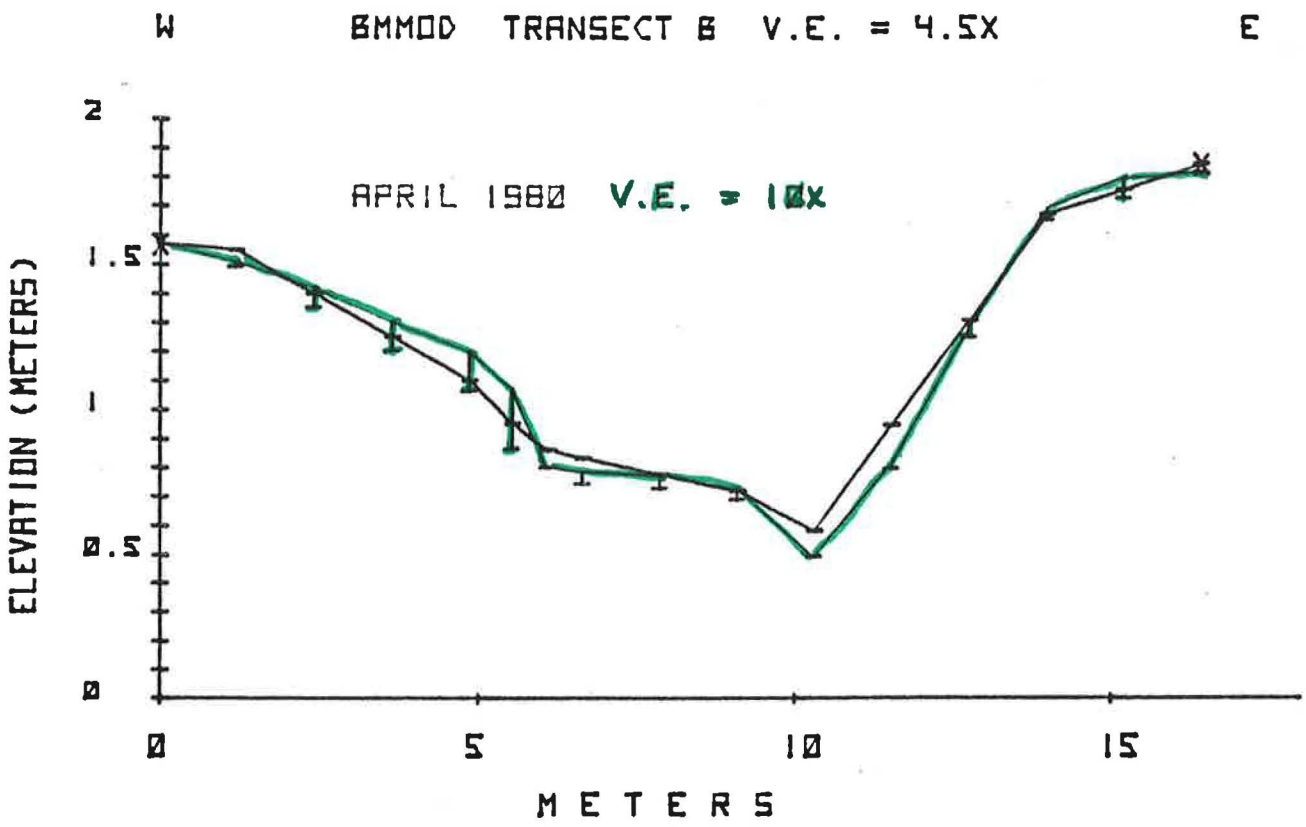


Figure 23: Topographic Profile and Change in Ground-Surface Elevation for Final Measurement of Erosion-Pin Transect B, BMMOD. Original Ground Surface Indicated in Black and Change in Ground-Surface Elevation Indicated in Green. See Text for Additional Information.

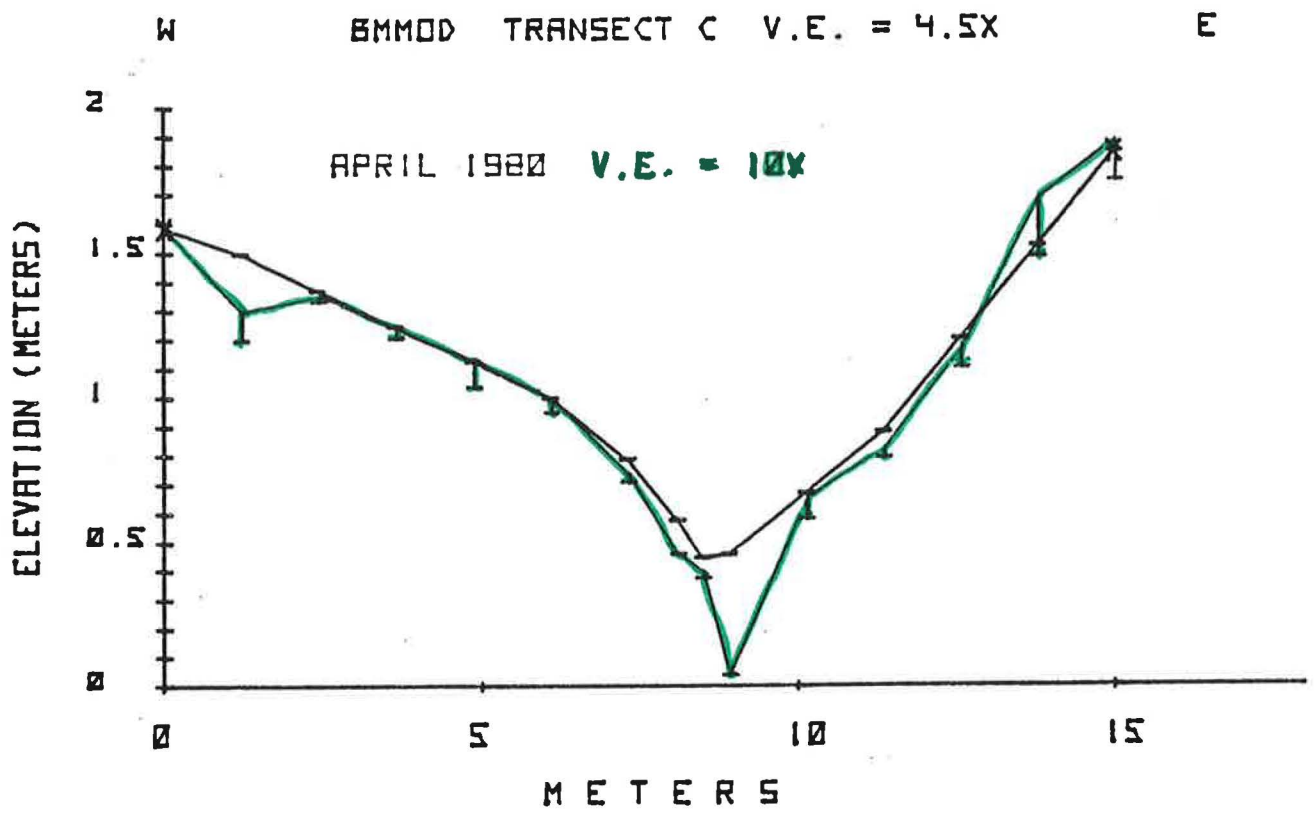


Figure 24: Topographic Profile and Change in Ground-Surface Elevation for Final Measurement of Erosion-Pin Transect C, BMMOD. Original Ground Surface Indicated in Black and Change in Ground-Surface Elevation Indicated in Green. See Text for Additional Information.

The green line represents the change in ground surface elevation relative to the datum (black line). The green line has an additional vertical exaggeration of 10 times to accentuate changes. The horizontal segments on the green line represent the maximum erosion and relative elevations of the washers on the pins at the time of measurement. Vertical line segments above the washer segments represent the amount of deposition on a given washer. The connecting green line segments represent the ground-surface expression at the time of measurement.

Profile segments which exhibit pronounced variations in lowering of ground-surface elevation from pin to pin are hillslope segments where rilling is the dominant erosive process (e.g., east and west ends of transect A, BMINT, Fig. 19; most of transect B, ASINT, Fig. 29). Profiles which exhibit fairly uniform lowering of ground-surface elevation from pin to pin are hillslopes where sheetwash is the dominant erosive process (e.g., transect A, BMMOD, Fig. 22; transect C, BMMOD, Fig. 24; transect B, ASMOD, Fig. 32). Pronounced gain from pin to pin along a given transect can arise from two different causes. The first is a result of a change in slope, from steep (> 10°) to shallow (< 10°), causing the deposition of debris in transit downslope (e.g., between 14 and 17 meters, transect B BMINT, Fig. 26). The second is the presence of post-fire needle cast trapping debris

in transit downslope (e.g., west end of transect B, BMMOD, Fig. 23; east end of transect A, ASMOD, Fig. 31; northeast end of transect A, ASLIGHT, Fig. 33).

Pronounced, singular peaks present on some profiles are the result of grass clumps trapping sediment (e.g., transect B, ASLIGHT, Fig. 34). The variations in ground surface elevation along the transects in BMLIGHT (Figs. 25, 26 and 27) are a result of the burrowing activity of gophers producing mounds and pits on the ground surface.

Appendix II contains the summaries of erosion-pin measurements for all study basins. The method of data reduction is explained in Appendix II. Table 4 is a summary of the data in Appendix II. The values in Table 4 represent the average annual change in ground-surface elevation ($\bar{\Delta}$/yr) per pin transect within each study basin. During the first year of study, all transects experienced a loss in ground-surface elevation. There were no distinct trends in erosion for the first year. However, the changes in ground-surface elevation within the intense-burn basins were greatest in the headwater and basin-mouth regions, a trend followed by nearly all basins during the second year following the fire. The magnitude of losses along the pin transects was the greatest during the second year. There was a net gain along nearly every pin transect during the third year.

Study Basin	Period	$\bar{\Delta}$/yr (mm)			
		TRANSECT			
		A	B	C	D
BMINT	9/77-6/78	-4.7	-2.7	-5.5	-
	6/78-6/79	-5.9	-4.1	-9.5	-
	6/79-4/80	+1.6	+2.6	+6.5	-
BMMOD	9/77-6/78	-2.4	-2.5	-0.7	-1.7
	6/78-6/79	-3.3	-2.2	-6.9	+7.9
	6/79-4/80	-0.5	+4.2	-2.2	-3.1
BMLIGHT	9/77-6/78	-4.3	-5.1	-4.3	-
	6/78-6/79	-5.7	-8.4	-8.9	-
	6/79-4/80	+5.3	+5.5	+7.7	-
ASINT	9/77-6/78	-3.5	-2.8	-4.3	-
	6/78-6/79	-3.4	-3.0	+2.7	-
	6/79-5/80	+4.6	+5.1	+0.5	-
ASMOD	9/77-6/78	-6.3	-2.5	-	-
	6/78-6/79	-4.6	-4.1	-	-
	6/79-5/80	+3.6	+1.4	-	-
ASLIGHT	10/77-6/78	-1.7	-4.8	-	-
	6/68-6/79	-6.7	-9.0	-	-
	6/79-5/80	+1.3	+5.1	-	-

Table 4. Average Annual Change in Ground-Surface Elevation ($\bar{\Delta}$/yr) per Transect for all Study Basins.

Erosion Grid Studies

Figures 35 through 37 are isopleth maps of the final measurements at the hillslope grid stations. The isopleths represent the changes in relief relative to the datum (taken November 1977) within the square meter at each grid station. Down gradient is toward the bottom of the page in all figures. The shading on the figures represents the areas of loss relative to the datum; gain is unpatterned. The erosion grids were not installed horizontally. Grid station B had an eight degree slope in the direction of the hillslope gradient and a one degree slope to the right side of the grid (looking upslope). Grid station C had a ten degree slope down gradient, a half degree slope to the right. Grid station D has a three degree slope down gradient, a half degree slope to the right. Burnt Mesa is the only area instrumented with the erosion grid, due to accessibility.

The isopleth pattern of these plots give an indication of the type of geomorphic processes operative within each grid station. The elongate trough and mound pattern of grid B (Fig. 36) suggests the cutting of rills

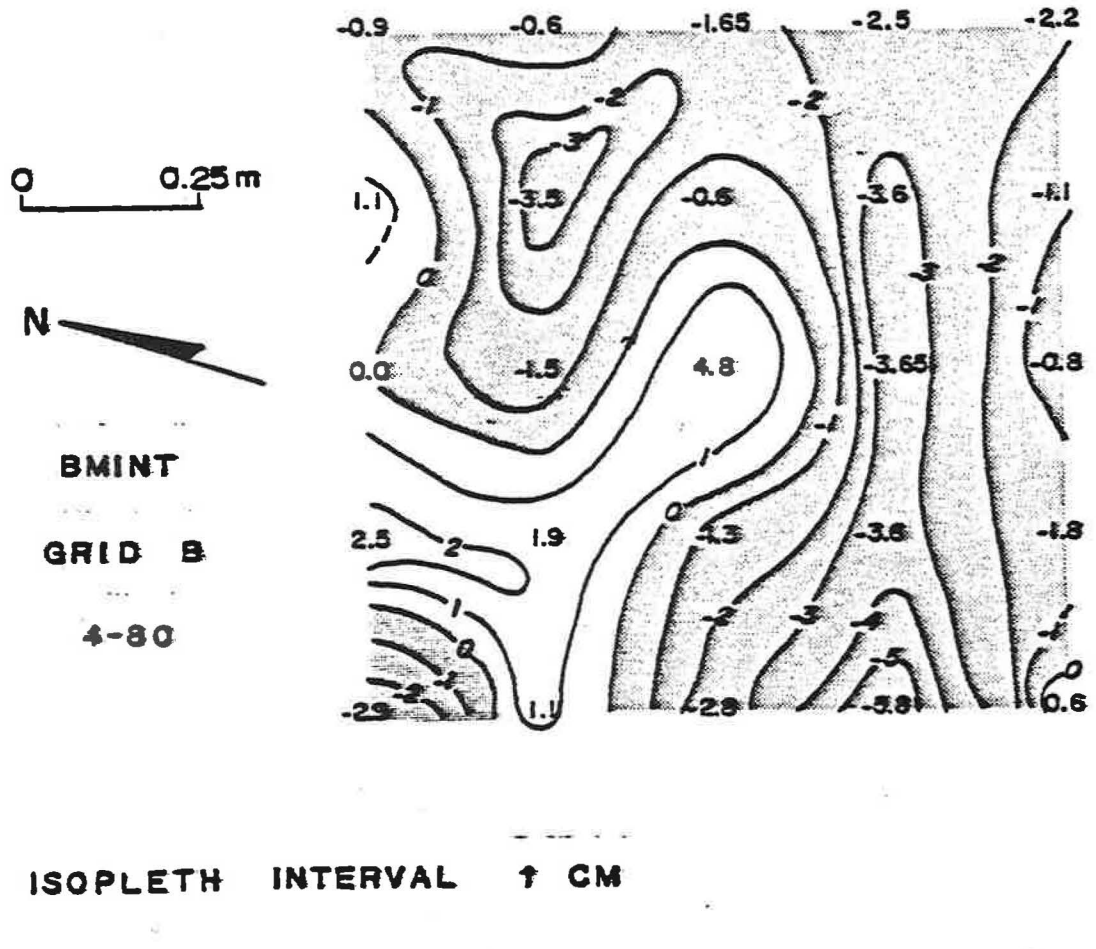


Figure 35: Net Change in Ground-Surface Elevation at Grid Station B, BMINT, April 1980. Shaded Areas Represent Erosion and Unshaded Areas Indicate Deposition.

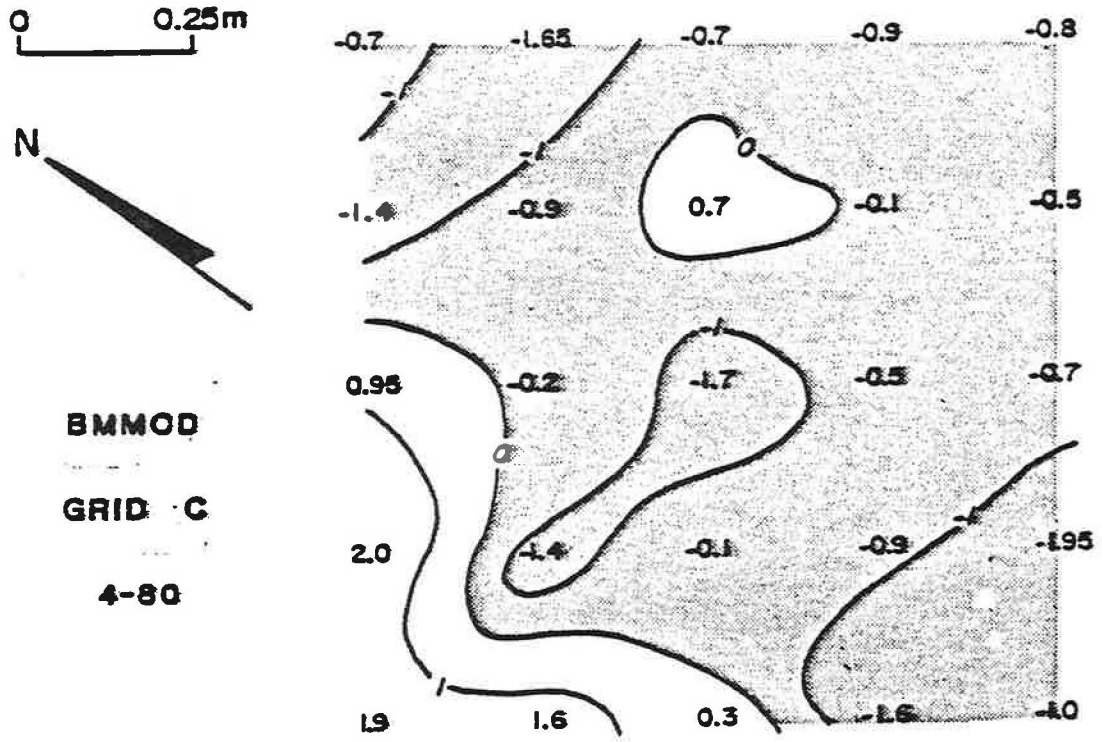


Figure 36: Net Change in Ground-Surface Elevation at Grid Station C, BMMOD, April 1980. Shaded Areas Represent Erosion and Unshaded Areas Indicate Deposition.

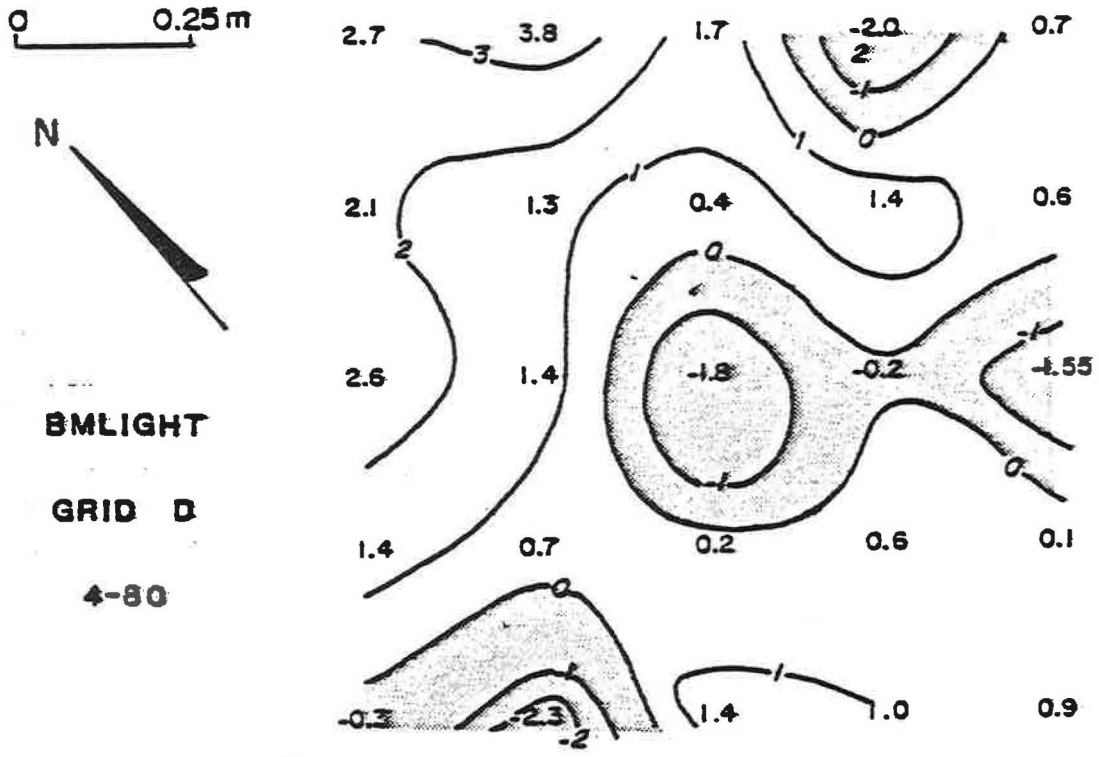


Figure 37: Net Change in Ground-Surface Elevation of Grid Station D, BMLIGHT, April 1980. Shaded Shaded Areas Represent Erosion and Unshaded Areas Indicate Deposition.

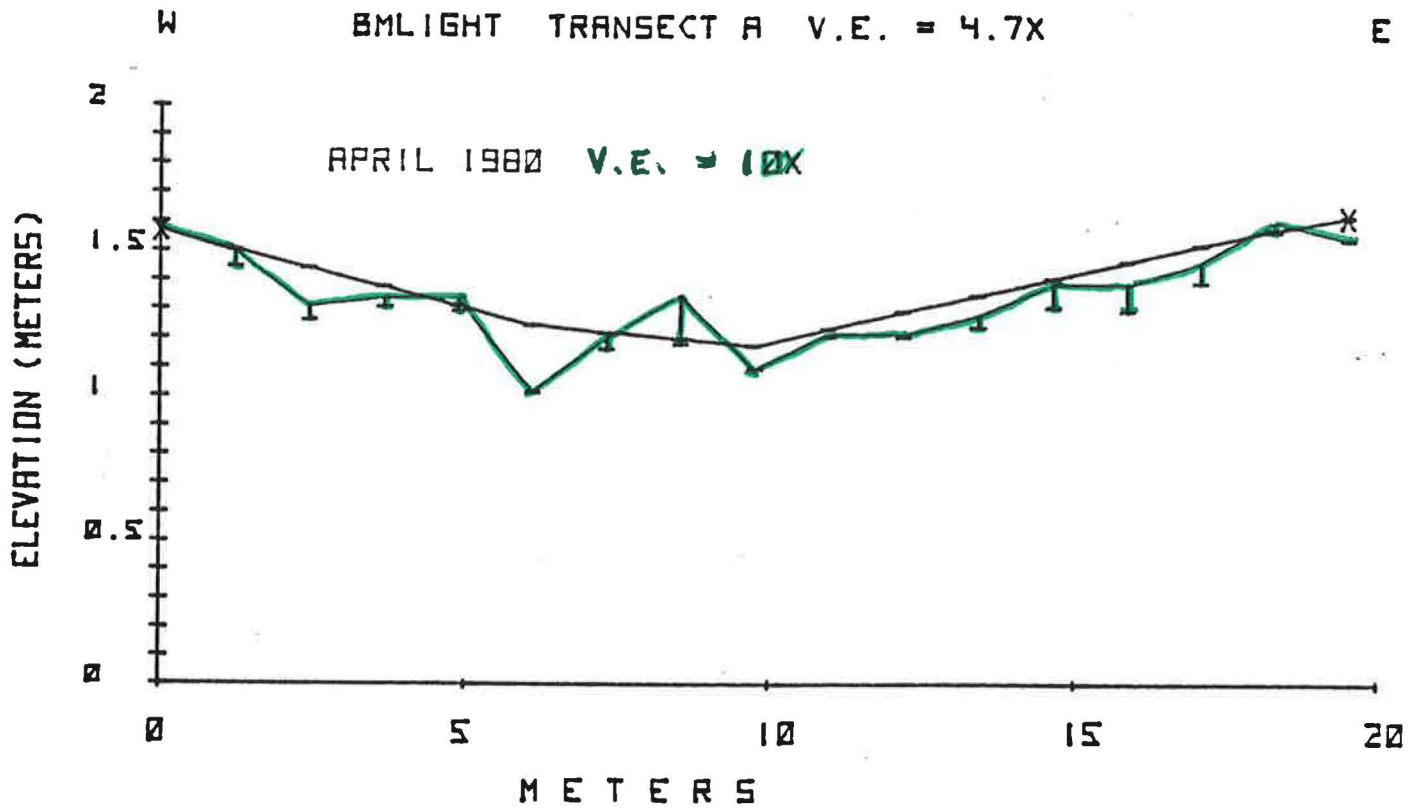


Figure 25: Topographic Profile and Change in Ground-Surface Elevation for Final Measurement of Erosion-Pin Transect A, BMLIGHT. Original Ground Surface Indicated in Black and Change in Ground-Surface Elevation Indicated in Green. See Text for Additional Information.

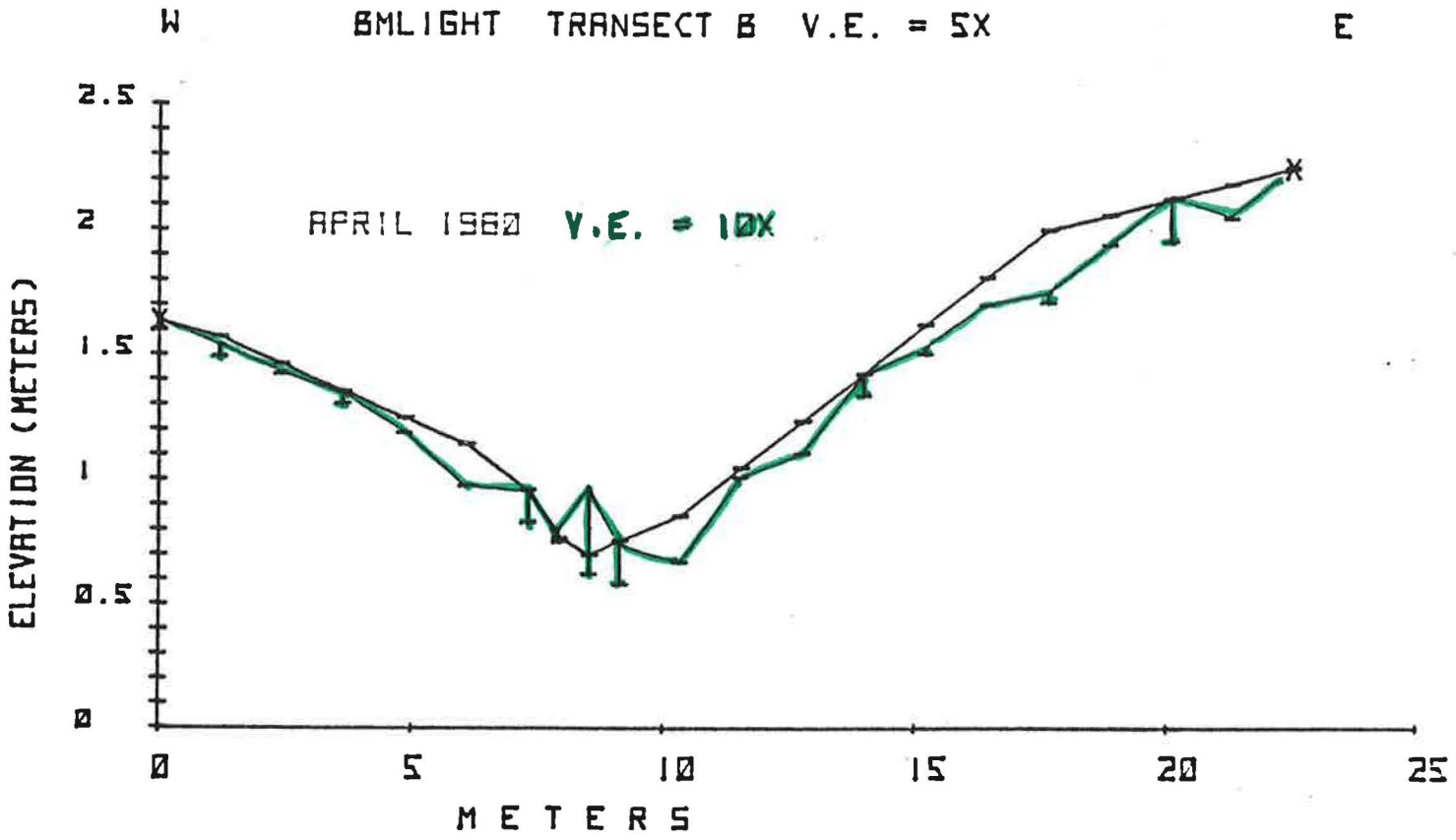


Figure 26: Topographic Profile and Change in Ground-Surface Elevation for Final Measurement of Erosion-Pin Transect B, BMLIGHT. Original Ground Surface Indicated in Black and Change in Ground-Surface Elevation Indicated in Green. See Text for Additional Information.

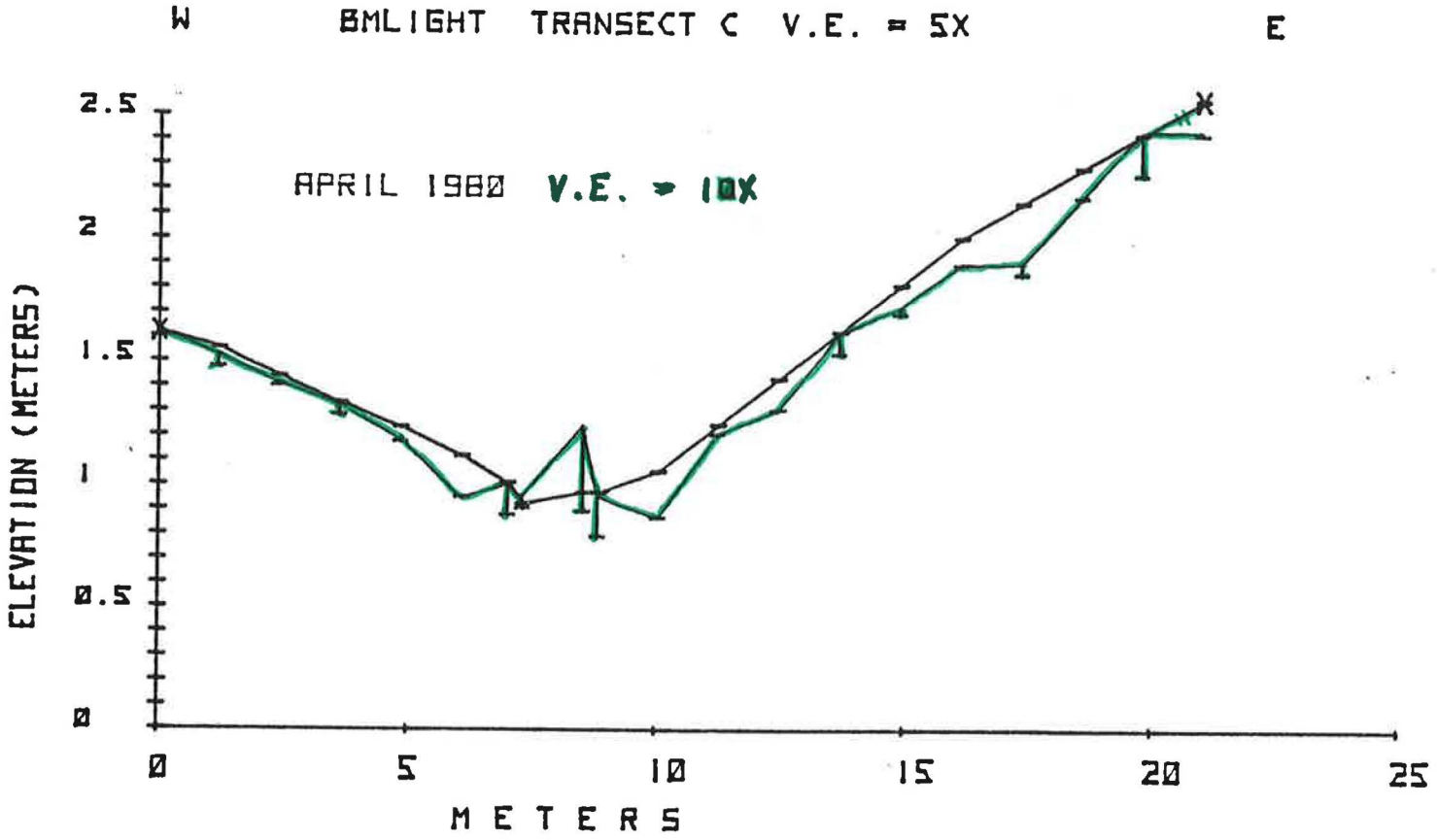


Figure 27: Topographic Profile and Change in Ground-Surface Elevation for Final Measurement of Erosion-Pin Transect C, BMLIGHT. Original Ground Surface Indicated in Black and Change in Ground-Surface Elevation Indicated in Green. See Text for Additional Information.

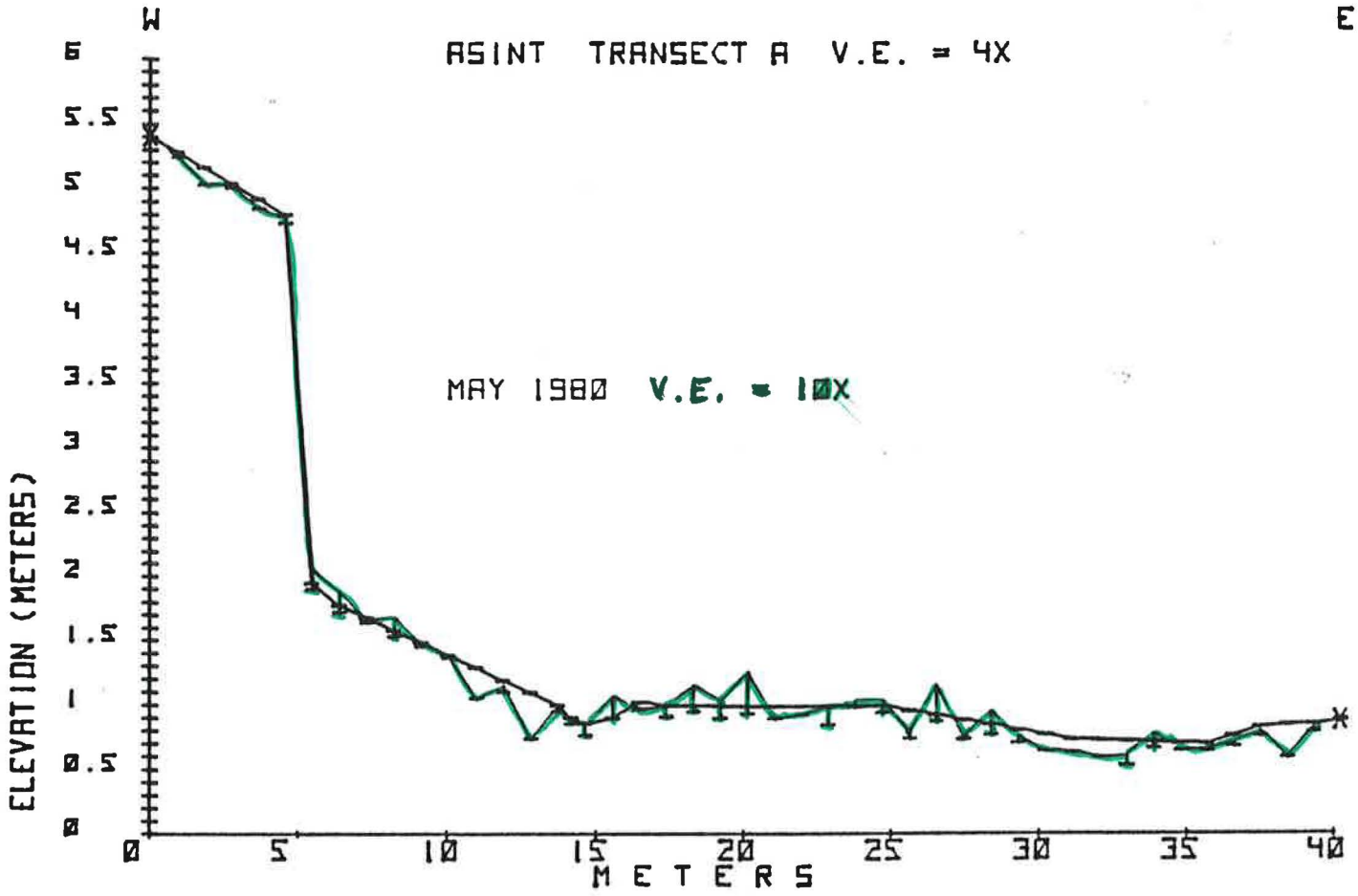


Figure 28: Topographic Profile and Change in Ground-Surface Elevation for Final Measurement of Erosion-Pin Transect A, ASINT. Original Ground Surface Indicated in Black and Change in Ground-Surface Elevation Indicated in Green. See Text for Additional Information.

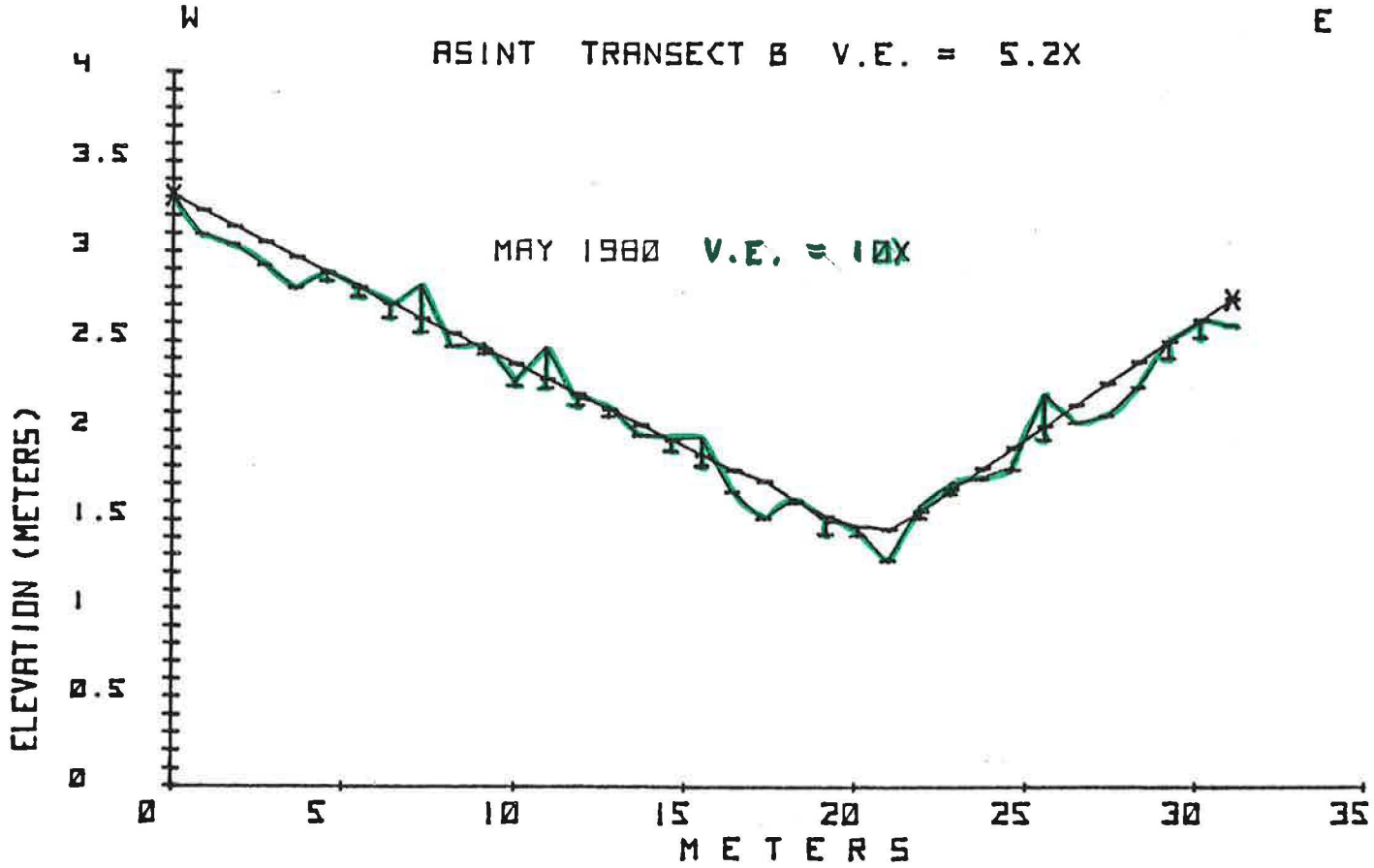


Figure 29: Topographic Profile and Change in Ground-Surface Elevation for Final Measurement of Erosion-Pin Transect B, ASINT. Original Ground Surface Indicated in Black and Change in Ground-Surface Elevation Indicated in Green. See Text for Additional Information.

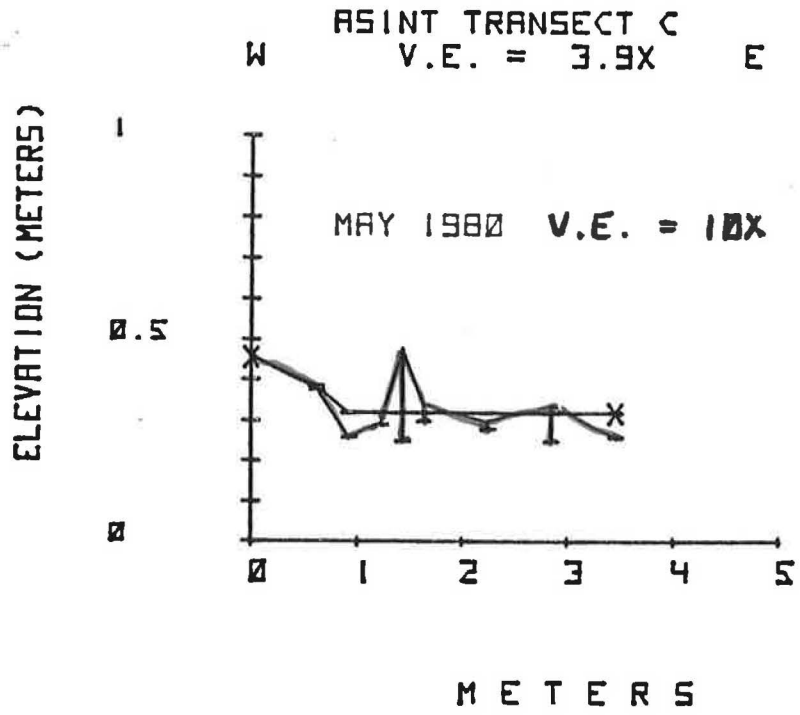


Figure 30: Topographic Profile and Change in Ground-Surface Elevation for Final Measurement of Erosion-Pin Transect C, ASINT. Original Ground Surface Indicated in Black and Change in Ground-Surface Elevation Indicated in Green. See Text for Additional Information.

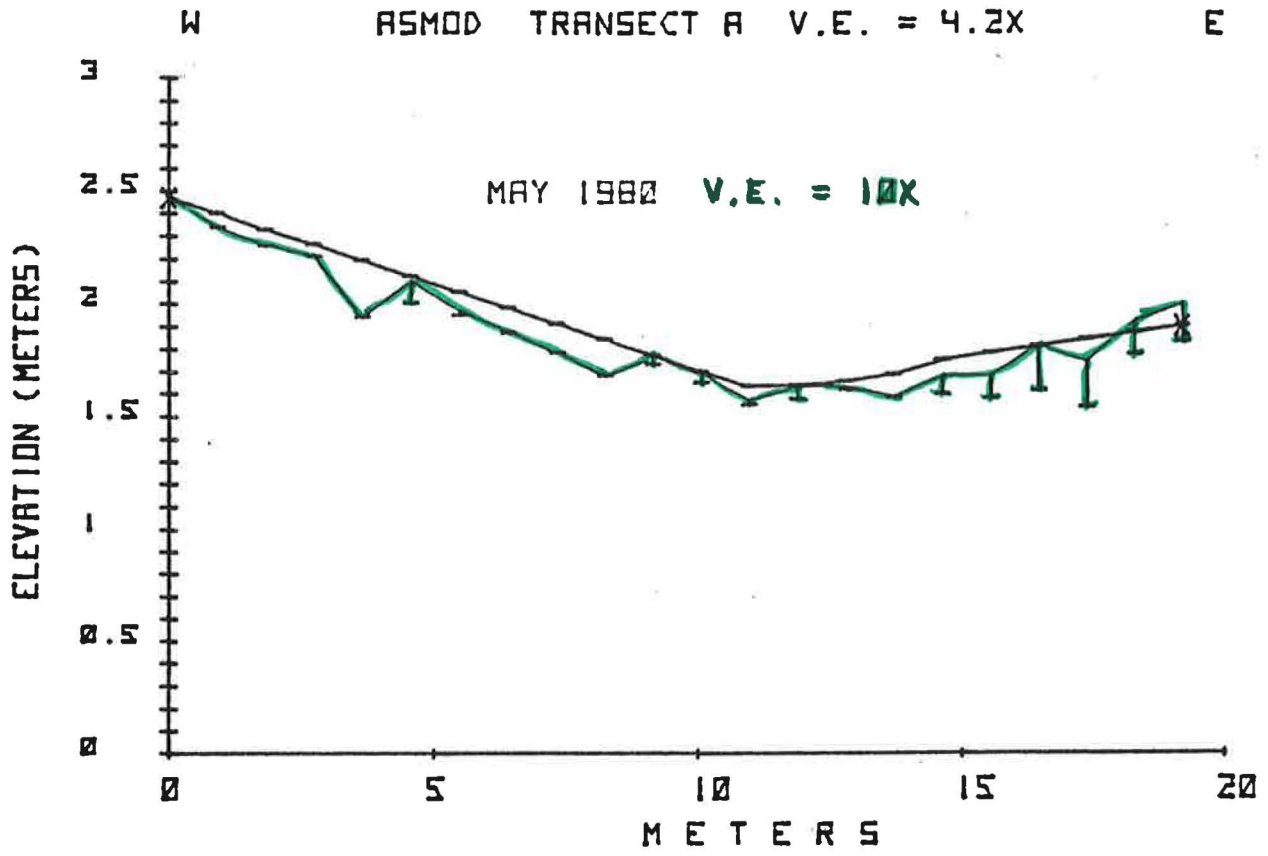


Figure 31: Topographic Profile and Change in Ground-Surface Elevation for Final Measurement of Erosion-Pin Transect A, ASMOD. Original Ground Surface Indicated in Black and Change in Ground-Surface Elevation Indicated in Green. See Text for Additional Information.

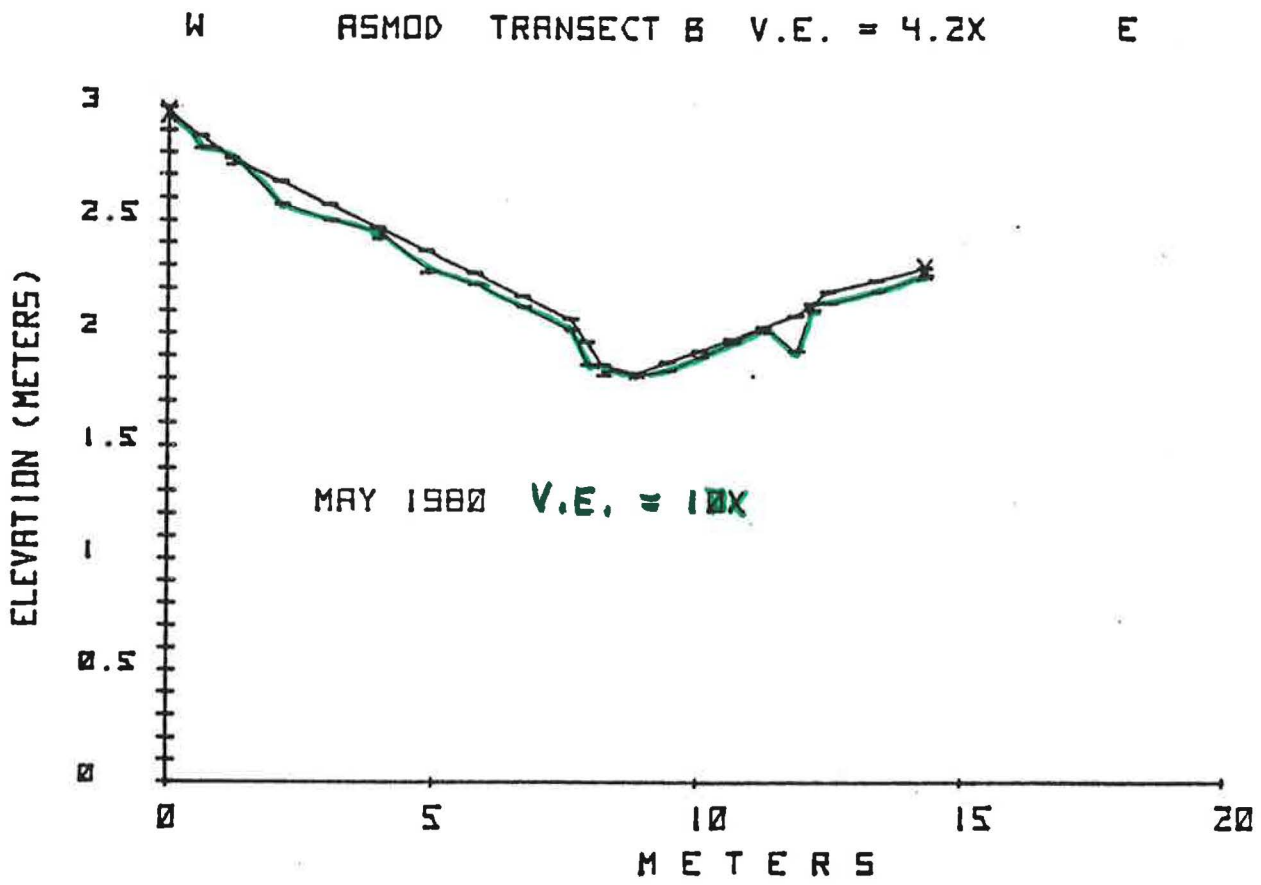


Figure 32: Topographic Profile and Change in Ground-Surface Elevation for Final Measurement of Erosion-Pin Transect B, ASMOD. Original Ground Surface Indicated in Black and Change in Ground-Surface Elevation Indicated in Green. See Text for Additional Information.

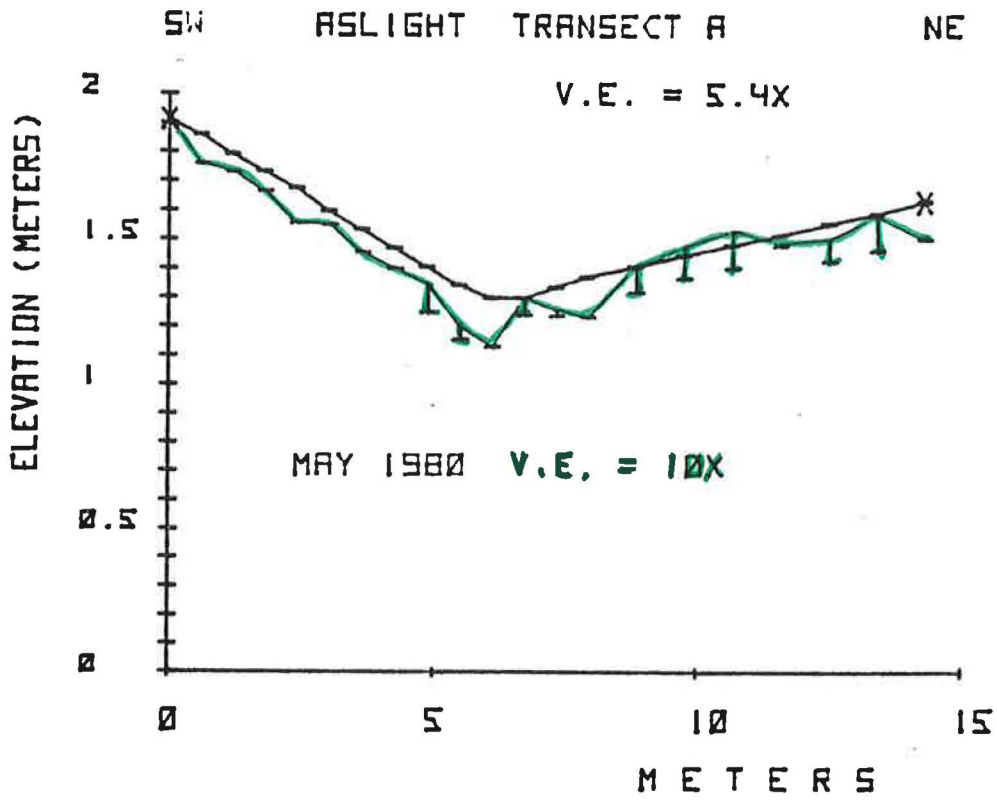


Figure 33: Topographic Profile and Change in Ground-Surface Elevation for Final Measurement of Erosion-Pin Transect A, ASLIGHT. Original Ground Surface Indicated in Black and Change in Ground-Surface Elevation Indicated in Green. See Text for Additional Information.

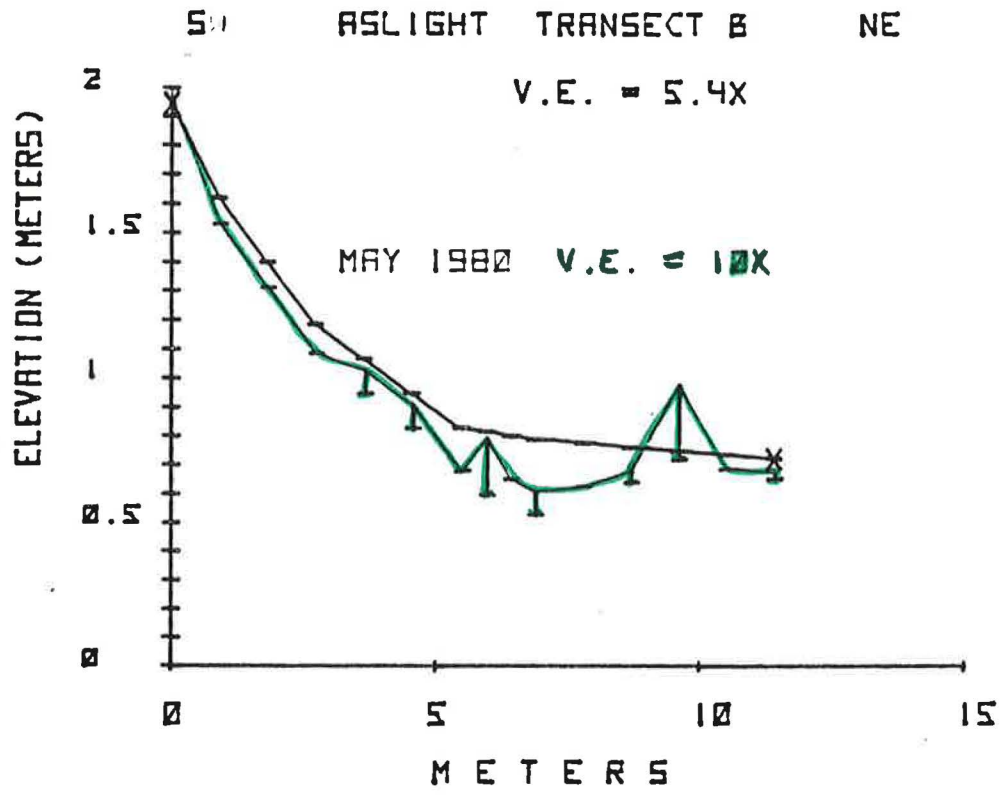


Figure 34: Topographic Profile and Change in Ground-Surface Elevation for Final Measurement of Erosion-Pin Transect B, ASLIGHT. Original Ground Surface Indicated in Black and Change in Ground-Surface Elevation Indicated in Green. See Text for Additional Information.

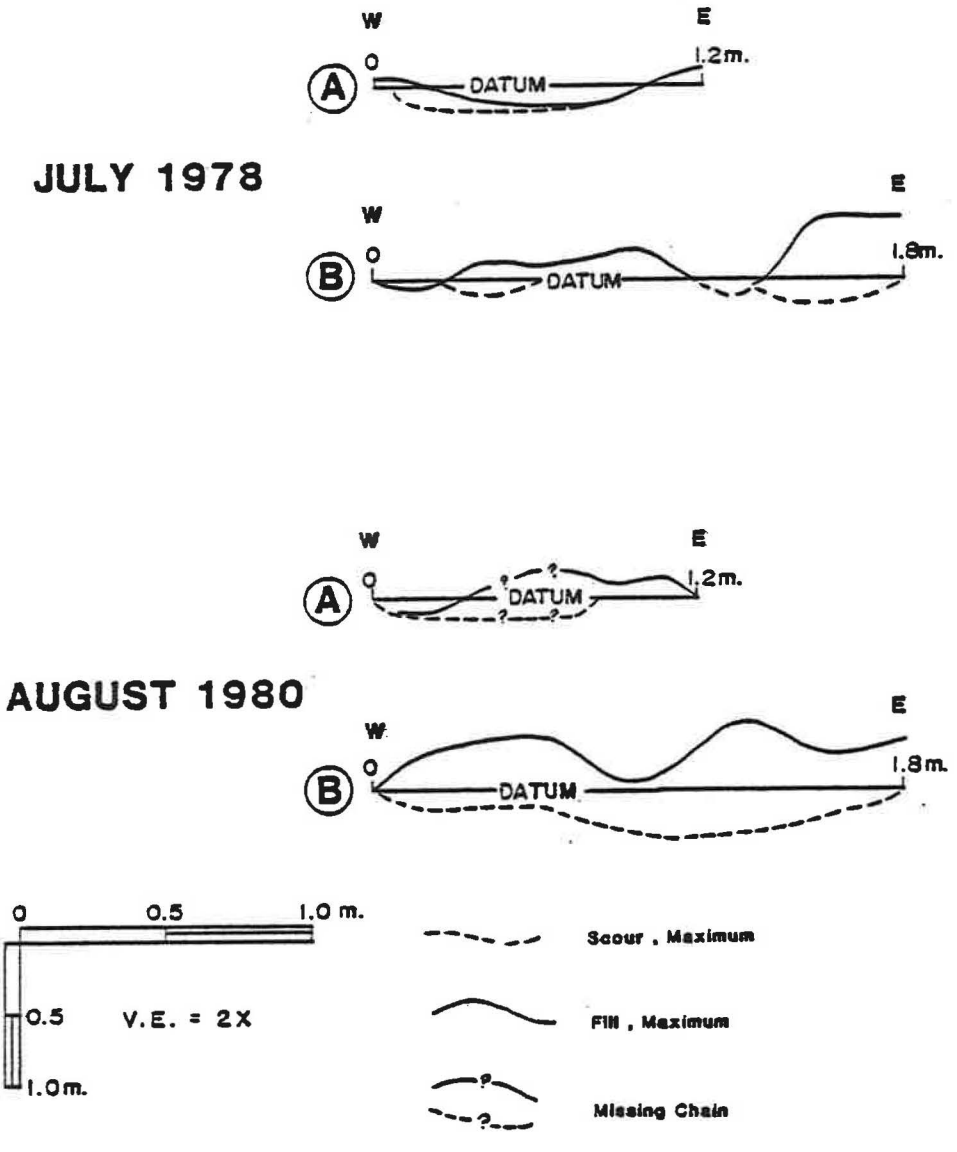


Figure 40: Changes in Channel Bed Elevation by Cutting and Filling, ASINT. See Figure 16 for Transect Locations.

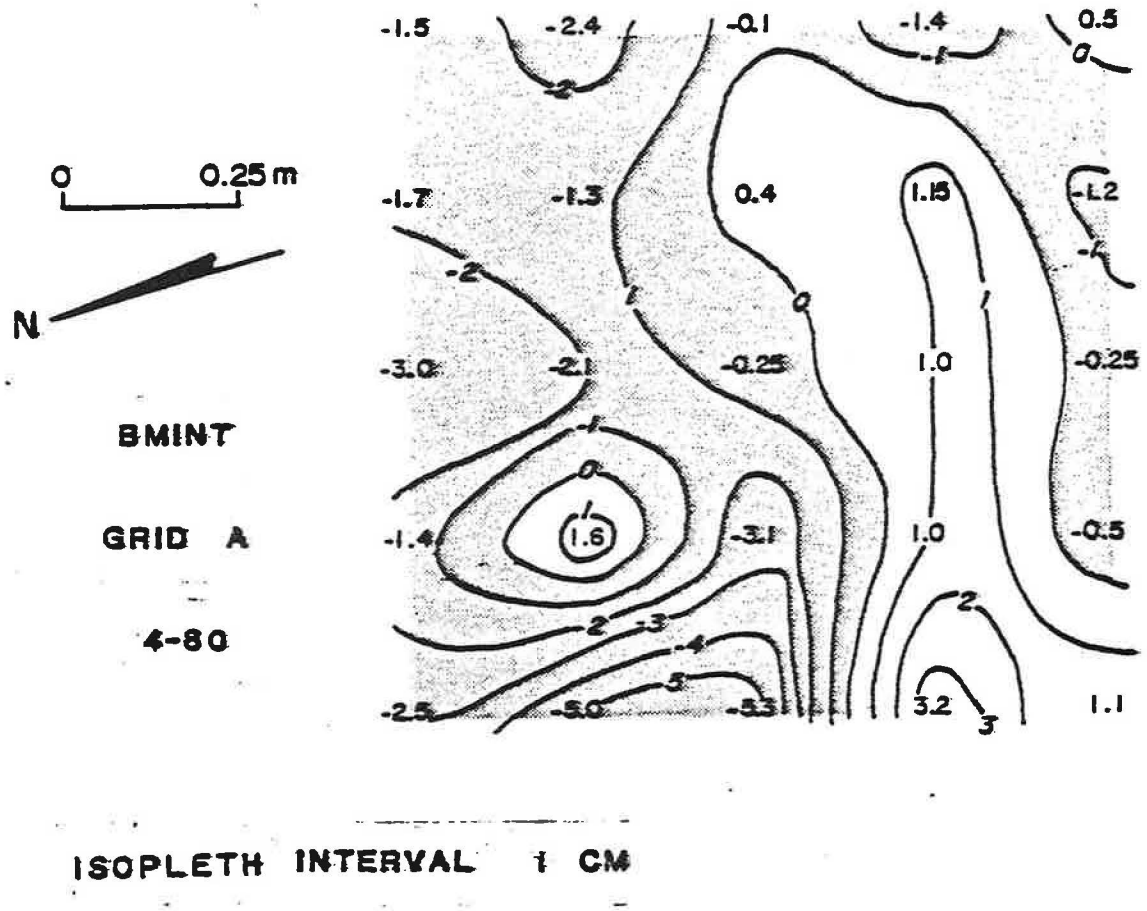
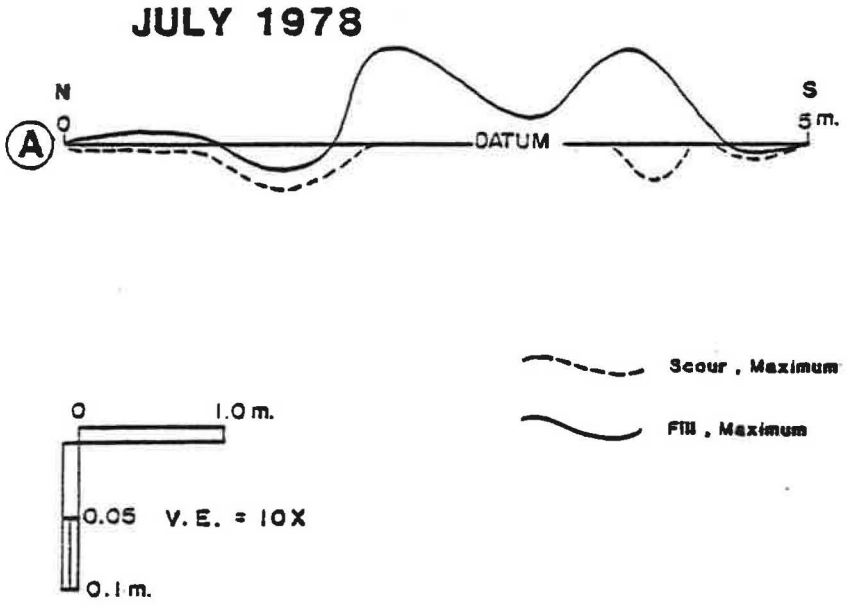


Figure 41: Net Change in Ground-Surface Elevation at Grid Station A, BMINT, April 1980. Shaded Areas Represent Erosion and Unshaded Areas Indicate Deposition.

Areas of gain (unshaded) represent the temporary storage of sediment on small steps of bedrock adjacent to and within the channel.

Figure 42 is a profile of the chain transect installed within the axial drainage below the confluence of the BMINT and BMMOD study basins. The chain transect is located between the rebar stakes at the margins of the channel shown in Figure 43. Cut and fill of the bar at the southern end of the chain transect indicates the intermittent storage and transportation of sediment (Fig. 42).

The ephemeral channel draining the BMMOD and BMINT study basins had already experienced aggradation at the time of instrumentation, three months following the La Mesa fire. A cross section measured in a trench at a constricted segment of the channel in September of 1977 revealed a heterogeneous deposit 15 cm thick of pumice and crystal fragments with ash particles (Fig. 44A). A cross section measured at a trench in the widest segment of this channel in May of 1980 revealed a stratigraphic layering of debris deposited following the La Mesa fire (Fig. 44B corresponds to Fig. 43). The first layer above the burn layer was comprised of fine gravel to coarse sand and ash. The second layer, which comprised the bulk of the bar represented in Figure 42, was a fine to medium sand. The bar was stabilized in May of 1980 by grasses



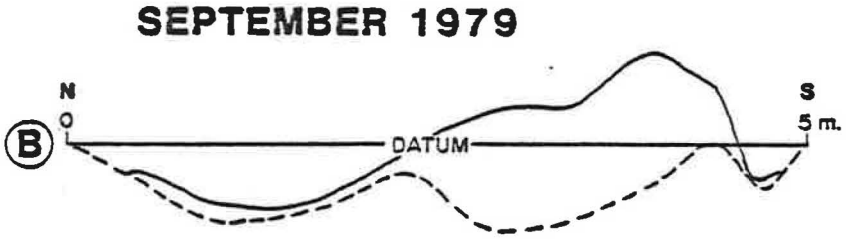


Figure 42: Changes in Channel Bed Elevation by Cutting and Filling, ASINT. See Figure 16 for Transect Locations.

(trough) and the filling of other rills by the regrowth of grasses (mound, center and lower left-center). Grid B occupies a steep side slope in the headwaters of BMINT (Fig. 8). The open contour pattern of Figure 36 is a result of sheetwash uniformly removing debris from the shoulder slope station of grid C, BMMOD (Fig. 11). The pit and sinuous, low-relief mound pattern of Figure 37 suggests sheetwash erosion on the vegetated, shallow gradient side slope (< 10°) station of grid D, BMLIGHT (Fig. 12). Raindrop impact was observed to splash debris out of bare spots (pits), with some debris being trapped by grasses (sinuous mound pattern).

Table 5 is a summary of the erosion-grid measurements in Appendix III for the grid stations within the Burnt Mesa study area. The tables in Appendix III were generated in the same manner as the erosion-pin tabulations. The 25 measurement points over each grid station were divided into the net change (Net Δ) to arrive at an average change (avg. Δ) in ground surface elevation for each station (Appendix III).

The values in Table 5 represent the average annual change in ground-surface elevation ($\bar{\Delta}$/yr) over the square meter of each grid station. There is gain or no change for the first annual period for the hillslope grid stations (B, C, D, Table 5). The second annual period shows the greatest changes (loss and gain), as did the erosion-pin transects (Table 4). Grid D (Figs. 37 and 12) exhibits gain during

	$\bar{\Delta}$/yr (mm)			
Study Basin	BMINT		BMMOD	BMLIGHT
Grid Station	A	B	C	D
11/77 - 6/78	+1.9	+5.3	+8.4	0.0
6/78 - 6/79	-7.1	-13.5	-7.0	+6.3
6/79 - 4/80	-3.8	-1.3	-7.2	+0.5

Table 5. Average Annual Change in Ground Surface Elevation ($\bar{\Delta}$/yr) per Grid Station for the Burnt Mesa Area.

the second two years. This condition may largely be attributable to station D's location on a vegetated, shallow slope (< 10°). Stations B and C (Figs. 35, 8, 36 and 11) are situated on devegetated slopes of 10° or greater. Station A, BMINT, is a grid station situated over an ephemeral channel. Although the data for grid station A are included in Table 5, the station is described in the following discussion related to stream channels.

Channel Instrumentation, Morphology, and Stratigraphy

In addition to the erosion-pin transects which cross the drainage lines within each study basin, ephemeral streams were instrumented with erosion-chain transects. Chain transects were installed only in the intense-burn basins of each study area. Figure 39 through 40 are graphic representations of erosion-chain masurements (changes in channel bed elevation with time) within the BMINT and ASINT study basins, respectfully.

The first-order channels of the lower elevation study area (BMINT, Figs. 38 and 39) exhibit scouring in the headmost channel segments (transects B and C, see Fig. 8 for transect locations). Bar deposition occurs in wide channel segments (transect D, Fig. 38 and 39). The first-order channels of the upper elevation study area (ASINT, Fig. 40) exhibit net filling (see Fig. 14 for transect locations).

Figure 41 is a isopleth map of the final measurement at the erosion grid station A. Grid station A straddles a first-order channel segment in the headwaters of BMINT Fig. 8). Down gradient is toward the bottom of the page.

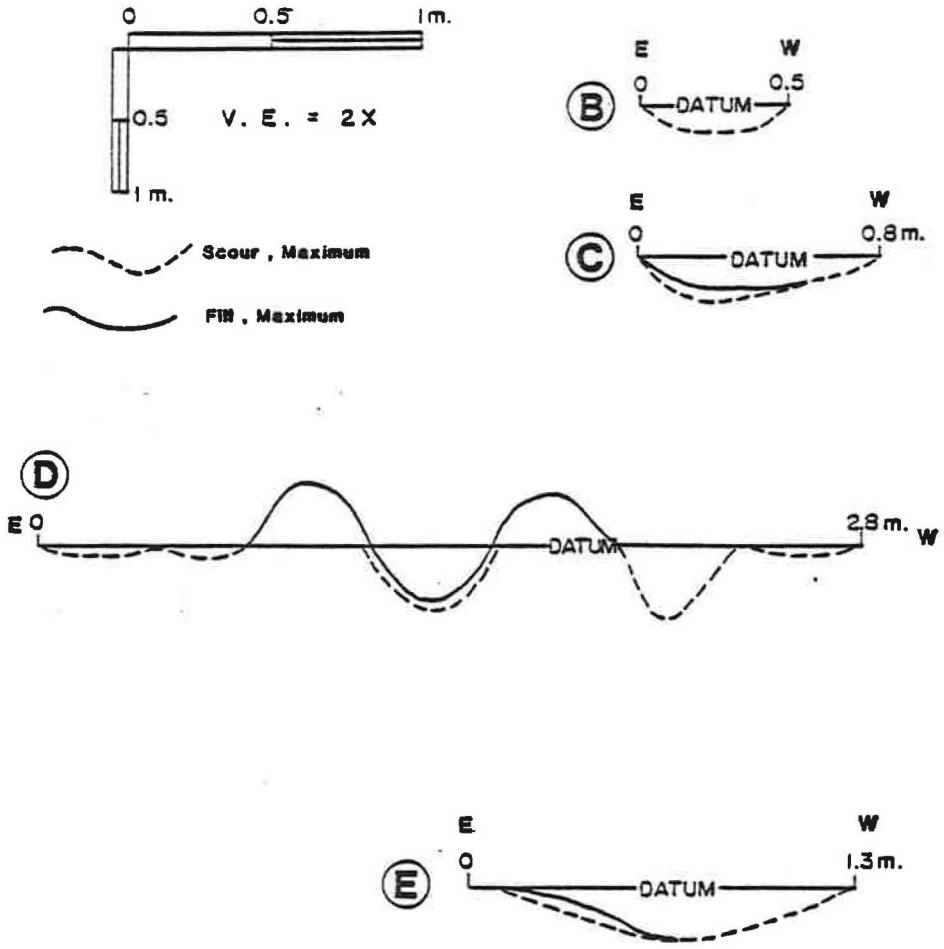


Figure 38: Changes in Channel Bed Elevation by Cutting and Filling, BMINT, July 1978. See Figure 10 for Transect Locations.

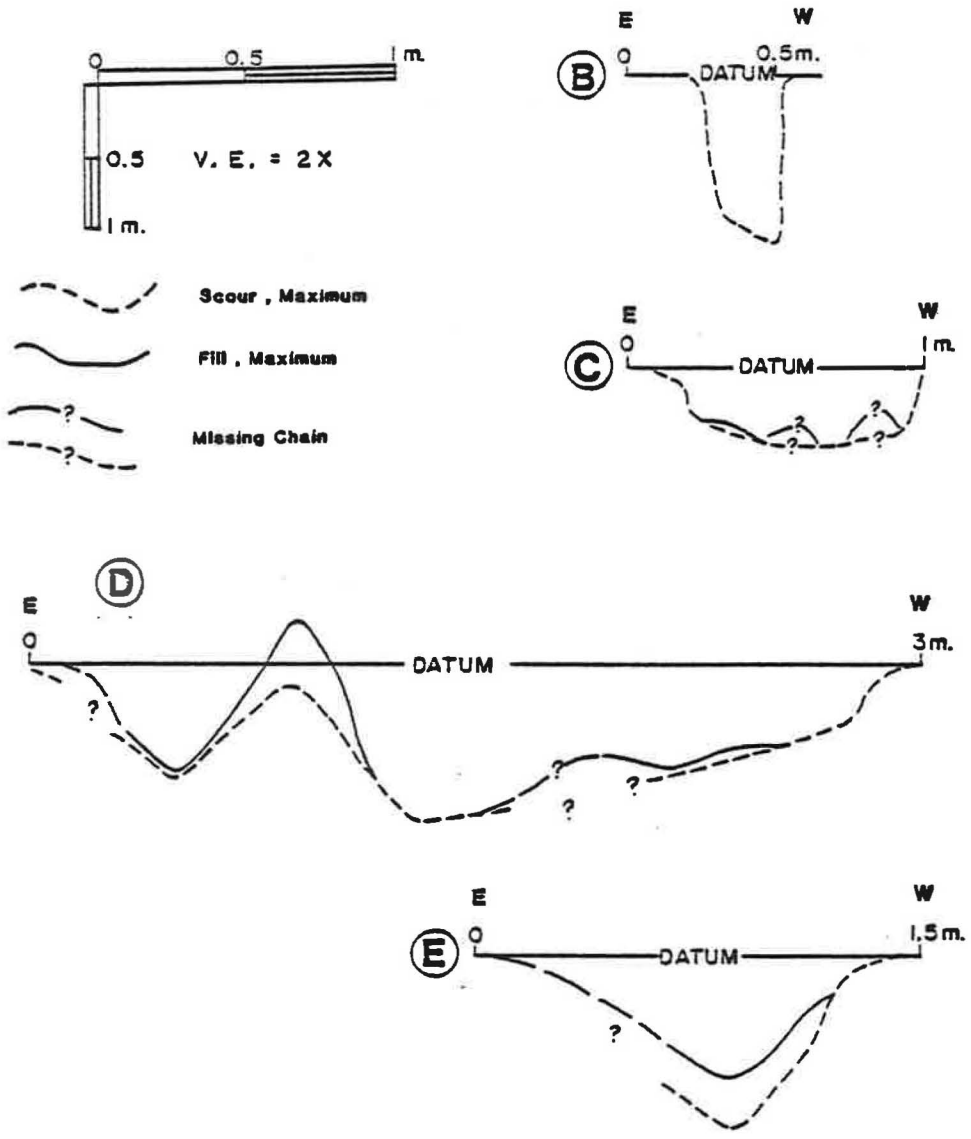


Figure 39: Changes in Channel Bed Elevation by Cutting and Filling, BMINT, September 1980. See Figure 10 for Transect Locations.



Figure 43: Post-Burn Channel Aggradation in the Axial Drainage Below BMMOD and BMINT Study Basins. Chain Transect of Figure 42 is Located Across Channel.

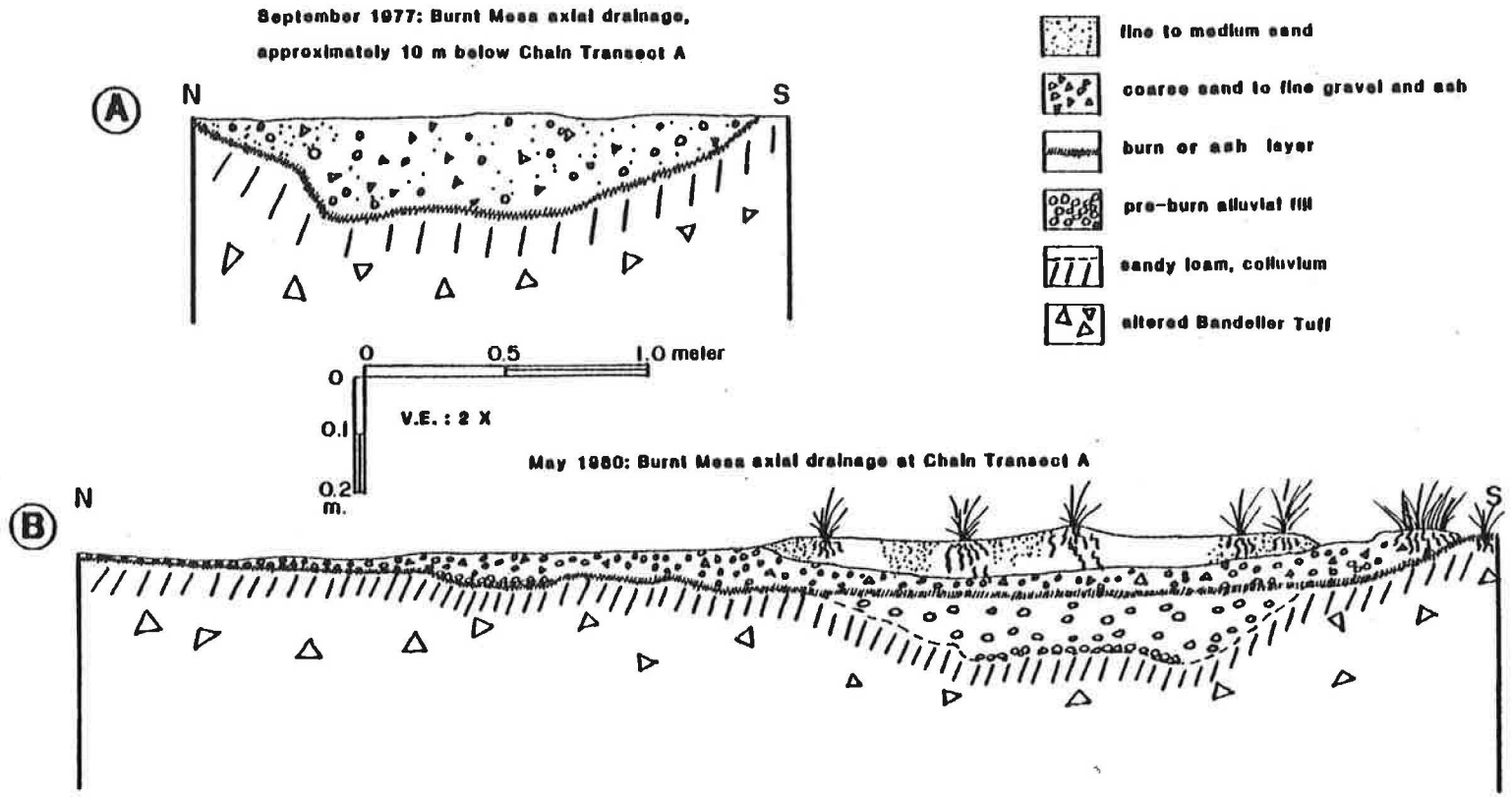


Figure 44 : Sketches of Channel Fill Deposits and Channel Cross Sections in the Burnt Mesa Axial Drainage.

which were rooted in the second layer of fine to medium sand. The pre-burn channel occupied the southern end of the cross section in Figure 44B. The southern end of the cross section received the thickest accumulation of post-fire detritus which diverted the active post-burn channel to the north.

Figure 45A through 45C are cross-sectional profiles of the probable maximum flood along the axial ephemeral canyon which drains sections of the upper and lower mesa-top catchments. Width and depth measurements were based upon the level of flood debris (ash and pine needles) on one or both banks. Figure 45A is the profile of the tributary reach draining the ASINT and ASMOD study basins. This tributary is a trunk drainage of the upper elevation study area. Figure 45B is the profile of the ephemeral canyon just below the confluence of the Burnt Mesa tributary reach and the main stem, and is approximately 3 km downstream of Figure 45A. Figure 45C is a constricted reach of the axial ephemeral canyon, approximately 1.5 km downstream of Figure 45B. The channel bed of this constricted section was found to have accumulated gravel 2 to 20 cm thick since the La Mesa fire. The sediment in this constricted reach probably represents an excess of sediment load deposited during the waning stages of a flood event.

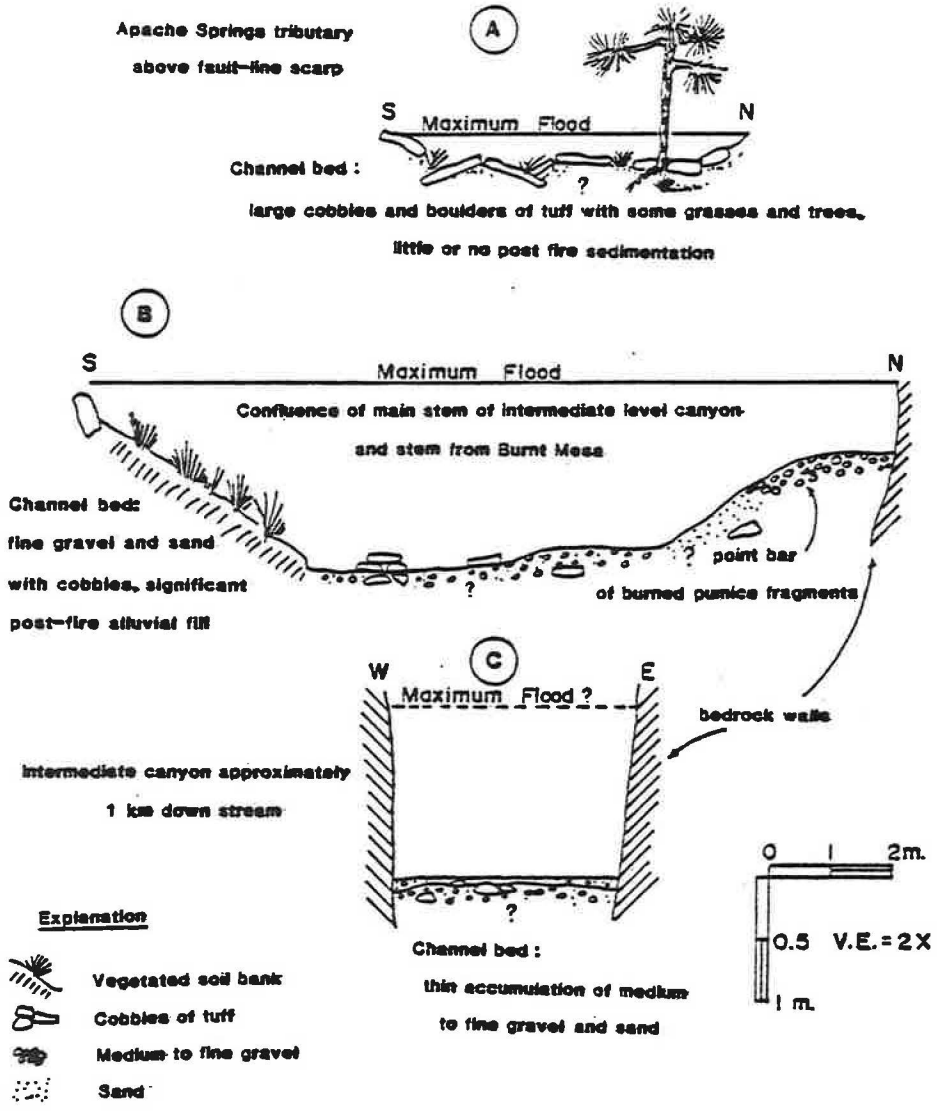


Figure 45: Three Cross-Sectional Profiles of Trunk, Mesa-Top Ephemeral Canyon Showing the Probable Maximum Flood. Figure 45C Corresponds to Figure 70.

Table 6 is a summary of slope-area discharge calculations for the Burnt Mesa study basins. The calculations are based upon high-flow marks on the ephemeral channel banks following runoff events. The July 1978 event resulted from a heavy thunderstorm one day previous to the field visit. The May 1979 event was apparently a much less intense shower, relative to the 1978 event. It should be noted, however, that the channel morphology of the 1979 event suggests that a large runoff event likely occurred before the mid-May event. No discernible flow marks could be found in the BMLIGHT study basin for the 1979 runoff event (Table 6). Runoff in the study basins of the Burnt Mesa area was found to be greatest from the intense-burn basin and least from the light-burn basin. This fact suggests that the amount of devegetation (i.e., burn intensity) influences the amount of runoff generated from a given thunderstorm event.

Light Burn	Moderate Burn		Intense Burn	
Area = 1426.0 m^2	Area = 813.8 m^2		Area = 4116.5 m^2	
Basin Mouth	**Lower Basin**		**Basin Mouth**	
7-4-78	**7-4-78**	**5-17-79**	**7-4-78**	**5-17-79**
S = 0.072	S = 0.130	0.013	S = 0.045	0.056
R = 0.087	R = 0.089	0.040	R = 0.131	0.031
n = 0.035	n = 0.028	0.028	n = 0.020	0.020
A = 0.107	A = 0.163	0.068	A = 0.770	0.088
V = 2.649	V = 4.494	0.880	V = 4.668	2.193
Q = 0.283	Q = 0.732	0.060	Q = 3.594	0.193
(=$8.0 \times 10^{-3} m^3$/sec)	(=$2.1 \times 10^{-2} m^3$/sec)	($1.7 \times 10^{3} m^3$/sec)	(=$1.0 \times 10^{-1} m^3$/sec)	($5.5 \times 10^{3} m^3$/sec)
	Mid Basin		**Mid Basin**	
	7-4-78		**7-4-78**	
	S = 0.128		S = 0.084	
	R = 0.083		R = 0.185	
	n = 0.028		n = 0.020	
	A = 0.135		A = 0.459	
	V = 4.276		V = 8.097	
	Q = 0.577		Q = 3.716	
	(=$1.6 \times 10^{2} m^3$/sec)		(=$1.0 \times 10^{-1} m^3$/sec)	

Q = discharge (cfs)
A = area (ft^2)
V = velocity (ft/sec)
R = hydraulic radius (ft)
S = slope (ft/ft)
n = roughness value

TABLE 6: Discharge Calculations of Runoff Events by the Slope-Area Method, Burnt Mesa Study Area.

Precipitation

The available records of precipitation during the course of this study are presented in Figure 46. Precipitation was greatest during the first year following the La Mesa fire (August 1977 through August 1978). Snowfall was greater during this period than during the second year (September 1978 through September 1979). The periods of greatest rainfall occur during the late spring and late summer seasons of both years. The post-burn average annual precipitation for 1977 was below the 10 year (1968 through 1978) annual average (F. Patton, personal communication, 1981). Figure 46 shows that the annual precipitation for 1978, 1979 and early 1980 are also below or near the average annual precipitation for the ten year period. However, the summer precipitation (July and August) of 1977 and 1978 was slightly above the normal amount of precipitation for that season for the 10 year record (F. Patton, personal communication, 1981).

The annual precipitation was similar during the pre- and post-burn periods. Changes in runoff and sediment yield of the Frijoles Canyon watershed after the La Mesa fire are not due to abnormal or large changes in average annual precipitation.

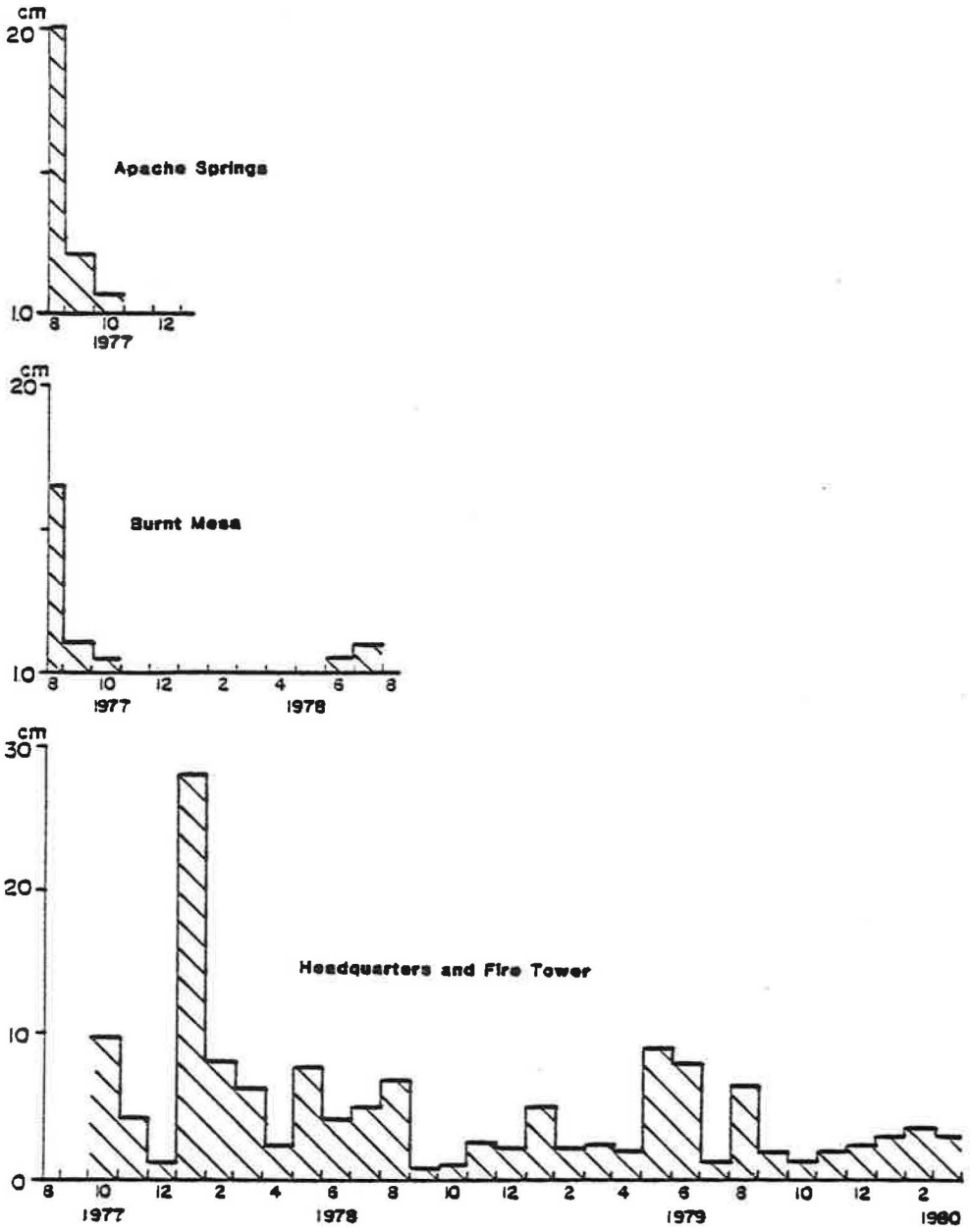


Figure 46: Monthly Precipitation Records Within Bandelier National Monument at Those Recording Stations Operative Following the La Mesa Fire. 1 Corresponds to January, 12 Corresponds to December.

Geomorphic Mapping

Plate 1 is a landform map (scale = 1:12,672) of the lower portion of the Frijoles Canyon watershed. The map was prepared using aerial photographs (1:6000) obtained from the National Park Service. Three landform units are identified: (1) The Frijoles Canyon walls, (2) the canyon floor, and (3) the mesas. Components of each landform unit are defined according to degree of slope, amount of vegetational cover, and the size of material comprising the slopes. The dominant components of the canyon wall, canyon floor, and the mesa units are the benched canyon wall, floodplain, and the gently sloping mesa tops, respectively. The map units reflect the type of geomorphic processes responsible for a given landform expression. The canyon wall map units (CW1 through CW4 of Plate 1) are formed by mass wasting processes such as rock fall and landslides. The canyon floor map units (CF1 and CF2 of Plate 1) are a result of fluvial erosion and deposition. The mesa map units are formed by a combination of mass wasting processes (creep, overland flow, rockfall; M1 and M2 of Plate 1)and fluvial processes

(ephemeral streamflow; M3 of Plate 1). The mesa map units comprise approximately 80 percent of the map area (M1 ≅ 64 percent, M2 ≅ 10 percent, M3 ≅ 6 percent). Canyon wall map units comprise approximately 15 percent of the area (CW 1 ≅ 4 percent, CW2 ≅ 5 percent, CW3 ≅ 7 percent, CW4 ≅ 1 percent). Canyon floor map units comprise approximately 5 percent of the area (CF1 ≅ 1 percent, CF2 ≅ 4 percent).

The La Mesa fire occurred mainly within the components of the mesa unit. The fire spilled over the mesa unit and burned only restricted portions of the canyon walls and canyon floors. The Burnt Mesa study basins have developed on the gently sloping mesa-top component of the mesa unit (M1).

Morphometric Analysis

There are two general physiographic units of the Frijoles Canyon watershed: (1) headwater catchment areas, and (2) mesa catchment areas. These two units are subdivided based upon their aspect. The headwater catchment is divided into: (1) the east fork of the Rito de los Frijoles, and (2) the west fork of the Rito de los Frijoles. The mesa catchments are subdivided by the drainage line of the Frijoles Canyon into: (1) the south mesas and south wall of the Frijoles Canyon, and (2) the north mesas and north wall of the Frijoles Canyon. These four areas are referred to as east fork, west fork, south canyon and north canyon (Fig. 47). The east and west forks of the Rito de los Frijoles drain domal features of the Valles Caldera rim (Fig. 2). The forks of the Rito de los Frijoles comprise 22 percent of the watershed system and are densely wooded, extremely rugged and steep relief with very limited mesa areas. The Rito de los Frijoles is deeply incised 150 m below the Pajarito Plateau. The north canyon catchment area comprises 55 percent of the watershed, and drains a large area of mesas (upper and

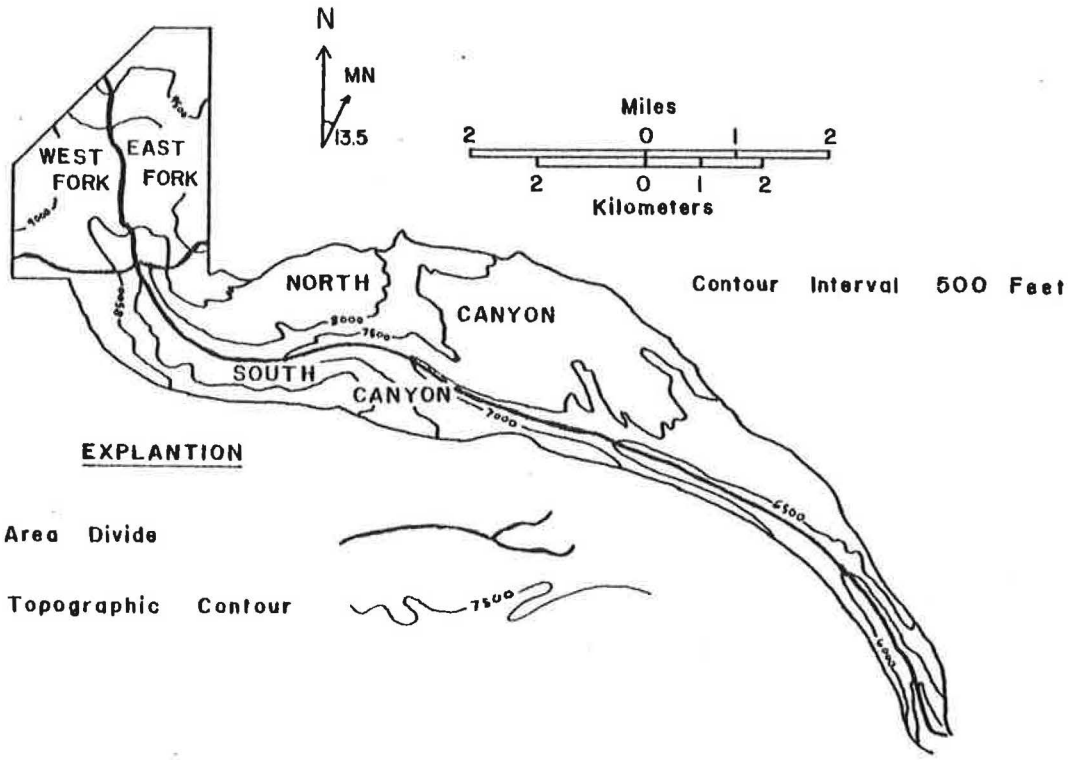


Figure 47: Physiographic Areas of the Frijoles Canyon Watershed, Bandelier National Monument.

Drainage Area (km^2)			Stream Order				
			1	2	3	4	5
East Fork	6.01	# Segments	204	48	12	3	1
		Total Length	41.35	8.53	4.34	1.29	3.22
		Mean Length	0.20		0.43	0.43	
North Canyon	27.79	# Segments	1177	252	40	7	1
		Total Length	164.44	50.21	29.6	10.94	6.6
		Mean Length	0.12	0.20	0.74	1.56	
West Fork	4.96	# Segments	178	40	11	3	1
		Total Length	32.02	9.81	4.67	2.57	1.79
		Mean Length	0.18	0.24	0.42	0.86	
South Canyon	11.45	# Segments	32	73	16	2	
		Total Length	56.79	18.35	7.07	2.25	
		Mean Length	0.17	0.25	0.44	1.12	

Table 7: Summary of Linear Parameters of Morphometric Analysis of the Rito de los Frijoles Watershed System.

lower) and the north walls of the Frijoles Canyon. The north walls of the canyon are of much smaller areal extent than the mesa-top catchments of the north canyon area. The south canyon catchment area drains mainly the southern canyon walls of the Rito de los Frijoles with segments of upper mesas. The top of the south wall of the canyon is the drainage divide for much of the lower portion of the Frijoles Canyon. Thus, the south canyon area comprises only 23 percent of the watershed system.

A morphometric analysis of the linear aspects of the Frijoles Canyon watershed system was conducted at a map scale of 1:12,000 on National Park Service topographic maps. For the four physiographic areas, the number of streams of each order were determined. Strahler's (1964) method of ordering streams was utilized in this analysis. The total stream length of stream segments of each order and the mean stream lengths are given in Table 7. The number of streams of each order is greatest for the north canyon area (Table 7). The similarity of morphology of the north and south canyon mesa-top catchments is shown by a parallel slope of the line segments for the two areas in Figure 48A. The difference between the headwater and the mesa catchment morphologies is evident by a different slope for the respective plots in Figure 48A. The different slopes of the east and west forks are due to a fewer number of low-order streams within these sub-areas.

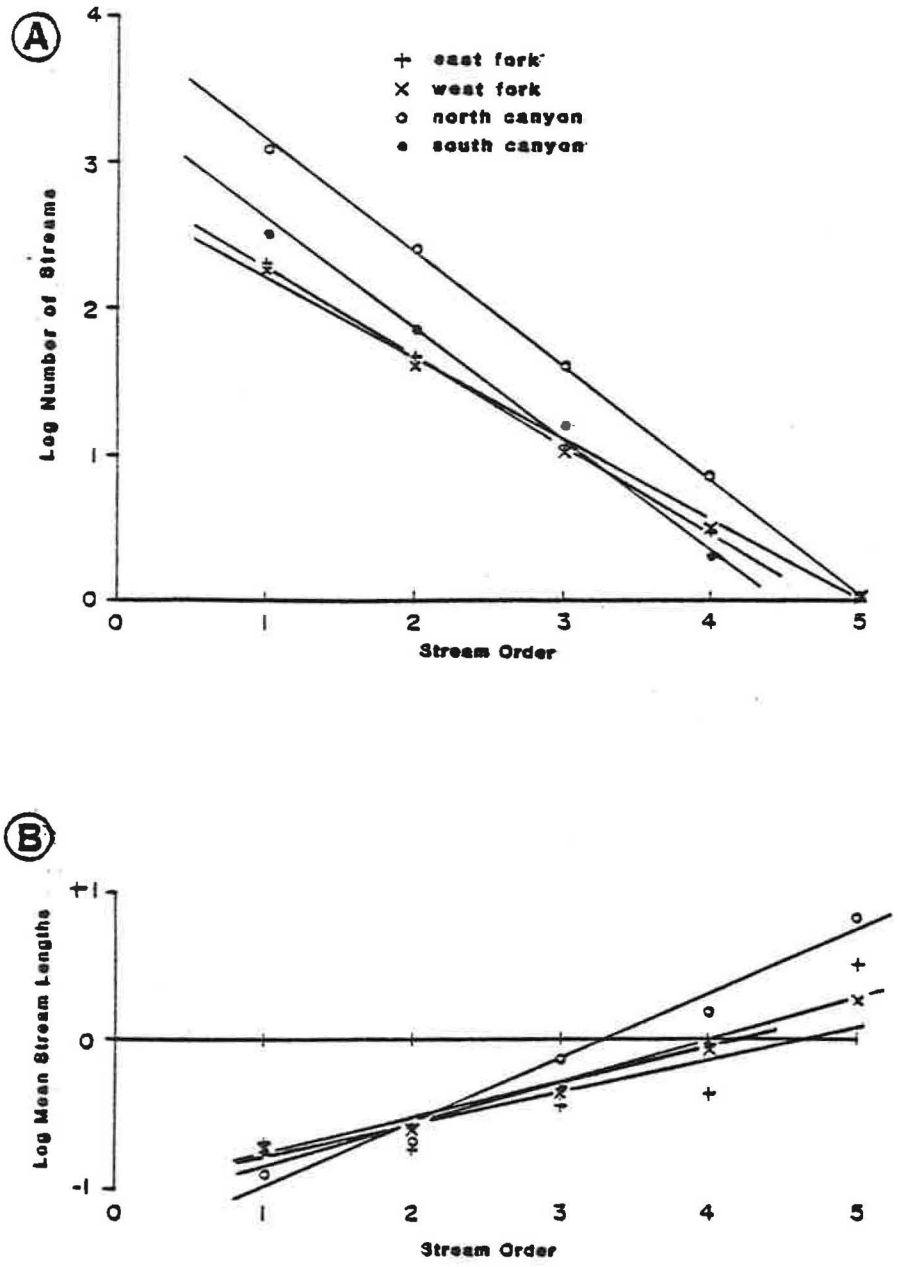


Figure 48: Semi-Log Plots of Stream Order Versus Log Number of Streams and Log Mean Stream Lengths for the Rito de los Frijoles Watershed.

In Figure 48B, the slope of the north canyon line is distinctly different from the slopes of the lines for all other physiographic areas. Figure 48B illustrates that the lengths of the high-order streams are greater for the north canyon area; whereas, the first-order streams are the shortest for the north canyon area.

DISCUSSION

Pre-Burn Geomorphic Conditions

EECI (contracted by the NPS) prepared a soil survey of the Bandelier National Monument (Earth Environment Consultants Inc., 1978). This survey indicates that the upper mesas of the Monument are characterized by a well-developed soil profile. EECI (1978) further noted that the lower mesas are actively eroding, based upon the observation of pedestaled grasses. Estimating the average height of pedestaling (3.8 cm) and the average life span of blue gramma grasses (7 years), the EECI concluded the lower mesas experience an erosion rate of 5.3 mm/year. EECI concluded that the well-developed soil profiles of the upper mesas are due to an apparent drying of the climate (Earth Environmental Consultants Inc., 1978).

A control area, an unexcavated archaeological site on Burnt Mesa instrumented with an erosion-pin transect, gives an erosion rate of 5.7 mm/yr for an 18 month period. The control area is on the uppermost

portion of a lower elevation mesa, and therefore has no upslope component. The post-burn erosion rate is in agreement with the EECI pre-burn estimate for the lower mesas. This is a general indication of a similar rate of erosion following the La Mesa fire on the lower mesas of the Monument. It should be noted that there is no contribution to this erosion rate by ferral burros. The burros, of concern in the lower portions of the Monument, are not present on the mesas north of the Frijoles Canyon.

Hillslope Processes in Devegetated Drainage Basins

Relationships of Weathering and Forest-fire Devegetation

Mechanical weathering processes in the devegetated study basins include the thermal effect of fire on grain-size reduction and frost heave of fine-grained surficial deposits. The effects of frost heave are of greater significance in fire-induced erosion than is the spalling of burned bedrock outcrops. This is due to the limited areal extent of bedrock outcrops in the study basins. Creep is observed to occur on steeper slopes with fine-grained colluvial cover in the upper mesa areas of the Frijoles Canyon watershed, but is not investigated in this study. Other mass-wasting processes, such as rock fall, are of such restricted occurrence in the relatively low-relief study basins that a study of their occurrences in a devegetated setting is not warranted.

In November of 1977, the ground-surface elevation along pin transects in the BMINT study basin was raised by frost heave in places as much as 3 to 4 cm above the level of the washers. The effect of frost heave on a devegetated

surface is shown in Figure 49. The diurnal temperature fluctation induced the growth and thawing of ice crystals in the soil. The ice growth disrupts the structure of the soil, and the thawing increases the porosity of the ground surface. The cycle results in an easily erodible ground surface.

In a vegetated setting, grass and small shrub root systems provide, to some extent, an anchoring effect to the soil during freeze-thaw cycles. In intensely burned areas, where the destruction of vegetation is the greatest, there is no masking of the frost action due to the lack of vegetation. Freeze-thaw cycles occur during the seasons when vegetation density is the least, the late fall and mid-spring. Therefore, the work done in the ground surface by freeze-thaw cycles is of even greater effect in a devegetated watershed. A given runoff event on these easily erodible ground surfaces would produce greater sediment yields than a comparable runoff event on a ground surface unaffected by freeze-thaw. Imeson (1977) observed an increase in suspended-sediment concentration following frost periods in a small, forested catchment in Luxembourg.

Frost heaving is areally extensive on the intensely burned areas of the lower mesas where diurnal temperature fluctuation is greater, and the recolonization of the grasses is slower (Potter and Foxx, 1979).



Figure 49: Effects of Frost Heave on Devegetated Ground-Surface. Ice Crystal Growth Raises Fine-Grained Material in the Ground Disrupting the Structure of the Soil Surface.

As the density of grasses and shrubs increase through time on the lower mesas, the enhanced effectiveness of frost heave will decrease. Other factors of importance in the effectiveness of frost heave include hillslope aspect and related moisture regimes, and the relative proportion of fine-grained sediment in the colluvial cover (White and Wells, 1979; see Appendix I for grain-size distributions of the study basins).

Types and Distribution of Hillslope Erosion Related to Forest-Fire Devegetation

Erosional processes responsible for hillslope reduction in the devegetated portions of the Bandelier National Monument are rillwash and sheetwash. In the study basins mapped in June and July of 1978, sheetwash is of greater areal extent than is rillwash (Figs. 8, 11, 12, 14, 16, and 17). This is due to the shallow slopes of most of the hillslope segments within the study basins. The shallow gradient of these hillslopes (<10°) generally will not concentrate overland flow into areas of channelized flow (rilling). Rillwash is more common in the intensely burned study basins, relative to the other study basins (Figs. 8 and 14). This is a result of a greater degree of devegetation within these study basins and the better developed impermeable ash layer associated with intensely burned areas. Both overland flow processes are of increased effectiveness in a devegetated setting due to the lack of the retarding influence of vegetation and the

decreased infiltration capacity of forest soils associated with fire.

The decreased infiltration rates on exposed soils can be attributed to two processes: (1) rain-splash impact plugging the ground-surface porosity (Zwolinski, 1971), and/or (2) a fire-induced water repellency of the ground surface (Krammes and Debano, 1965). Campbell and others (1977) observed that fire-induced water repellency was an important factor in reducing infiltration rates in their case study of an Arizona ponderosa pine ecosystem. In the Bandelier National Monument, it was observed that the ash layer, produced by the consumption of forest litter during the La Mesa fire, decreased the infiltration rate of the exposed soils. In the study basins, an ashed ground surface had a lower infiltration rate (mean = 30 cm/hr) than did an unashed, or stripped, ground surface (mean = 42 cm/hr; Table 3)

To test the relative contribution of the plugging of surface porosity by rain-splash impact and the development of an impermeable layer on decreased infiltration capacity, bulk density was determined for the samples collected at the infiltration sites. It was found that ashed ground surfaces had lower bulk densities (0.56 - 1.09 gm/cm^3) than did unashed ground surfaces (1.20 - 1.43 gm/cm^3; Table 3). The lower bulk densities of the ashed surfaces is a result of the combustion of organic debris

in the ground surface producing void spaces. The lower infiltration rates associated with lower density, ashed ground surfaces appears to be due to the generation of an impermeable ash layer and not due to a plugging of surface porosity by rain splash impact. It is assumed that the water repellency of a burn layer is due to the organic resins which are concentrated in the ashed remains of the forest litter.

The decreased infiltration capacity of the forest soils as a result of the La Mesa fire promotes an increase in overland flow. With greater overland flow, there will be a corresponding increase in runoff and sediment yield from a given basin. Influencing the amount of sediment that is entrained on hillslopes and delivered to the drainage lines is the length of overland flow. The efficiency of sediment removal from hillslopes will be greatest where the length of overland flow is the least (White and Wells, 1979). Table 8 is a tabulation of the mean overland flow distances for the headwaters, mid-basin, and basin mouths of the study basins. For three of five basins, the greatest length of overland flow occurs in the mid-basin region of the study basins. The relative degree of dissection by drainage lines is the least in the mid-basin regions; the distance from divides to drainage lines is generally greatest in the mid-basin regions. For example, most of the first-order drainages within BMINT (Fig. 8) join the trunk drainage line above the mid-basin region.

Study Area	Location	Mean Overland Flow Distance (m)
Burnt Mesa		
INTENSE	Headwaters	5
	Mid-Basin	16
	Basin mouth	10
MODERATE	Headwaters	10
	Mid-Basin	12
	Basin mouth	8
LIGHT	Headwaters	26
	Mid-basin	14
	Basin mouth	6
Apache Springs		
INTENSE	Headwaters	12
	Mid-basin	15
	Basin mouth	9
MODERATE	Headwaters	15
	Basin mouth	10
LIGHT	Headwaters	No defined drainage
	Basin mouth	

Table 8: Mean Length of Overland Flow on Interfluves for the Study Basins in the Apache Springs and Burnt Mesa Areas.

The first-order stream segments provide a greater degree of dissection in the headwater region, and correspondingly a shorter length of overland flow. In the basin-mouth region, the drainage divides taper toward the mouth of the basin, which decreases the area of overland flow with respect to the area of the channel. Sediment entrained on the mid-basin hillslopes will have greater distances to travel to drainage lines which subsequently remove sediment from the basin. The headwater and basin-mouth regions, being generally more dissected by drainage lines, will be more susceptible to erosion due to the shorter lengths of overland flow.

The reduced infiltration capacity on burned hillslopes leads to greater volumes of overland flow. As the flow concentrates and moves downslope, new rills are cut into the devegetated ground surfaces. The development of new rills decreases the pre-burn overland-flow distances, effectively increasing the drainage density within a devegetated basin. The increased drainage density allows an increased amount of sediment to be delivered from a devegetated basin.

Figure 50A was taken in November of 1977, five months following the La Mesa fire, and exhibits the maximum development of rilling. The photograph is of a valley-side slope within the BMINT study basin. The view is nearly perpendicular to transect B, which crosses the

Photo A



Figure 50: Rill Development (Photo A = November 1977) and Obliteration (Photo B = April 1980) on a Valley-Side Slope Within BMINT.



Photo B

bottom of the photograph (not visible). Infiltration test sites C and D (Table 3) were located behind the tree at right center. The infiltration rate on the rilled, impermeable ash was 21.6 cm/hr, whereas the infiltration rate on the unashed surface was 64.8 cm/hr. The decreased infiltration capacity of the ashed surface increases the surface runoff which, in turn, promotes the development of rills and an increase in channelized flow. Note that the unashed surface is not rilled (Fig. 50A).

The first post-burn freeze-thaw cycle was in November of 1977. During this period, the frost action began the initial break up of the ash layer. With time, the impermeable ash layer was destroyed by continued freeze-thaw cycles and the regrowth of vegetation. Figure 49B is the same rill complex as Figure 50A, 29 months later, in April of 1980. The rill complex is indistinct due to regrowth of vegetation and destruction of the impermeable ash layer. The regrowth of grasses and the downed trees on the ground surface increase the surface roughness from an approximate value of 0.015 in November 1977 (Fig. 50A) to an approximate value of 0.067 in April 1980 (Fig. 50B). The increased surface roughness decreased the velocity of overland flow, thereby decreasing the capacity of overland flow to entrain sediment. The trees fallen across the slope above the rill complex in Figure 49B reduced the overland flow contribution from upslope to the rill complex, further

hastening the obliteration of the rill complex.

Factors important in post-fire hillslope erosion are listed below in decreasing order of importance:

(1) degree of ash development;

(2) amount of upslope catchment area;

(3) degree of slope; and

(4) type of slope.

A shallow gradient hillslope (< 10°) with a relatively large upslope catchment and with a well developed ash layer (prevalant in the intense-burn basins) will be susceptible to rill erosion. Rill systems will develop master (main stem) rills with tributary rills that fill and switch courses over the ground surface. The resultant ground surface along a given erosion-pin transect (e.g., west end of transect A, BMINT, Fig. 19) will exhibit variable amounts of gain and loss from pin to pin. Sheetwash is the dominant erosional process on a shallow gradient hillslope without a significant upslope catchment area. Changes in ground-surface elevation, along a given pin transect where sheetwash is operative, will be more evenly distributed, with minor variations (e.g., the east end of transect B, BMINT, Fig. 20; also see Fig. 8). Steep, short side slopes adjacent to drainage lines are highly susceptible to post-burn erosion due to the degree of slope and rapid removal of sediment via the drainage line (e.g., Fig. 19, between 35 and 40 meters). Complex hillslopes, slopes with both

waxing (increasing slope) and waning (decreasing slope) segments, will experience erosion on the waxing segment and deposition on the waning segment. The gain along transect B, BMINT (Fig. 20, between 14 and 18 meters), is a waning toeslope segment (also see Fig. 8).

The regions of the study basins most susceptible to post-fire erosion are the headwaters and basin mouths. This is primarily due to the short overland flow distances and greater drainage densities of these regions. Steep hillslopes (> 10°), generally present in the headwater regions, are susceptible to rillwash. Slopes with a well-developed ash layer (prevalent in the intense-burn basins), coupled with a relatively large upslope catchment area, are also susceptible to rillwash, even on shallow gradient (< 10°) hillslopes. Shallow-gradient hillslopes lacking a well-developed ash layer, and waning hillslope segments are susceptible to sheetwash. Shallow and waning hillslopes are generally present in the mid-basin and distal regions of the study basins and are the most stable hillslope types under post-fire conditions.

Runoff, Erosion Rates, and Sediment Yield in Devegetated Drainage Basins

Forest-fire devegetation contributes to increased runoff. The runoff calculations for the Burnt Mesa study basins (Table 6) show that runoff increases with increasing burn intensity (i.e., increasing devegetation) (Fig. 51). Table 1 indicates that the smallest basin in the Burnt Mesa study area (BMMOD) is also the steepest. Figure 51 shows that the BMMOD basin yields a smaller amount of runoff than the larger BMINT basin, but a greater volume of runoff than the larger BMLIGHT basin. Therefore, drainage basin area and basin slope are not the significant factors in runoff in devegetated basins. This is an indication that basin relief and burn intensity may be of greater significance in runoff than basin area and slope.

Table 9 is a summary of the calculated annual rates of mean surface-elevation change ($\bar{\Delta}$/yr) for each study basin. The $\bar{\Delta}$/yr values are calculated for each basin by summing the values in Table 4 for each annual period and dividing by the number of pin transects per basin. Total sediment yield (m^3/yr) is computed for the first two annual periods by multiplying the $\bar{\Delta}$/yr values by the length and width (0.04 cm) of the erosion-pin transects.

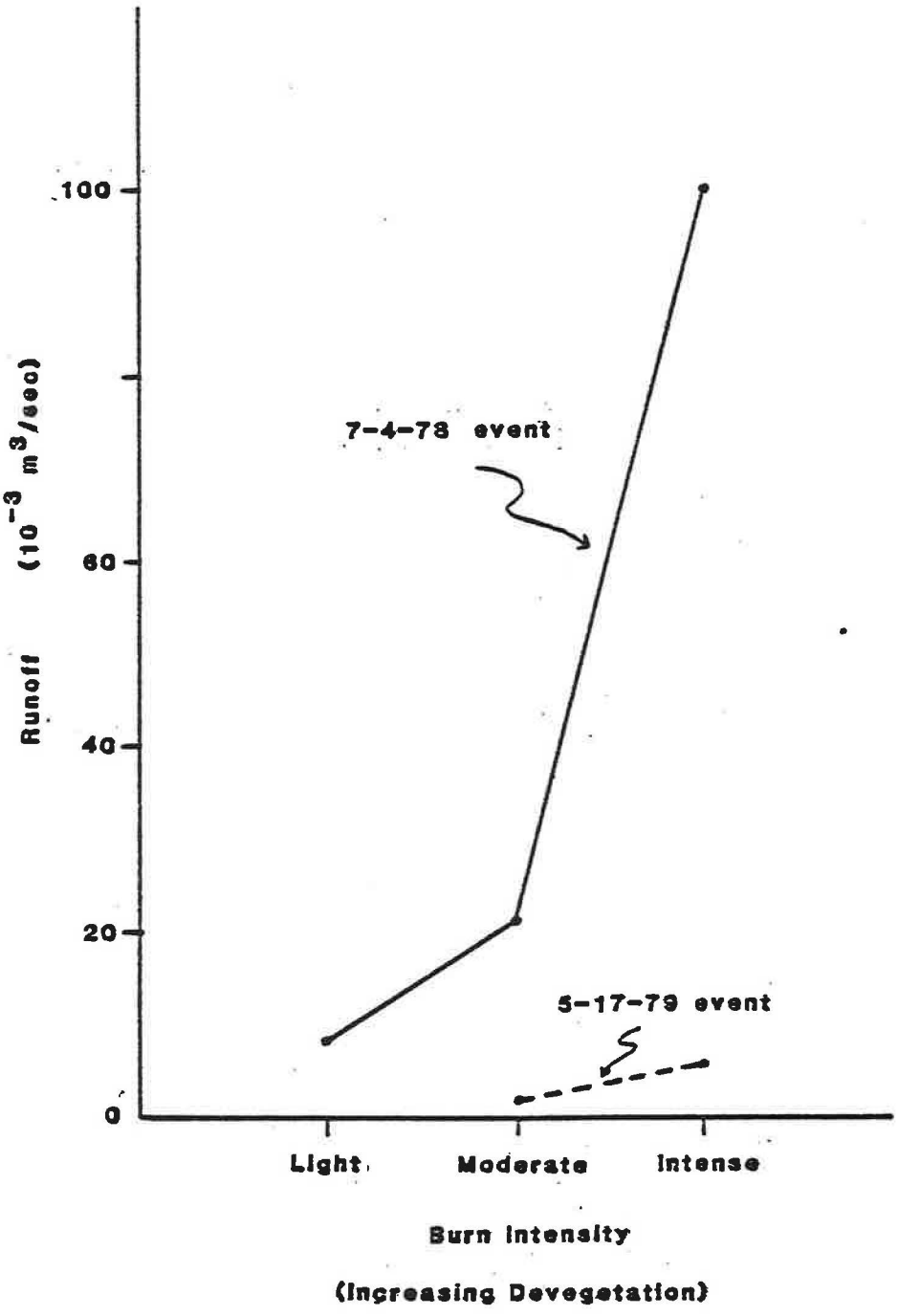


Figure 51: Relationship Between Runoff and Forest-Fire Devegetation for Two Precipitation Events, Burnt Mesa Study Basins.

Study Basin	Time Period	$\bar{\Delta}$/yr (mm/yr)	Total Sediment Yield ($m^3/yr \times 10^{-3}$)	Sediment Yield per Unit Area ($m^3/m^2/yr \times 10^{-6}$)
BMINT	9/77-6/78	-4.3	17.2	4.18
Area = 4116.5m^2	6/78-6/79	-6.5	26.0	6.32
	6/79-4/80	+3.6		
BMMOD	9/77-6/78	-1.8	3.6	4.42
Area = 813.0m^2	6/78-6/79	-1.1	2.2	2.70
	6/79-4/80	-0.4		
BMLIGHT	9/77-6/78	-4.6	12.1	8.50
Area = 1426.0m^2	6/78-6/79	-7.7	20.2	14.2
	6/79-4/80	+6.2		
ASINT	9/77-6/78	-3.5	9.1	6.42
Area = 1421.4m^2	6/78-6/79	-1.2	3.1	2.20
	6/79-5/80	+3.4		
ASMOD	9/77-6/78	-4.4	5.5	8.18
Area = 677.7m^2	6/78-6/79	-4.4	5.5	8.18
	6/79-5/80	+2.5		
ASLIGHT	10/77-6/78	-3.2	2.2	5.85
Area = 380.4m^2	6/78-6/79	-7.8	5.4	14.3
	6/79-5/80	+3.2		

Table 9: Summary of Mean Annual Surface Change and Sediment Yield for Each Study Basin.

Sediment yield per unit area is computed by dividing the m^3/yr values by their respective basin areas. This allows the relative degree of erosion between study basins to be compared; the sediment yield values are calculated and not actually measured volumes of sediment. The use of sediment yield values is limited due to the restricted area actually covered by erosion pins within each basin. Sediment yield is not computed for the third annual period because nearly all the basins experienced a net gain along erosion-pin transects. Although the study basins were yielding sediment, the total sediment yield must have been significantly decreased as the hillslopes and channels became revegetated.

Erosion rates ($\bar{\Delta}$/yr) were generally of greater magnitude during the second year following the La Mesa fire. However, precipitation was greater during the first year following the fire (Fig. 46). The greater magnitude of erosion during the second year is attributed to the destruction of the ash layer. Directly after the fire, the ash layer was hard to wet (water repellency of organic resins in the ash (Debano and others, 1970)) and promoted overland flow. The ash layer was only beginning to be incised locally and removed by rilling and sheetwash during the first year after the fire. During the second year, the extensive disruption of the ash layer by frost action, and the expansion of rill systems led to widespread

erosion of the ash layer. Even though the total amount of precipitation was less during the second year following the fire (Fig. 46), the extensive destruction of the ash layer accounts for the higher erosion rates during the second year.

Table 9 indicates that the ASMOD basin has relatively high rates of erosion for the first two years of the study. The relatively high rates of erosion are problematic. The basin had already accumulated a thick carpet of pin needles by the time of instrumentation (September 1977). It is possible that the pine needles interfered with the instrumentation. The high erosion rates of the ASMOD basin are postulated to be partially a result of this possible interference by the pine needles with the erosion-pin washers.

Figure 52 illustrates total sediment yield (m^3/yr) and sediment yield per unit area ($m^3/m^2/yr$) versus burn intensity for both the Apache Springs and Burnt Mesa study areas. It is evident from the plots that there is not a direct relationship between burn intensity and sediment yield (Fig. 52), as the runoff versus burn intensity plot seemed to indicate (Fig. 51). This is a result of factors other than burn intensity which may have an overriding effect on sediment production in a devegetated setting. These other factors will be discussed in detail in the Camparison of Drainage Basins of Differing Burn Intensity section.

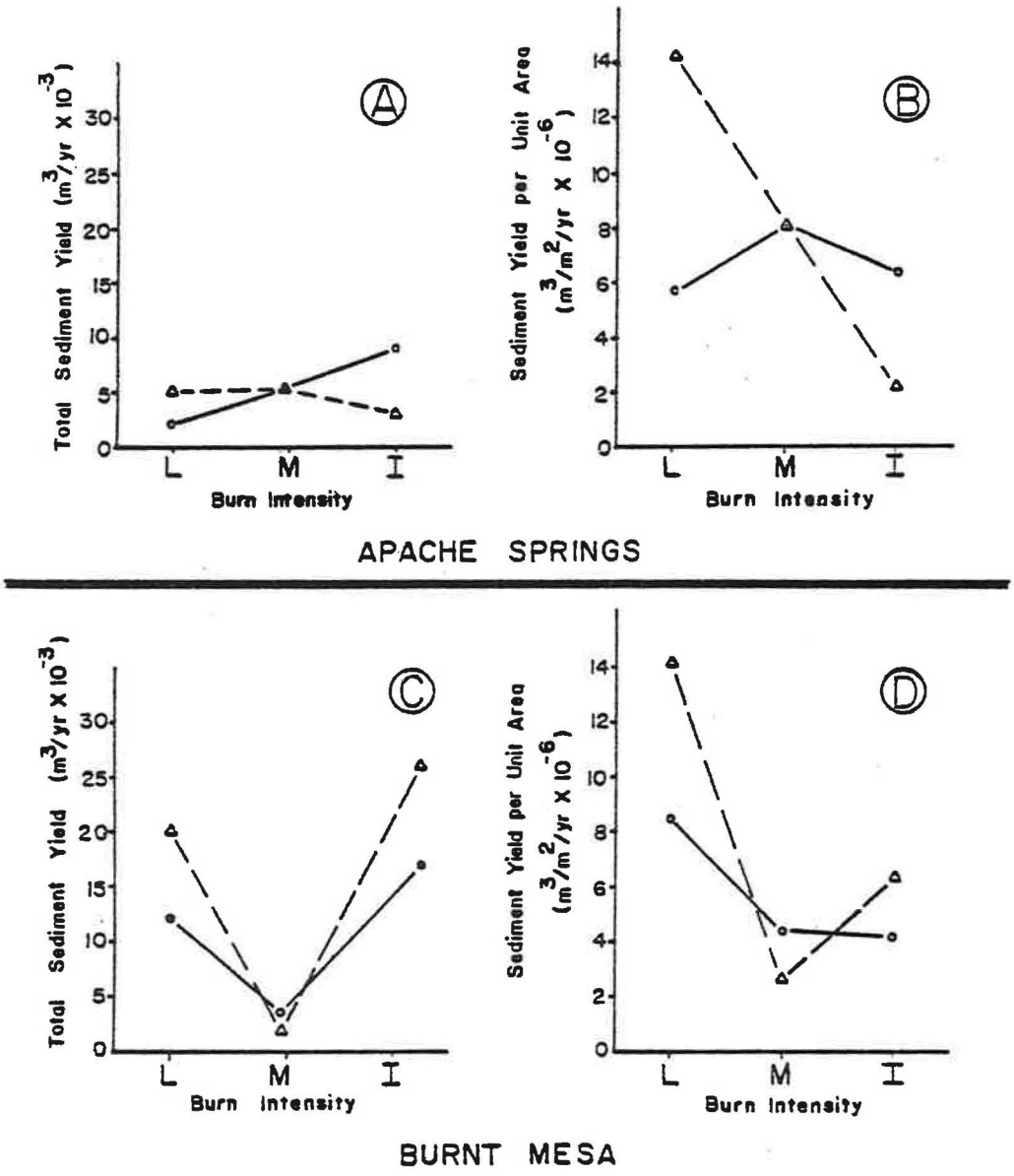


Figure 52: Sediment Yield Versus Burn Intensity Relationships for the Apache Springs Study Basins and the Burnt Mesa Study Basins. Solid Line Represents First Year of Data, Dashed Line Represents Second Year of Data.

Comparison of Drainage Basins in Differing Climatic and Topographic Settings

Figure 52B shows that during the second year of this study, the smallest basin (ASLIGHT, Table 9) produced the greatest amount of sediment for the upper-elevation study basins. The largest basin on the upper mesas (ASINT, Table 9) produced the least sediment. However, the smallest basin on the lower-elevation mesas (BMMOD, Table 9) produced the least sediment in the Burnt Mesa study area (Fig. 52D), while the largest basin (BMINT) produced a comparatively moderate amount of sediment (Fig. 52D). These relationships further illustrate the fact that the principle factors in erosion in a devegetated terrain are not burn intensity or drainage area size, but that other factors play a greater role in a devegetated terrain.

The total sediment yield (m^3/yr) for the Apache Springs study basins (Fig. 52A) is less than the Burnt Mesa basins (Fig. 52C) because the area covered by the erosion-pin transects within the Apache Springs basins is less. Figure 52B and 52D show that the range or magnitude of sediment yield per unit area ($\cong$ 2 to 14 $m^3/m^2/yr$) is similar between the study areas. This

indicates that both areas are producing similar amounts of sediment following the La Mesa fire. However, the axial drainage below ASINT (≅ 30 m downslope from the basin mouth) exhibits very little fire-associated sediment (Fig. 53). The axial drainage below the BMINT and BMMOD study basins (≅ 5 m downslope from their basin mouths). exhibits large amounts of fire-associated sediment in the channel (Fig. 43). The physiography of the upper mesas as compared to the physiography of the lower mesas is a contributing factor as to why the upper-mesa axial drainages exhibit less deposition of fire-associated sediment. The sediment produced from the Apache Springs study basins must traverse long valley-side slopes to reach the axial drainage (Fig. 54A), whereas the sediment produced from the Burnt Mesa study basins is delivered directly to the axial drainage (Fig. 54B).

The soil survey performed by EECI (1978) and the study of Potter and Foxx (1979) both concluded that the post-fire reseeding was most successful on the upper mesas. Better soil development and the greater precipitation on the upper mesas promoted a more rapid regrowth of vegetation (Earth Environmental Consultants Inc., 1978). The Apache Springs basins produce similar amounts of sediment as the Burnt Mesa study basins (Figs. 52B and 52D). Collectively, however, the Apache Springs study basins deliver less sediment to the Frijoles Canyon drainage net because



Figure 53: Densely Vegetated, Axial Drainage Below ASINT. The Trunk Drainage is not Well Defined and Has Very Little Fire-Associated Sediment, August. 1980.

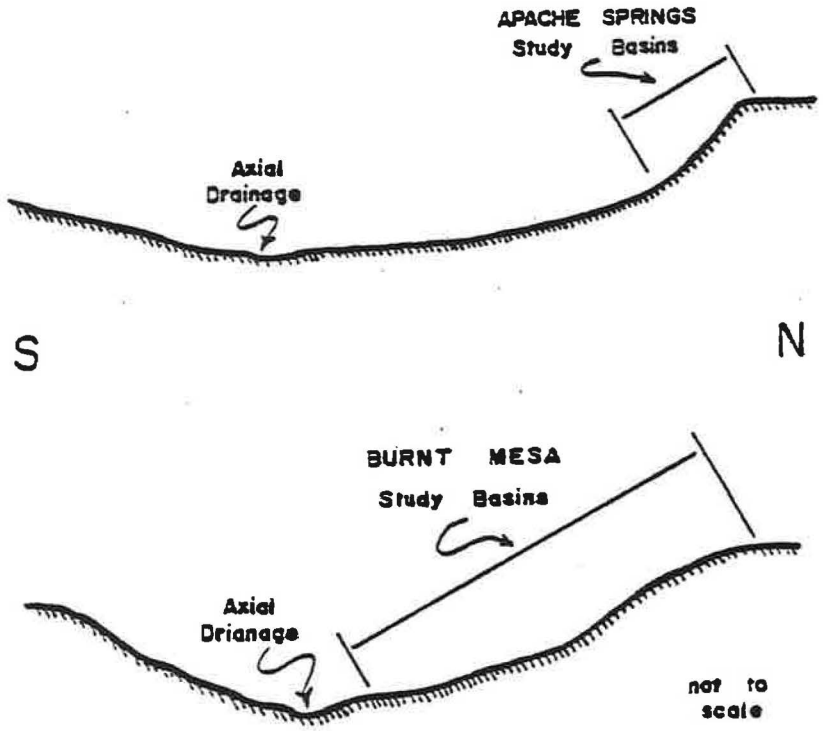


Figure 54: Schematic Cross Sections Illustrating the Physiographic Settings of the Study Basins within each Study Area. The Apache Springs Basins are Separated from Axial Drainage by Shallow Gradient Valley-Side Slopes.

the dense and rapid regrowth of vegetation on the valley-side slopes of the upper mesas traps fire-associated sediment before it reaches the axial drainages (Fig. 55). Therefore, the combination of the physiograpy of the study areas, the location of the study basins within the upper- and lower-elevation study areas, and the success of the reseeding on the upper mesas, all combine to result in the upper-elevation mesas being less affected by the La Mesa fire.



Figure 55: Dense and Rapid Revegetation of the Valley-Side Slopes Between the Apache Springs Study Basins and the Upper-Elevation Axial Drainages Provides Storage of Fire-Associated Sediment.

Comparison of Drainage Basins of Differing Burn Intensity

The sediment yields ($\bar{\Delta}$/yr) within the BMMOD study basin are the lowest for all the study basins (Figs. 52C and 52D). The low erosion rates within the BMMOD basin are due to the protection of the denuded ground surface by post-fire needle cast. Pine needles burned, but not consumed by the fire, on the upper portions of the trees were cast off by the trees (Fig. 56). These needles provide a protective carpet that breaks the fall of rain drops and retards overland flow (Megahan and Molitor, 1975). Throughout the National Monument, the post-fire needle cast greatly enhanced the success of revegetation of native grasses (Potter and Foxx, 1979).

The burrowing activity of gophers produces mounds of fresh sediment at the ground surface without a protective cover of vegetation (Fig. 57). These mounds of unvegetated, loose sediment are susceptible to rain splash and entrainment by overland flow (Imeson, 1977). The BMLIGHT study basin, which is largely a meadow, supports a gopher population (D. Guthrie, personal communication, 1978). The high sediment yields (Figs. 52C and 52D) of the



Figure 56: Needle Cast Covering the Ground-Surface in the BMMOD Study Basin. Rebar Stake in Center of Photograph is Approximately 0.3 m in Height.



Figure 57: Mounds of Colluvium (Light Areas in Upper Half of Photograph) Produced by the Burrowing of Gophers. Ground-Surface Has Been Subjected to Freeze-Thaw. Ruler is 16 cm long.

BMLIGHT study basin are a result of the burrowing activity of the gophers. The variability in ground-surface elevation along transects A and B (Figs. 25 and 26) is due to the mounding of sediment on some pins (peaks on green line) and the subsidence of the ground surface over gopher tunnels (low points on green line).

The high total sediment yield for the BMINT study basin is due to a number of factors (Fig. 52C). The most important factor contributing to the high erosion rates is the impermeable ash layer. The ash layer is most apparent in the headwaters of BMINT, and is best developed in intensely burned areas (Fig. 58). Also of importance is the lack of needle cast to protect the ground surface (Fig. 58). Mechanical weathering is a significant factor in intensely burned areas, where the degree of devegetation is the greatest, and correspondingly frost action is most effective. The high drainage density, relative to the other study basins, of the BMINT basin (Fig. 8) allows rapid and efficient sediment removal from the basin.

In the Apache Springs area, the intense-burn basin experienced a moderate sediment yield during the first year following the fire (Fig. 52B). During the second year, the ASINT basin experienced a very low sediment yield (Fig. 52B). The change from a moderate to a low erosion rate in this intensely burned area can best be attributed to the rapid and dense regrowth of vegetation



Figure 58: Headwaters of BMINT Study Basin. Ash Layer is Medium to Dark Gray Areas on the Ground-Surface (November 1977). Note the Development of Rills on the Shallow Gradient, Ashed Headwater Slope.

within the basin. The rapid regrowth of vegetation is due to the better developed soils and greater amounts of precipitation on the upper mesas (Earth Environmental Consultants Inc., 1978).

The large sediment yields in the ASMOD basin (Figs. 52A and 52B) may be due to the large headwater catchment area of the basin, relative to the other Apache Springs study basins (Fig. 14, 16, and 17). The large headwater catchment may have contributed larger volumes of runoff for sediment entrainment from the pin transects. Since the basin was protected by a dense needle carpet, the runoff could not channelize into rills and the sediment was removed by sheetwash. The fairly uniform change in ground surface elevation from pin to pin along the pin transects supports this explanation for the large erosion rates within this moderate-burn basin (Figs. 31 and 32).

The high sediment yields within the ASLIGHT study basin are due to its development on the waxing portion of a mesa-side slope (Figs. 52A and 52B). The convex longitudinal profile distinguishes the ASLIGHT basin from all other study basins (Fig. 15). Revegetation was not as successful within this study basin, which, in combination with its convex profile, resulted in a high sediment yield during the second year of this study (Fig. 52B).

Seasonality of Erosion Rates

Figure 59 through 68 are graphic representations of the seasonal changes in ground-surface elevation along pin transects and grid stations for each study basin. Months circled on the time scale in these figures are the months in which field measurements were taken. Months boxed on the erosion grid plots are measurement periods when the ground surface was affected by frost heave. The value plotted, $\bar{\Delta}$/month, is derived from the erosion pin and grid measurements as explained in Appendix II. The $\bar{\Delta}$/month values are plotted as gain (+) or loss (-) from zero, assuming the previous date as zero (datum) for each following measurement date. The slope or length of the line segments are of no significance, only the relative grouping of the values above or below zero (datum) through time are of significance.

There is a pronounced grouping of values below the zero line during the months of May and June (Figs. 59 through 68). A general increase in the values follows as the summer season progresses. Late in the fall, there is a general decrease in ground-surface elevation within the study basins. This trend is due to a number of factors, the most

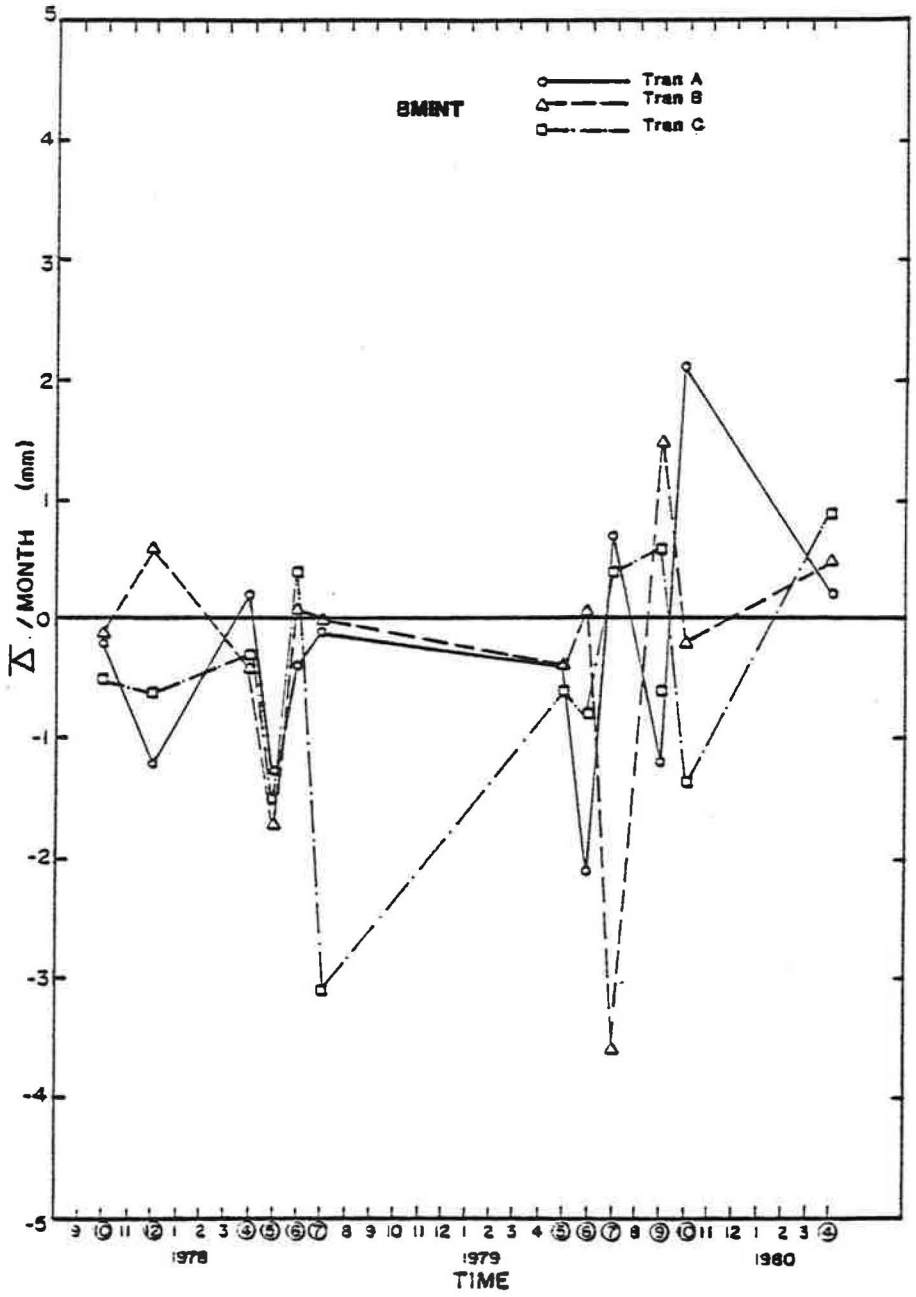


Figure 59: Seasonal Variations in Ground-Surface Elevation for the BMINT Study Basin. Numbers on Time Axis Indicate Months of Year With 1 = January and 12 = December. Circled Months are Months of Field Measurements.

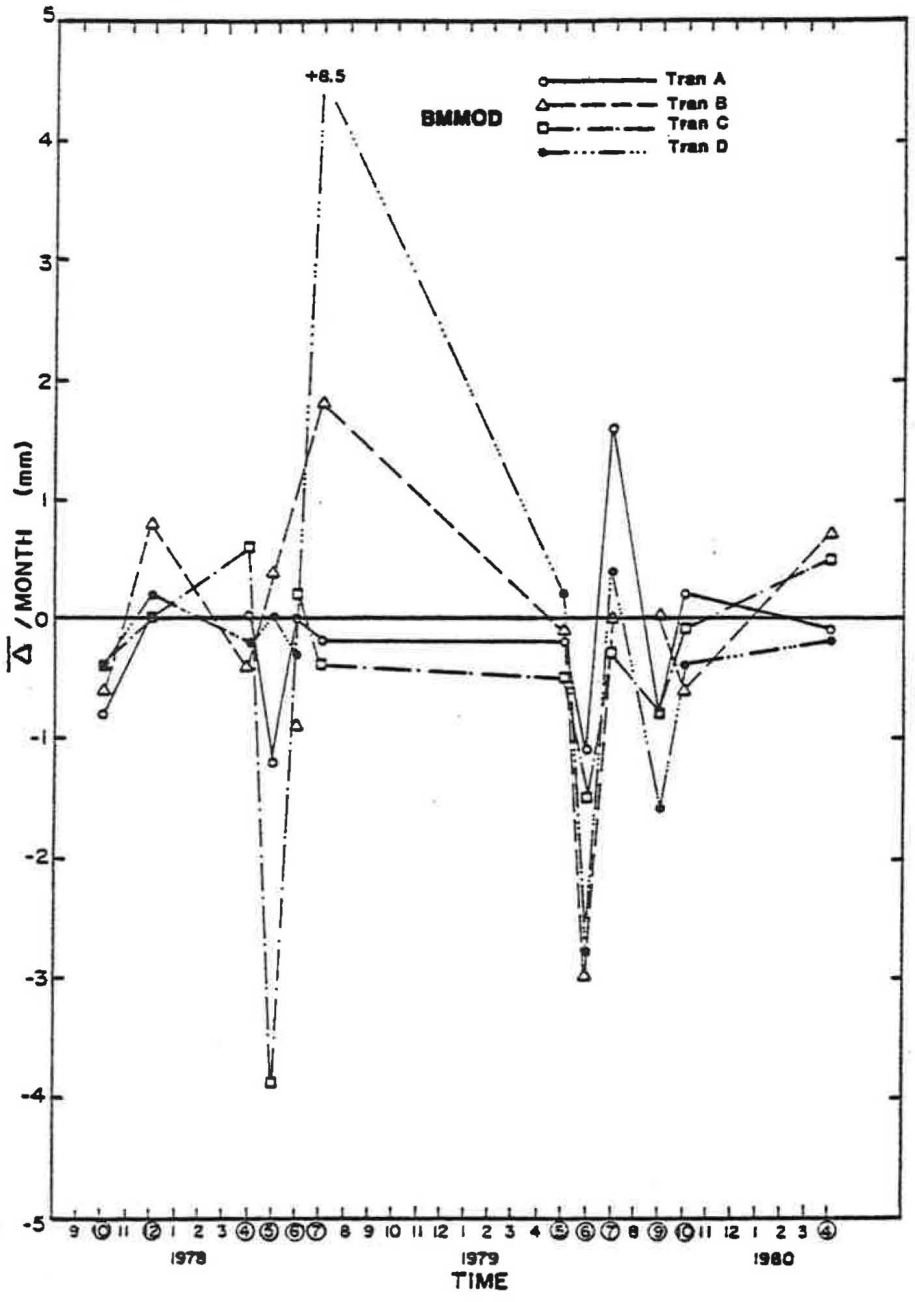


Figure 60: Seasonal Variations in Ground-Surface Elevation for the BMMOD Study Basin. Explanation of Time Axis in Figure 59 Caption.

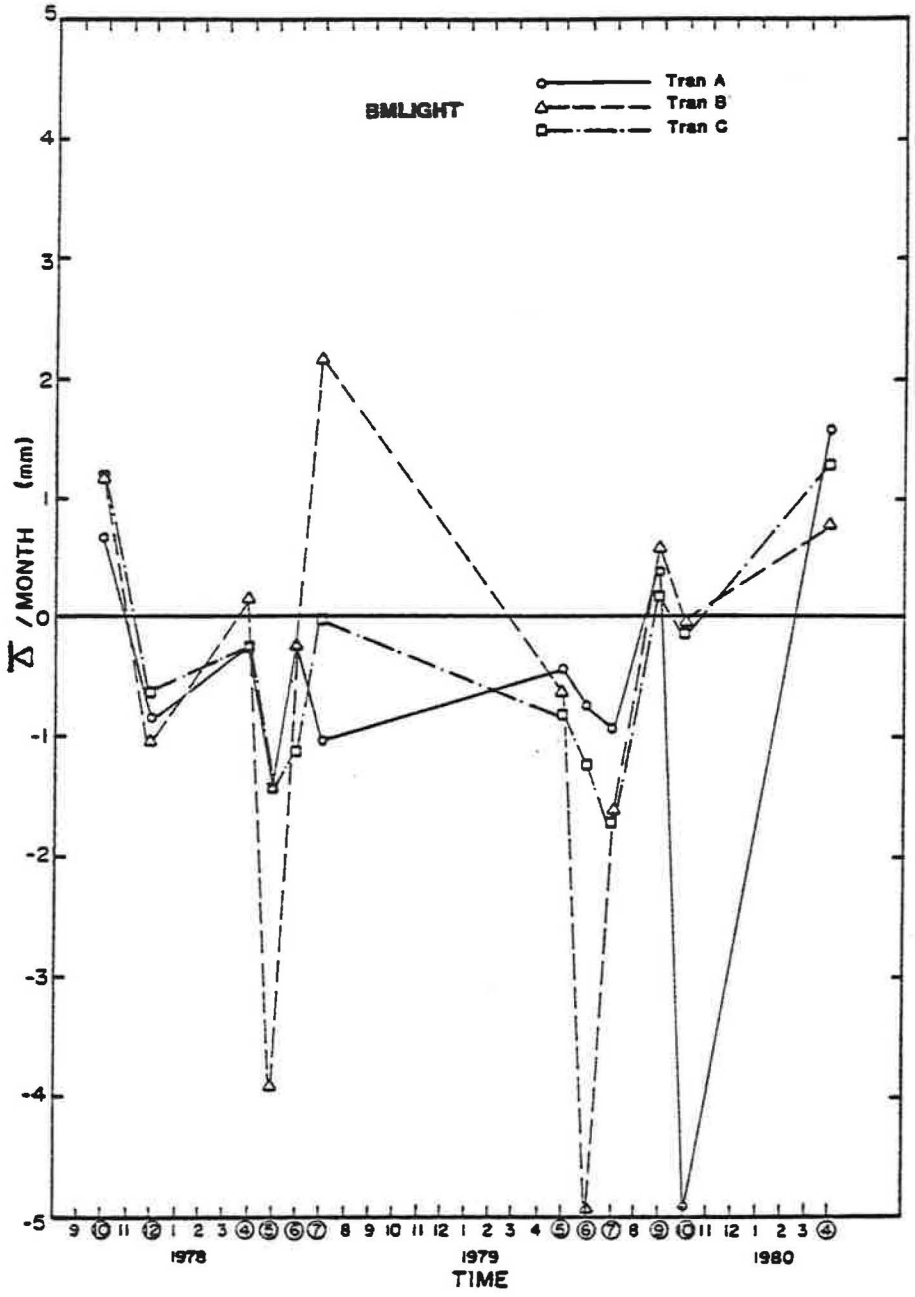


Figure 61: Seasonal Variations in Ground-Surface Elevation for the BMLIGHT Study Basin. Explanation of time axis in Figure 59 Caption.

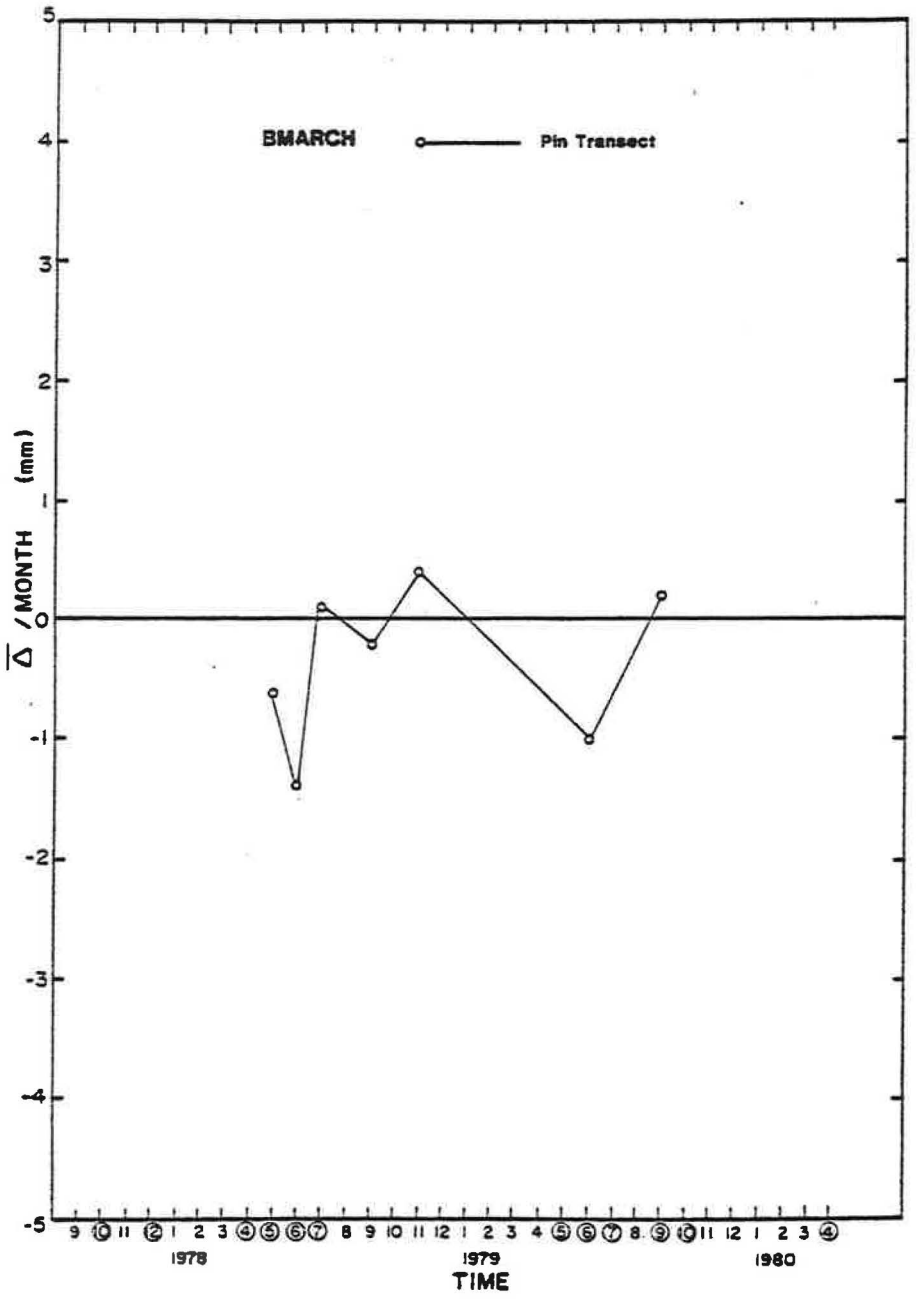


Figure 62: Seasonal Variations in Ground-Surface Elevation for the BMARCH Study Basin. Explanation of time axis in Figure 59 Caption.

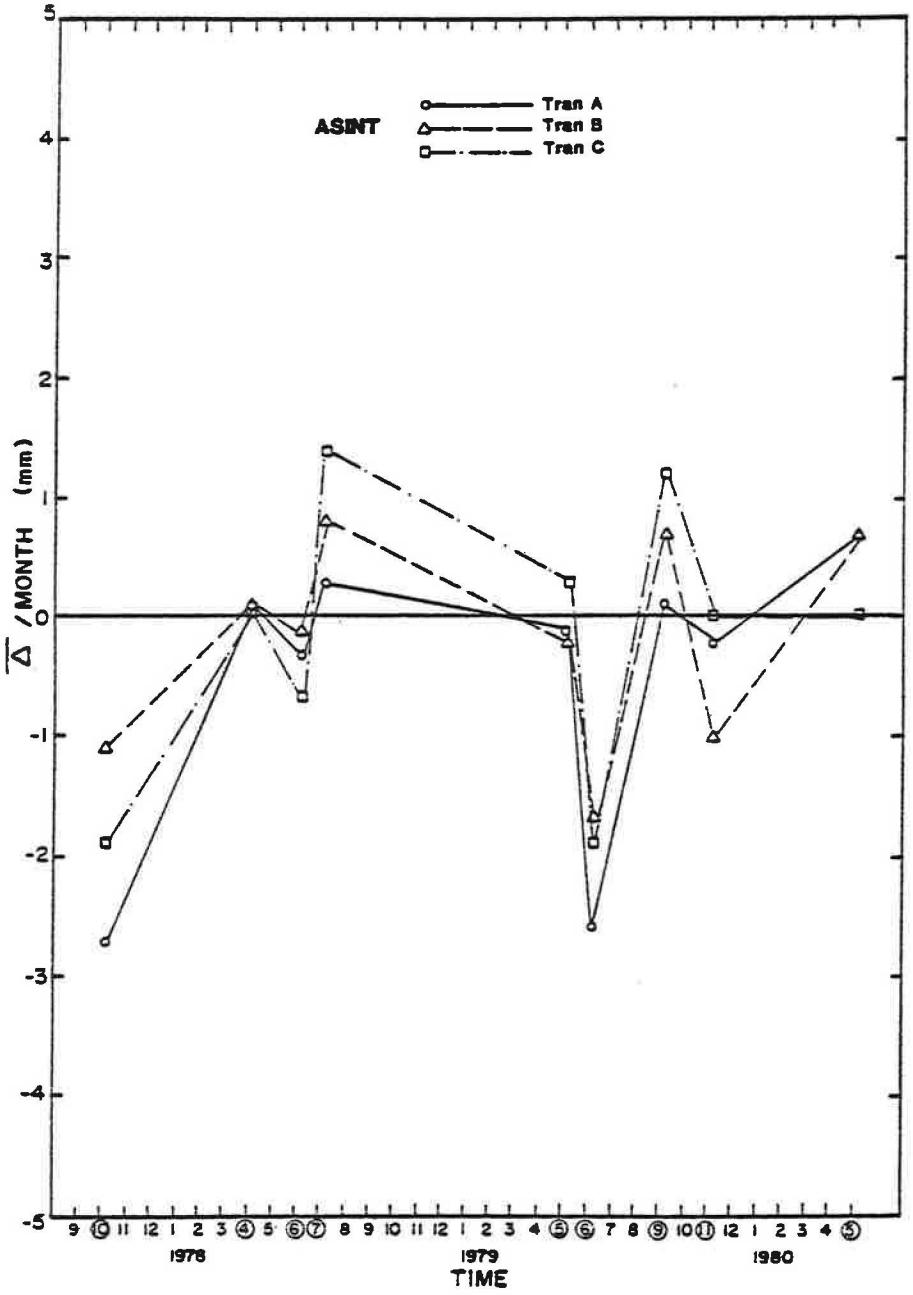


Figure 63: Seasonal Variations in Ground-Surface Elevation for the ASINT Study Basin. Explanation of time axis in Figure 59 Caption.

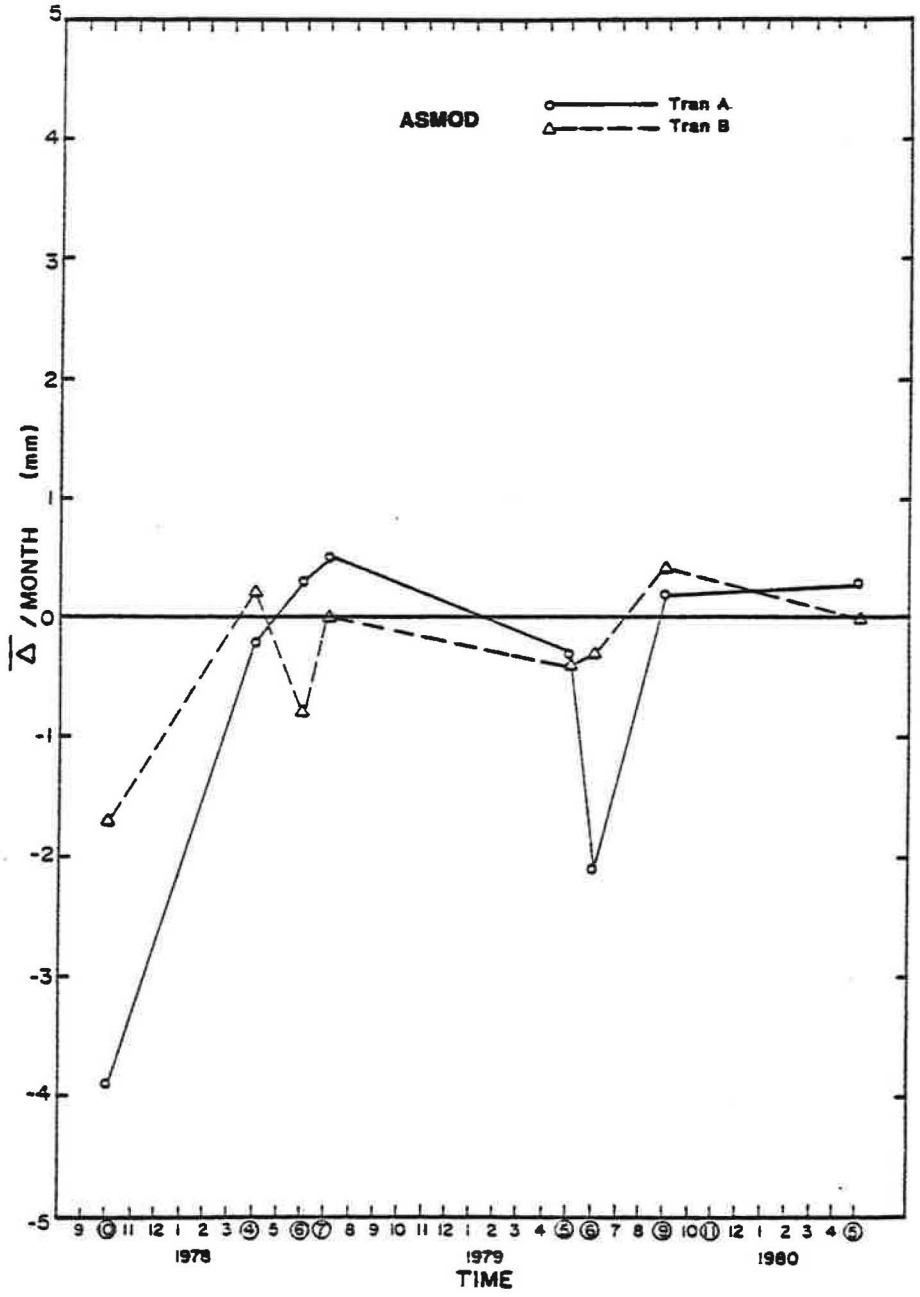


Figure 64: Seasonal Variations in Ground-Surface Elevation for the ASMOD Study Basin. Explanation of time axis in Figure 59 Caption.

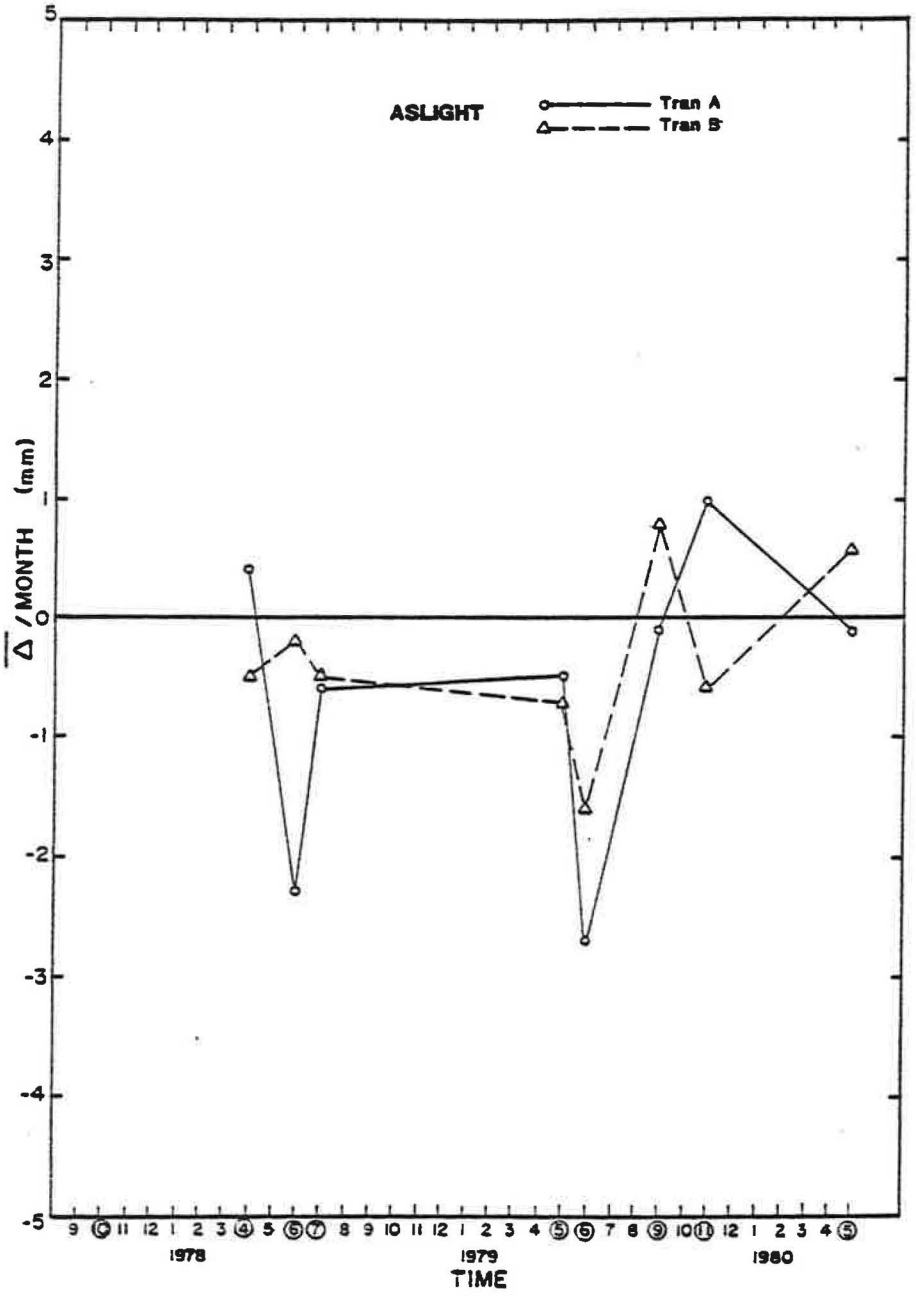


Figure 65: Seasonal Variations in Ground-Surface Elevation for the ASLIGHT Study Basin. Explanation of time axis in Figure 59 Caption.

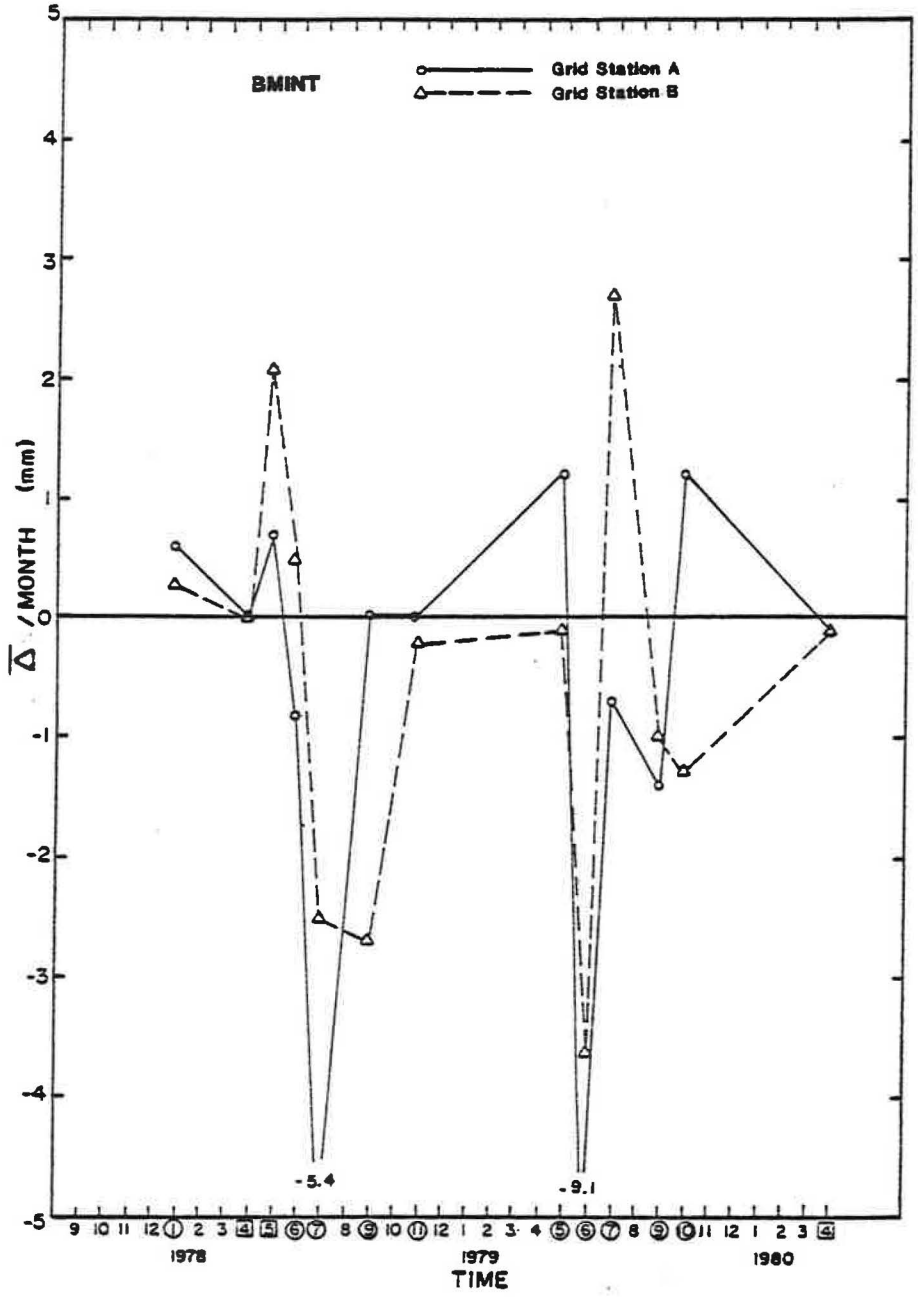


Figure 66: Seasonal Variations in Ground-Surface Elevation for the Erosion-Grid Stations within the BMINT Study Basin. Circled Numbers on Time Axis are the Months of Field Measurements. Boxed Numbers are Field Measurements Affected by Frost-Heave.

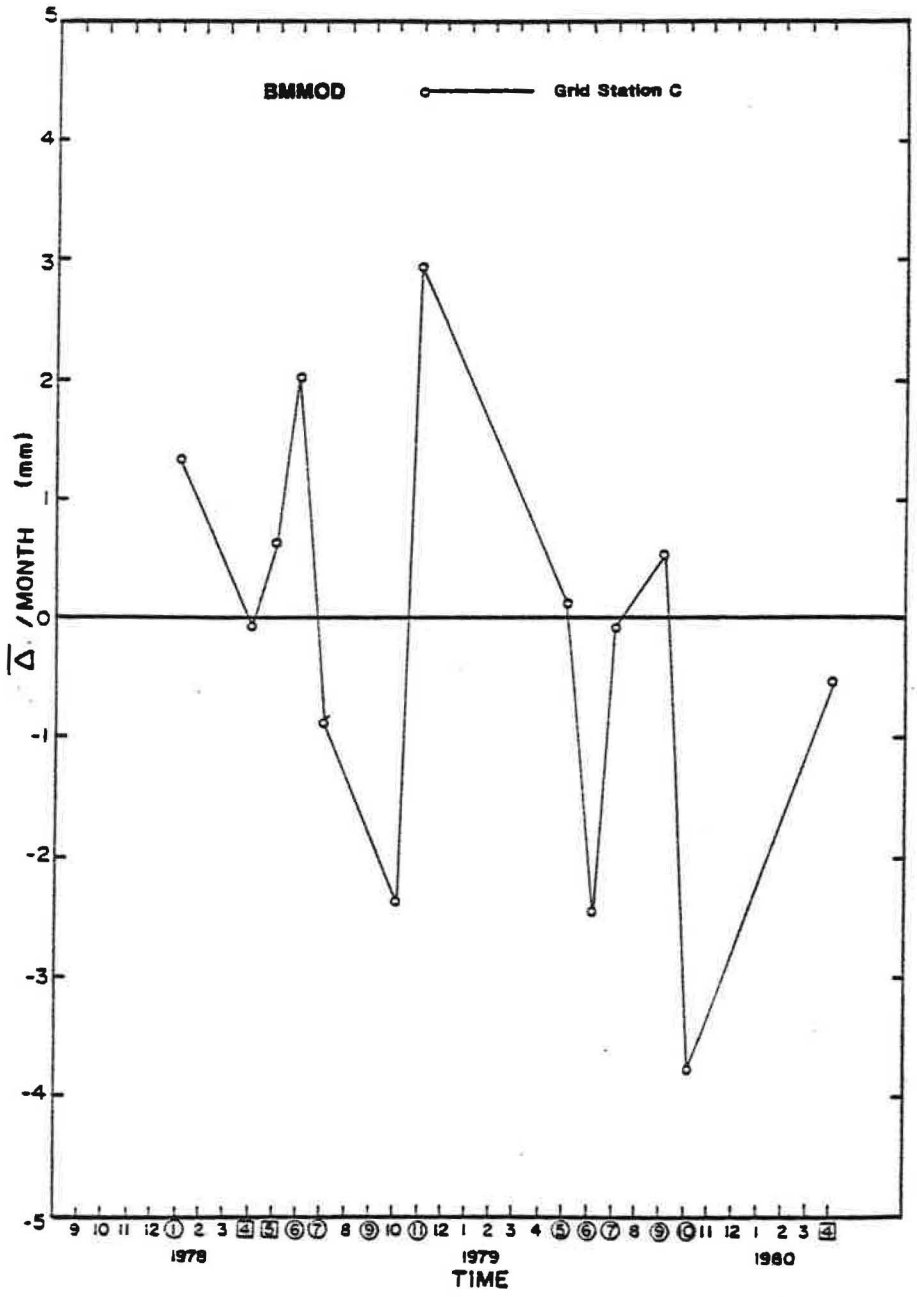


Figure 67: Seasonal Variations in Ground-Surface Elevation for the Erosion-Grid Station with in the BMMOD Study Basin. Circled Numbers on Time Axis are the Months of Field Measurements. Boxed Numbers are Field Measurements Affected by Frost-Heave.

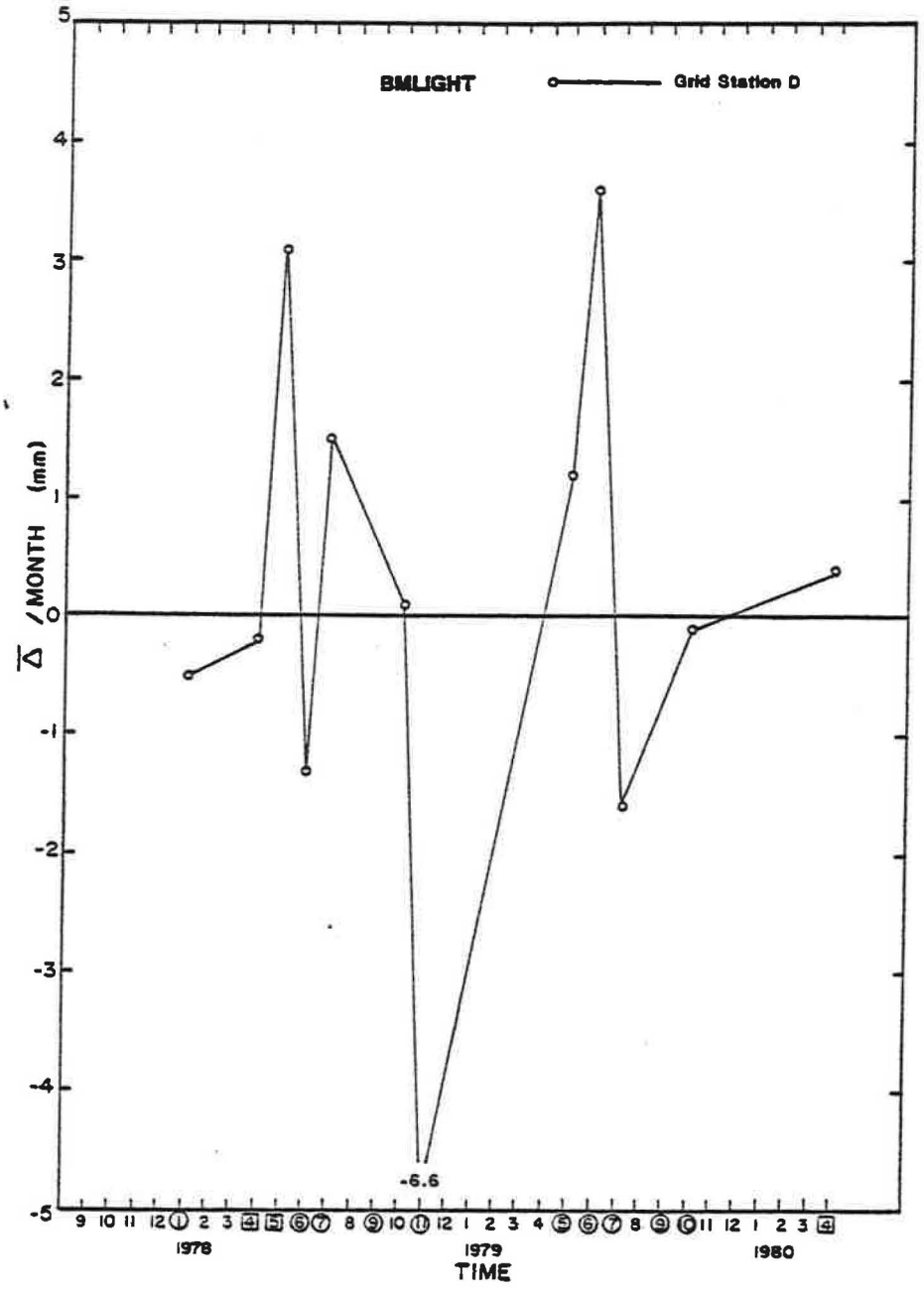


Figure 68: Seasonal Variations in Ground-Surface Elevation for the Erosion-Grid Station within the BMLIGHT Study Basin. Circled Numbers on Time Axis are the Months of Field Measurements. Boxed Numbers are Field Measurement Affected by Frost-Heave.

important of which is the enhanced effect of mechanical weathering in devegetated watersheds at the time of the year when the perennial vegetation is the sparest. The beginning and end of a growing season are marked by diurnal temperature fluctuation around the freezing point. If there is significant soil moisture at this time, the ground surface will be disrupted by the heaving of fine-grained soil with ice crystal growth. When the ice thaws, the ground surface has an increased porosity, lacks cohesion, and is easily entrained by a runoff event (Fig. 49). The regrowth of perennial vegetation can reduce the effect of frost heaving in two ways. The roots can provide an anchoring effect during the ice crystal growth, or the vegetation can trap sediment in transport as the vegetation density increases through the growing season. The net aggradation within most of the study basins during the third year following the fire is largely due to grasses trapping sediment in transport on the hillslopes ($\bar{\Delta}$/yr of Table 9).

The monthly values for change in ground-surface elevation generally cluster around the zero line (datum) previous to and following the winter season (Figs. 59 through 68). The clustering around the datum during these periods can be interpreted as an indication that the winter season is a quasi-stable period during which the ground

surface is protected by snowpack. Should the snowpack be removed or not present at some point during the winter season, the ground surface would be as susceptible to erosion as during the spring and late fall season.

Grid-station plots exhibit larger seasonal variations in erosion rates than the erosion-pin plots (Figs. 66 through 68; Figs. 59 through 65, respectively). This disparity is due to the limited area within a grid station. The square meter of a grid station covers only a single slope type, and therefore, documents only one erosional process. Erosion-pin transects traverse all degrees of slope inclination, ground surface textures, and vegetational conditions present within a given basin. Therefore, the average change in ground-surface elevation for erosion-pin transects will represent a more moderate value for erosion than a restricted, meter-square measurement representing only one slope type and one erosional process.

Channel Processes and Morphologic Adjustments in Devegetated Watersheds

Ephemeral Channels in Mesa-Top Catchment Areas

The soils of the Frijoles Canyon watershed are better developed on the upper mesas, relative to the lower mesas, due to the greater amounts of precipitation the upper mesas receive (Earth Environmental Consultants Inc., 1978). The degree of soil development influences the pre-burn ephemeral channel morphology. The axial ephemeral drainage on the upper mesa in the Apache Springs area has a shallow, parabolic cross section with a loamy bed and dense vegetation (Fig. 51). On the lower mesas, where the degree of soil development is less, bedrock outcrops influence the morphology of the ephemeral channels to a greater degree (Fig. 69). The pre-burn morphology of the trunk ephemeral channel draining the upper and lower mesas can be described as a wide-to-confined, U-shaped, bedrock channel with varying densities of vegetation and thickness of sediment (Fig. 70).

The post-burn ephemeral channel morphology is dependent on the degree of revegetation. The upper mesas



Figure 69: Lower-Elevation Mesas Have a Thinner Colluvial Cover Than the Upper Mesas. Bedrock Outcrops Thereby Control the Morphology of the Ephemeral Channel to a Greater Degree.



Figure 70: Bedrock Constrictions in a Major Ephemeral Channel. Photograph Corresponds to Figure 45.

revegetated quickly, such that there is no significant change in channel morphology. The ephemeral channels of the lower mesas have a distinctly different post-burn morphology. Higher-order channels (e.g., the fourth-order channel draining the BMMOD and BMINT study basins) are choked with sediment resulting in wide, flat-bottomed, braided channels (Fig. 43). High-order (greater than third order) ephemeral channels are areas of significant temporary storage of the excess sediment being produced as a result of the La Mesa fire (Fig. 71).

A secondary, but still significant, storage area of fire-associated sediment is the plunge pools marking the junction of trunk ephemeral canyons with the Rito de los Fijoles (Fig. 72). Sediment delivered over these nickpoints is splashed to the margins of the plunge pool and builds high channel banks along the exit of the pool. The portion of sediment being discharged to the Frijoles Canyon bottom is deposited along point bars, and as overbank deposits on the floodplain.



Figure 71: Wide Channel Reaches of High-Order (> Third Order) Drainages Provide Storage for Fire-Associated Sediment.



Figure 72: Plunge Pools Provide Storage of Fire-Associated Sediment. Notebook Measures 13 by 19.5 cm.

Perennial Channel - Rito de los Frijoles

The pre-burn morphology of the Rito de los Frijoles varies along the length of its course. In general, the Rito de los Frijoles occupies an incised alluvial floodplain bounded by steep walls of Bandelier Tuff. The channel is a meandering, flat-bottomed channel with a shallow to deep, U-shaped cross section. The cut banks range in height from 0.4 to 2 m and point bars range 0.1 to 0.6 m in height. The width/depth ratio is low, indicating a high percentage of silt-clay in the channel banks (Schumm, 1977). The channel bed is armored with cobbles.

In an erosion study following a wildfire in a ponderosa pine setting in Arizona, Rich (1962) observed that deposition of fire-derived sediment occurred on the floodplain, above the level of normal discharge for the perennial stream. The low-water channel experienced some deepening and scouring. In the Bandelier National Monument, fire-derived sediment that is delivered to the perennial channel is carried by flood waters and deposited as overbank deposits on the floodplain (Fig. 73).



Figure 73: Overbank Deposits (Gray Area on Right) of Fire-Associated Sediment on the Floodplain of the Rito de los Frijoles.

The adjustments (i.e., channel widening) of the low-flow channel are most pronounced in the Headquarters area of the Monument. There was a distinct increase in bank undercutting following the La Mesa fire (J. Lissoway, personal communication, 1979). Figure 74 is a photograph of the Rito de los Frijoles channel upstream of the picnic area bridge at the Headquarters. Note the undercutting of the point bar bank and the lag gravel at the base of the cut bank in Figure 74.

The low-flow channel is transporting an increased bed load as a result of the La Mesa fire. Shifting of bars of fine gravels and sands over the cobble-armored bed of the Frijoles channel indicates bed-load transport. According to a treatment of hydraulic geometry by Schumm (1977), a channel experiencing an increased bed load may adjust width, depth, meander wavelength, channel slope and channel sinuosity to accomodate the increased bed load. In the Rito de los Frijoles channel, an increase in channel width initiated by bank undercutting is the most pronounced change in morphology in response to the increased bed load (Fig. 74). Channel depth likely decreases due to the observed presence of shifting bars of fire-derived sediment on the channel bed, but this is insignificant relative to the bank undercutting. The energy of the normal discharge of the Rito de los Frijoles is not sufficient to transport



Figure 74: Undercutting of the Banks of the Rito de los Frijoles, in Response to an Increased Bed Load Following the La Mesa Fire. Cobbles Derived From the Banks Further Armor the Channel Bed.

the cobbles being derived from the banks. The cobbles being derived from the channel banks provide additional armor to the channel bed. Down cutting of the channel is thereby inhibited.

Streamflow Behavior of the Rito de los Frijoles Watershed As Affected by the La Mesa Fire

The USGS operated a stream-gaging station on the Rito de los Frijoles in Bandelier National Monument from October 1963 to September 1969. The station was discontinued at the end of that period and was again made operational on July 7, 1977, 15 days following the La Mesa fire.

The shapes of the post-burn hydrographs are dramatically different from the pre-burn hydrographs (Figs. 75A and 75B). The hydrographs have been separated into surface-runoff and base flow components by a simple visual separation, as described by Gregory and Walling (1973). The separation is intended to define the relative amounts of surface runoff and base flow in each hydrograph. Interflow has not been considered here. The hydrographs are of runoff events which occurred during the summer thunderstorm season of each period of record.

Post-burn runoff is more flashy. That is, the flood peak is sharp, with steep limbs displayed on the hydrograph.

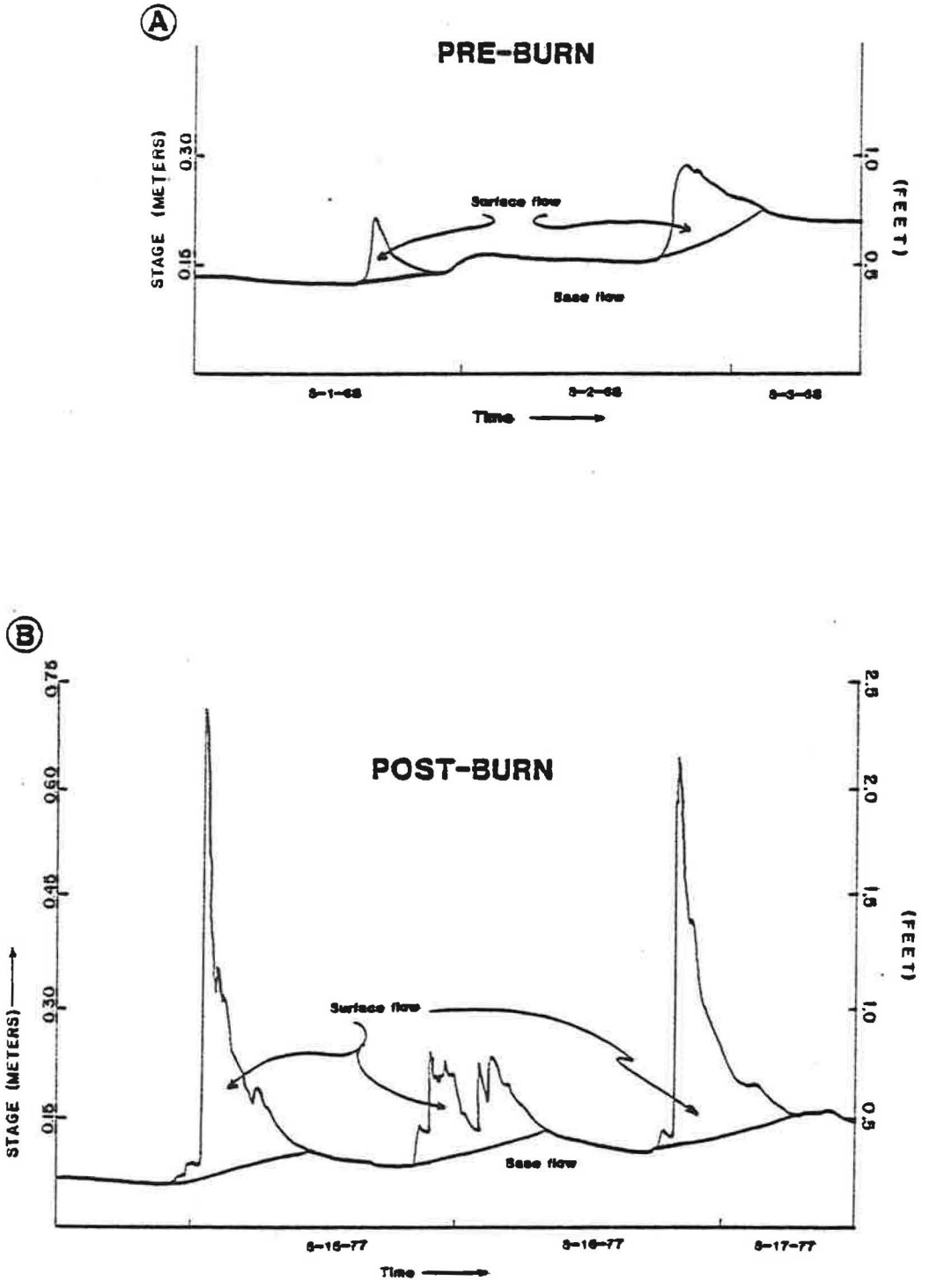


Figure 75. Hydrographs of Pre- and Post-Burn Streamflow for the Rito de los Frijoles, Bandelier National Monument.

The post-burn hydrograph illustrates a much larger surface runoff component, whereas the pre-burn hydrograph has a greater base-flow component (Figs. 75A and 75B). Vegetation and forest litter retards overland flow and promotes infiltration. The presence of vegetation in the pre-burn case gives rise to a reduced runoff peak and a large base flow which will recharge the stream for a longer period following the event, compared to the post-burn case. In the post-burn case, the removal of large areas of vegetation from the catchment areas produces a large surface runoff component which results in a rapid rise and fall in stage. Without the retarding influence of vegetation, in addition to many other fire-induced factors, there is little infiltration. Correspondingly, base flow contribution from the mesa-top catchments is less in the post-burn hydrograph relative to the pre-burn hydrograph.

Figure 76 and 77 are plots of mean discharge per month for the respective periods of record (U. S. Geological Survey, 1963-1969, 1977-1979). The season of peak runoff for the pre-burn record is the spring and late summer. This is also the trend in the post-burn record. However, it is apparent that the magnitude of the events is much greater in the post-burn record.

The variability of the stream flow can usefully be demonstrated by a flow duration curve (Gregory and Walling,

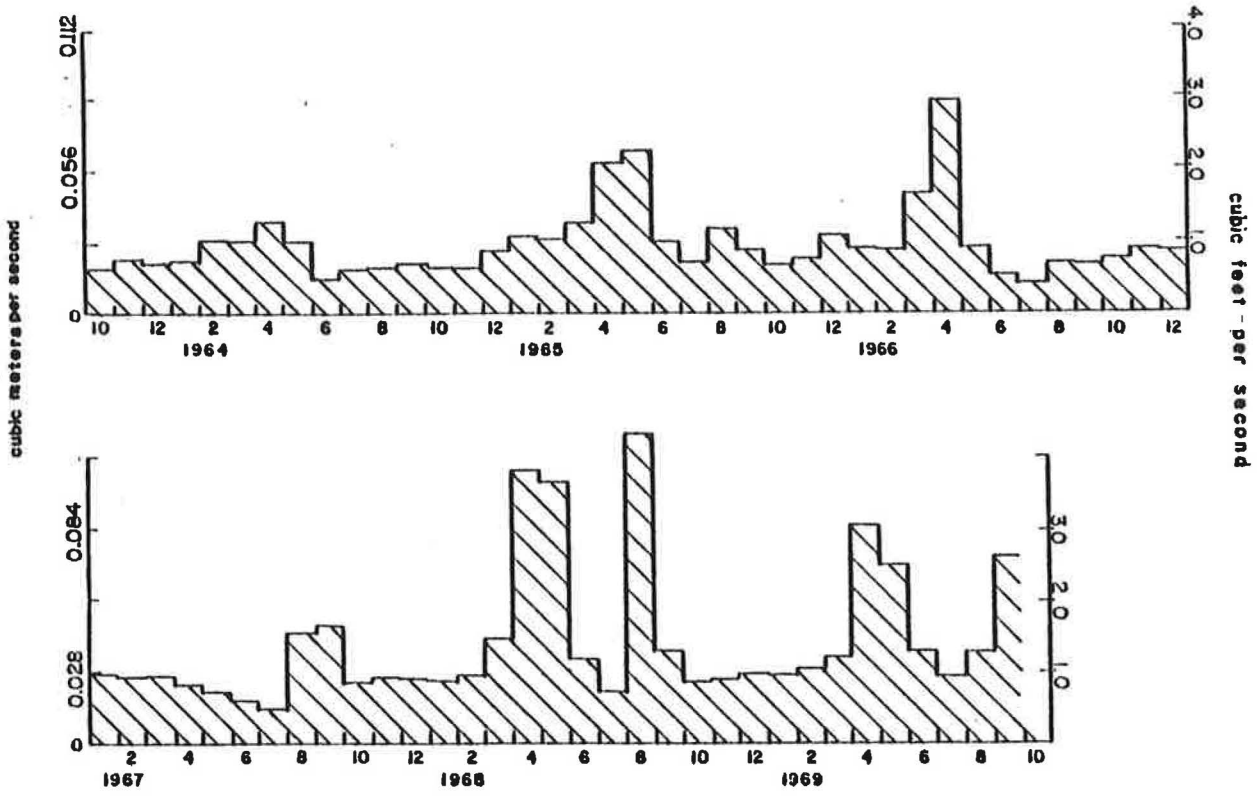


Figure 76. Mean Monthly Discharge for the Pre-Burn Record of the Rito de los Frijoles, Bandelier National Monument. Length of Record Requires a Break in the Histogram at the End of 1966. Numbers Correspond to the Month of the Year.

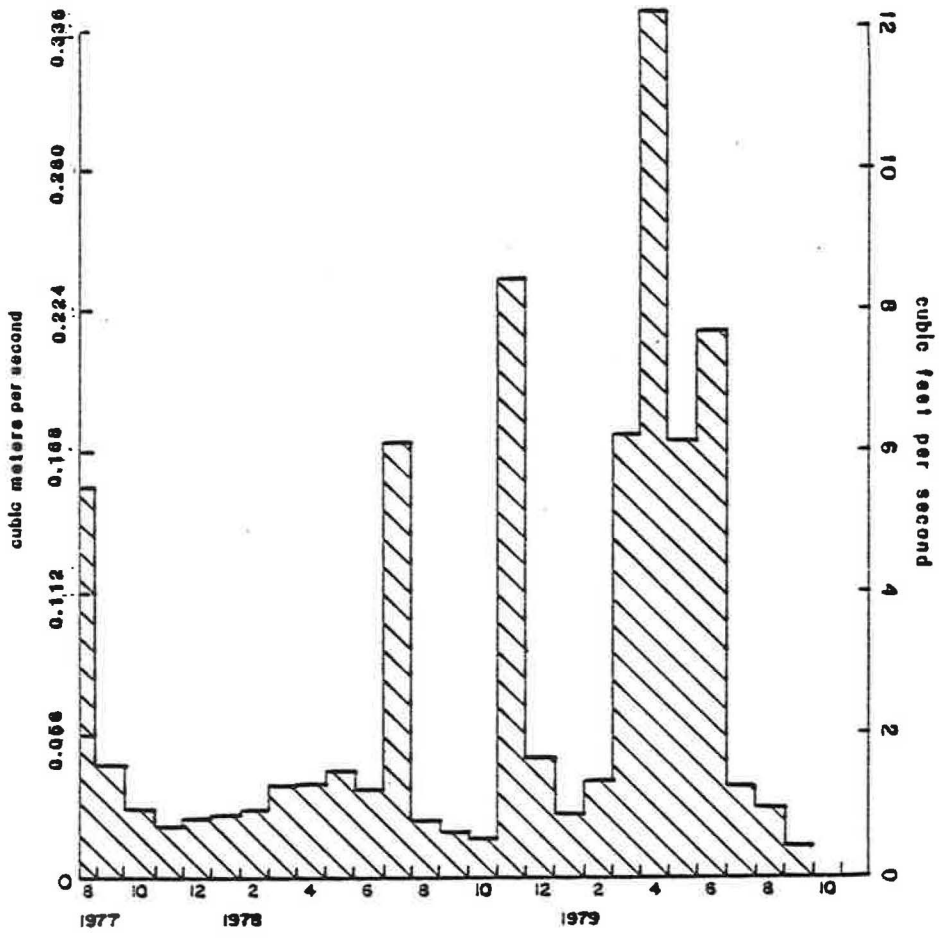


Figure 77: Mean Monthly Discharge for the Post-Burn Record of the Rito de los Frijoles, Bandelier National Monument.

1973). The flow duration curve displays the frequency at which flows of various magnitudes are equalled or exceeded. Figure 78 is a plot of the pre-burn and post-burn flow duration curves.

The departure of the post-burn trend from the pre-burn trend further illustrates the impact of the La Mesa fire on the hydrology of the Frijoles watershed. Figure 78 indicates that 60 percent of the time the post-burn discharge of the Rito de los Frijoles is greater than the discharge of the same frequency for the pre-burn record. Furthermore, 10 percent of the time the flow of the post-burn record exceeds the 0.1 percent frequency event of the pre-burn record. Figure 78 indicates that the high frequency events are of smaller magnitude following the La Mesa fire.

The three years of post-burn, stream flow records exhibit distinct changes from the trend of the six years of pre-burn record. With time, the difference between the lines in Figure 78 should diminish. The post-burn flow duration curve will approach the pre-burn flow duration curve based upon the fact that the study basins have experienced a net aggradation during the third year following the fire ($\bar{\Delta}$/yr of Table 9). The net aggradation is a result of the regrowth of vegetation. The vegetation will increase in density, providing greater obstruction to overland flow and promoting infiltration. A five year period is considered a minimum time required to accurately depict

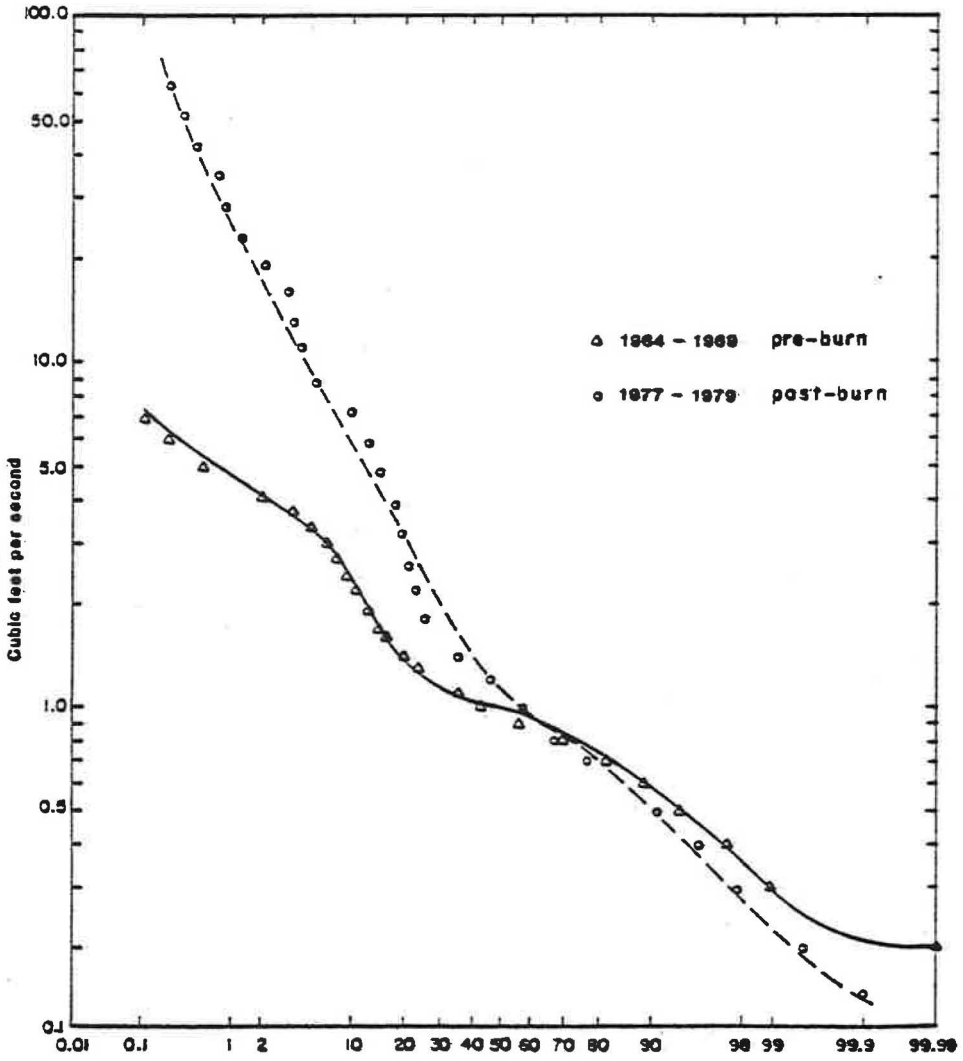


Figure 78: Flow Duration Curves for the Pre- and Post-Burn Records of the Rito de los Frijoles, Bandelier National Monument.

the long-term adjustments of the hydrologic behavior of a watershed to altered environmental conditions (B. Dean, personal communication, 1980). Irregularities of the post-burn flow duration curve are possibly a reflection of the brevity of the record.

Morphometry and Forest-Fire Devegetation

There are differences in drainage pattern, drainage density, and stream bifurcation between the physiographic areas within the Frijoles Canyon watershed. The headwater physiographic unit has developed a different drainage pattern than the mesa-top physiographic region. The headwater region has a dendritic to sub-parallel drainage pattern due to the long slopes of the volcanic domes. The mesas have a dendritic to trellis pattern. The dendritic drainage pattern is a result of the homogeneity of the bedrock. The trellis drainage pattern is due to the numerous first-order stream segments draining the mesa side slopes, joining trunk canyons at nearly right angles. The north canyon can be distinguished from all other areas by: (1) greater number of stream segments for all stream orders, (2) shorter first-order streams, and (3) longer high-order streams (Table 7).

Area	Drainage Density km/km^2	Weighted Mean Bifurcation Ratio
East Fork	9.77	4.86
West Fork	10.22	5.13
North Canyon	9.42	5.97
South Canyon	7.38	5.54

Table 10: Drainage Density and Bifurcation Ratios for the Physiographic areas of the Frijoles Canyon Watershed.

Table 10 is a summary of the drainage density and bifurcation ratios (the ratio of the number of streams of given order (n) to the number of streams of the next highest order (n + 1)) for each area. The range in drainage density and weighted mean bifurcation ratio is not great due to the near homogeneity of the lithology of the watershed.

The headwater areas have a high relative drainage density and low bifurcation ratios. This is a result of the domal features of the caldera rim. The first-order drainages are closely spaced (sub-parallel) on the domal slopes and are elongate, giving rise to the low bifurcation ratios.

The mesa-top areas have relatively lower drainage density and high bifurcation ratios. The low drainage densities are due to the low relief (relative to the headwater areas) of the mesa-top catchments, and larger areas of canyon wall with no mesa-top catchment contributing surface runoff

to the canyon wall (south wall of Frijoles Canyon, especially in the lower basin). The high permeability of the uniform bedrock lithology (Bandelier Tuff) contributes to a low drainage density. The high bifurcation ratios are a result of the low relative relief of the mesa tops, and are a reflection of a high number of stream segments within the mesa-top catchments (Table 7).

Morphometric analysis yields relationships which define landform components that are most susceptible to erosion. The morphometric analysis of the Frijoles Canyon watershed indicates a high number of first-order drainages dissecting the gently to moderately sloping mesa tops of the north canyon area. This is reflected by a high bifurcation ratio (Table 10). The high number of short, first-order stream segments are efficient at delivering sediment from hillslopes to higher-order streams. At the scale at which the analysis was conducted, the axial drainage below the confluence of the BMMOD and BMINT study basins is a first-order stream segment. At the scale of field instrumentation, the drainage line is fourth order. Cut and fill processes are documented by the chain transect traversing the axial drainage (Figs. 42 and 43). The cutting and filling of the channel indicates that the drainage network is efficient in delivering sediment to the trunk ephemeral drainage line.

The north canyon area is the largest area of the Frijoles watershed (55 percent of the watershed area) and

is comprised of upper and lower mesa segments. As discussed earlier, the upper mesas have stablized within two growing seasons following the La Mesa fire. The lower mesas are dissected by a high number of short, first-order stream segments. The high number of first-order streams is an indication that the lower mesas are the landform components most susceptible to erosion (map unit M1 of Plate 1). The south canyon area contains segments of upper mesas only.

The north canyon area is cut by long, trunk drainage lines. The long, trunk ephemeral drainages provide temporary storage of fire-associated sediment that is rapidly flushed to these drainage lines by short, first-order stream segments. These trunk ephemeral drainages are, therefore, the second most susceptible landform component affected by the La Mesa fire (Map unit M3 of Plate 1). A heavy precipitation event in the north canyon area will produce large volumes of storm runoff and sediment yield. The confluence of the ephemeral tributaries draining the north canyon area with the Frijoles Canyon occur primarily in the lower portion of the Frijoles Canyon, above the Monument Headquarters. The concentration of large flood events occurs in the lower Frijoles Canyon, and correspondingly, the modern floodplain in the lower Frijoles Canyon (Map unit CF2 of Plate 1) is the third most susceptible landform to fire-induced changes.

Process-Response Model in Devegetated Watersheds

The La Mesa fire directly altered runoff and sediment yield relationships in the Frijoles Canyon watershed. As a result of the fire, greater volumes of runoff and sediment are delivered to the trunk drainage line. The responses of the trunk stream (Rito de los Frijoles) to the altered conditions affect tributary drainages. However, the Frijoles fluvial system is characterized by a perennial, trunk stream with 20 to 60 m nickpoints at the confluences of major tributaries. Adjustments of the Rito de los Frijoles cannot be transmitted upstream beyond these nickpoint confluences. Adjustments can be transmitted upstream along first-order drainages developed on the Frijoles Canyon walls.

White and Wells (1979, p. 217) developed a process-response model for devegetated fluvial systems in the Jemez Mountains. Their model is presented herein with little modification:

> "The model shows the importance of seasonal variations in sediment delivery from the mesa-top tributaries. In Figure 79 geomorphic responses and sediment transport

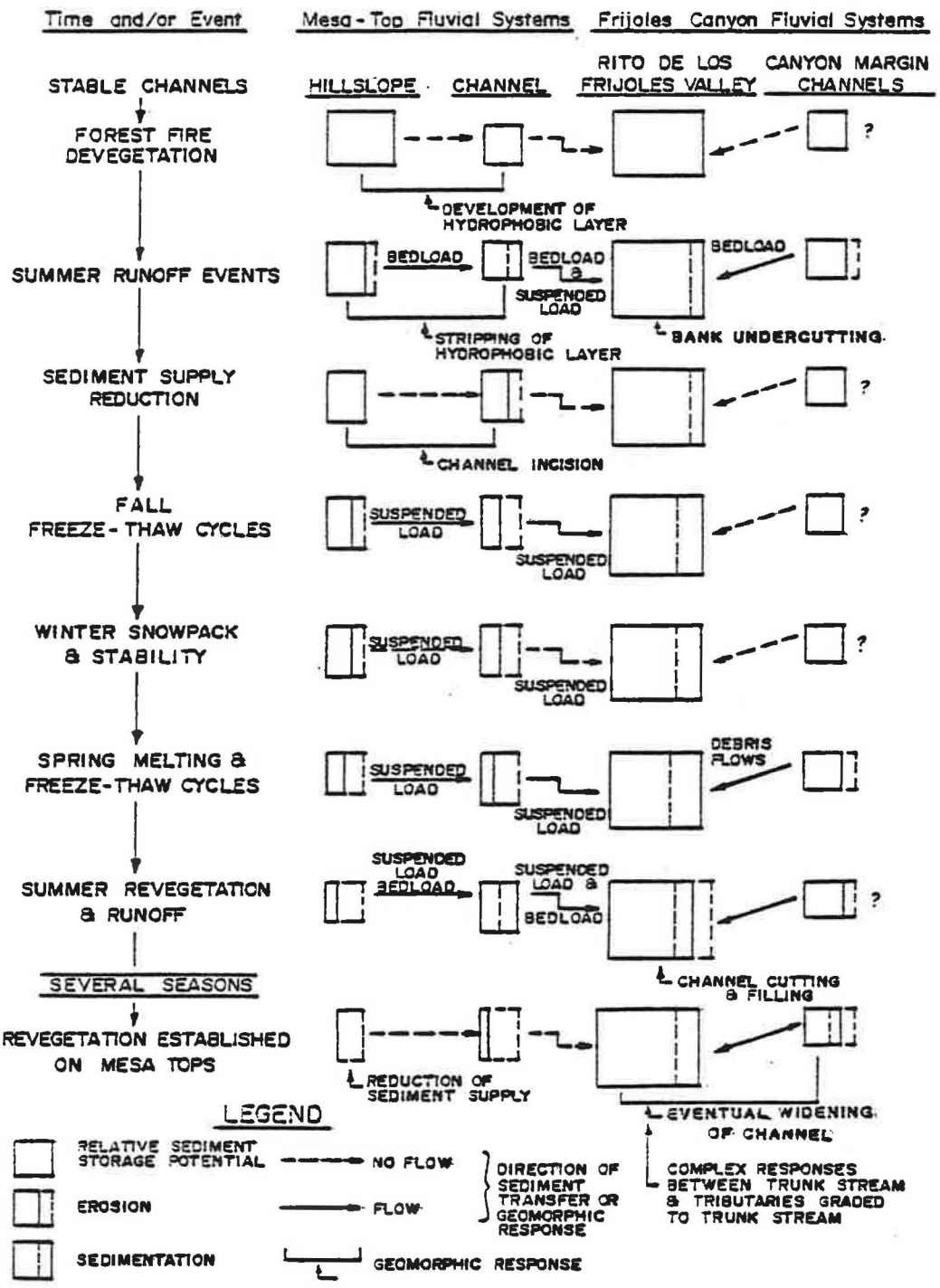


Figure 79: Process-Response Model of Devegetated Fluvial Systems (Modified from White and Wells, 1979).

are illustrated by the arrows, and the volume of sediment storage on hillslopes, in channels, and in valleys is indicated by the relative size of the boxes. The model (1) illustrates the continuous decrease in sediment supply from the mesa-top systems to the Frijoles Canyon, (2) illustrates the continued response of fluvial systems in the canyon to devegetation after geomorphic stability is attained on the mesa tops, and (3) emphasizes that tributaries in a fluvial system may adjust dependently or independently of the master drainage line. Complex responses (Schumm, 1977) are typical in streams with alluvial valleys, whereas in mountainous terrain the bedrock nickpoints act as barriers to interactions between components of the fluvial systems and reduce adjustments between tributaries and trunk streams."

SUMMARY AND INFERENCES

Catastrophic events, such as forest fires, can trigger complex geomorphic responses in watersheds due to removal of the protective cover of vegetation and exposure of the soil to raindrop impact. If removal of the vegetational cover coincides with the rainy season of the area, then the geomorphic work (runoff and erosion) done on the watershed system is maximized. Schumm's (1977) figure relating abrupt climatic change to vegetational change and geomorphic response has been modified to illustrate this point (Fig 80). A forest fire can reduce the vegetation from a maximum density to a minimum density in a short period of time. The coincidence of maximum seasonal precipitation with the devegetation results in the maximum geomorphic work being done on a watershed system. The period following the fire shows a gradual revegetation and a corresponding reduction of geomorphic work (i.e., erosion), except during periods of intense seasonal precipitation. With time, the revegetation is maximized and the geomorphic work done on the system is minimized.

Factors which influence the amount of geomorphic work done in the devegetated Frijoles watershed system are:

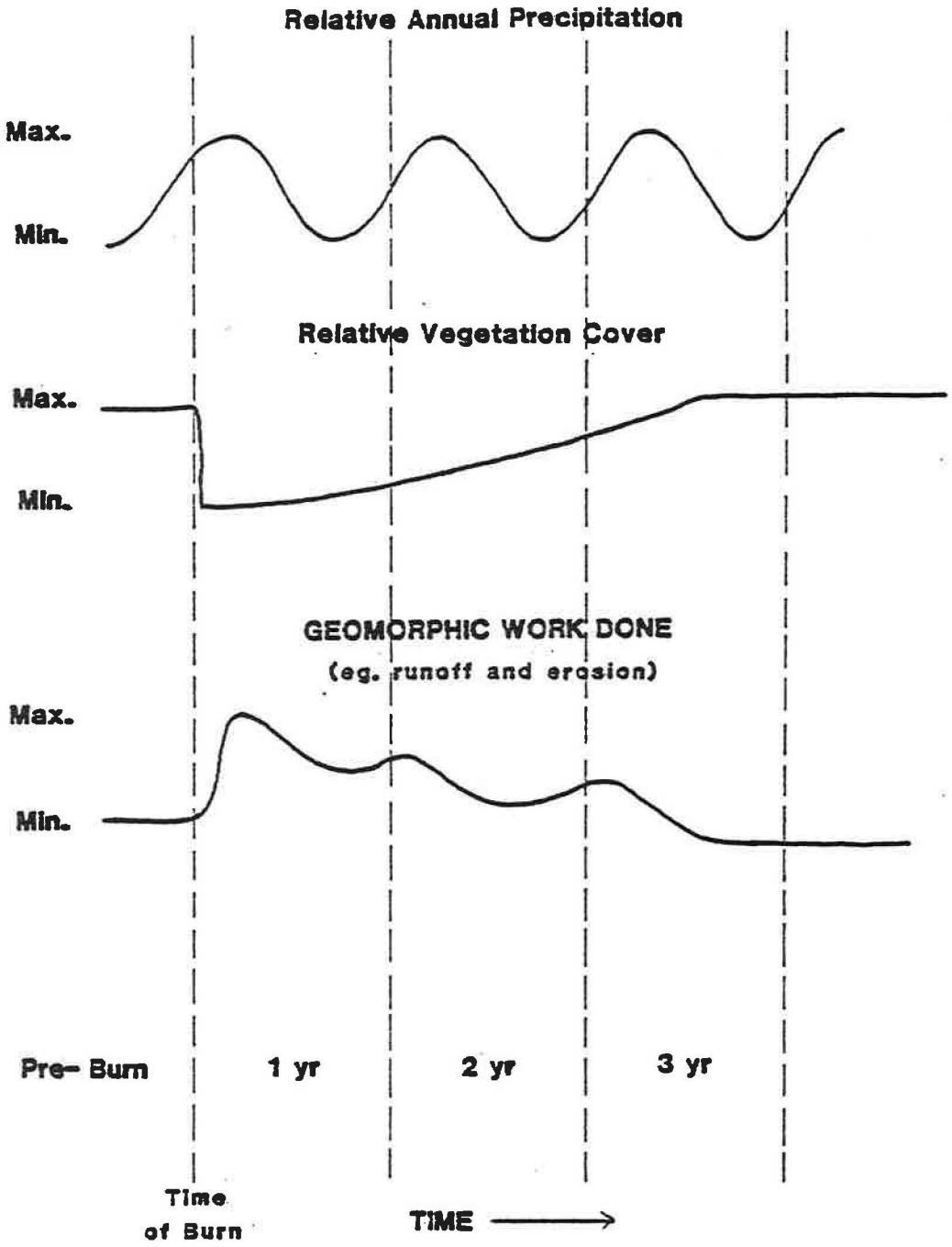


Figure 80: Geomorphic Response to Precipitation Events Following Devegetation by Forest Fire (modified after Schumm, 1977).

(1) mechanical weathering (i.e., frost heave),

(2) development of an impermeable ash layer,

(3) burrowing activity of animals, and

(4) post-burn needle cast.

The relief provided by the fault-line scarp occurring in the mid-portion of the Rito de los Frijoles watershed influences the climatic characteristics of the watershed. The upper mesas (to the west of the fault-line scarp, Fig. 2) receive a greater amount of annual precipitation (relative to the lower mesas) and have a better developed soil profile (Earth Environmental Consultants Inc., 1978). The degree of soil development and the greater amounts of precipitation the upper-elevation mesas receive contribute to the success of revegetation on the upper mesas. The rapid revegetation stabilized erosion of the valley-side slopes. This stabilization is evident by the lack of sediment in the axial drainage (Fig. 51).

The lower-elevation mesas are found to be the landform components most susceptible to erosion. Following the La Mesa fire, overland flow is increased due to the lack of vegetation and the decreased infiltration capacity of the burned forest soils. The greater volumes of overland flow promotes the development of new rill systems. Rill development is most active in the extension of headwater drainage lines and in the dissection of side slopes below bedrock outcrops usually associated with the headwaters of the

study basins. The increase in channelized flow increases the runoff and sediment load the channel of these headwater drainage basins must carry. The channel at the basin mouth will alternately cut and fill, depending on the season and the availability of sediment. Steep (> 10°) slopes adjacent to drainage lines and slopes with a well-developed ash layer are most susceptible to fire-induced erosion. These conditions (i.e., steep slopes, ash layers) promote rilling and rapid sediment removal from hillslopes. The mid-basin regions are less dissected by drainage lines, the length of overland flow is greater, and the mid-basin hillslopes are generally less steep relative to the headwater regions. Therefore, the primary source areas of fire-derived sediment are the headwaters and the basin mouths of headwater basins on the lower mesas. Furthermore, in an area already dissected by a high number of first-order drainages, the post-fire increase in rilling enhances the efficiency of sediment removal from the hillslopes and delivery to the trunk drainage lines. With time, the continued effect of frost heave and the regrowth of vegetation will destroy the character of the impermeable ash layer. The extent of post-fire rilling will decrease, resulting in a decrease in the efficiency of sediment removal.

EECI (1978) determined a pre-burn erosion rate of 5.3 mm/yr for the lower mesas of the Bandelier National Monument. The post-burn erosion rate calculated during

this study for a rapidly burned-over archaeological site on the lower mesas (BMARCH) is 5.7 mm/yr. The calculated value for the BMARCH site suggests the continuance of the pre-burn erosion rate. Both values exceed most of the calculated annual erosion rates for the study basins (Table 9). Areas within a naturally eroding (i.e., not fire-induced erosion) environment will not experience the same erosion rate throughout. Some areas may contribute greater amounts of sediment than others; some areas may not contribute any sediment at all. It is proposed that fire-induced erosion may not increase the erosion rate of a previously actively eroding environment, but only temporarily increases the number of areas contributing sediment to trunk drainage lines.

The length of the ephemeral trunk drainages of the north canyon area allows for the accumulation and temorary storage of fire-associated sediment. The channel morphology of the trunk drainages at lower elevations was changed from a wide-to-narrow, shallow parabolic bedrock channel with some sediment, to a wide-to-narrow, flat-bottomed braided channel. Runoff events occurring in the summer of 1980 were observed to be cutting and transporting the fill in the ephemeral channels as evidenced by inset terraces of fire-associated sediments along the channels Fig. 71).

The low-flow channel of the Rito de los Frijoles is experiencing bank undercutting. However, the post-burn

volume of flow for high-frequency events (occurring often) is less than the pre-burn record (Fig. 78). The lower-volume, high-frequency runoff is not responsible for bank undercutting. Bank undercutting is suggested to be a result of the increased frequency of larger magnitude runoff events, and to abrasion of the channel banks by the increased bed load. The regrowth of vegetation will gradually reduce runoff; sediment temporarily stored along ephemeral drainages will either be discharged or stabilized by the returning vegetation. As the frequency of larger magnitude runoff events decreases, and the bed load of the Rito de los Frijoles decreases, the accelerated bank undercutting will decrease. The undercut banks of the Rito de los Frijoles will collapse with time, and a net widening of the perennial channel will result.

The lower mesas of the Frijoles watershed were found to be the most susceptible to erosion following wildfire devegetation. The La Mesa fire altered the runoff characteristics of the watershed system. However, with time, the continued regrowth of vegetation on the lower mesa tops will reduce the volume of sediment delivered to the trunk drainage lines. Net gain within the study basins during the third year following the fire (Table 9) is an indication that fire-induced erosion peaked two years following the La Mesa fire.

The responses of a different portion of the Pajarito Plateau to another large wildfire could be predicted by a morphometric analysis. Areas dissected by a high number of first-order stream segments will produce large quantities of sediment. The presence of long, ephemeral trunk drainages will mark areas of fire-derived sedimentation. If there is no ephemeral trunk drainage providing storage of fire-derived sediment, it is expected that floodplain deposition and channel widening of a perennial channel would be more pronounced.

CONCLUSIONS

1. Factors of importance in the erosion of devegetated hillslopes within the Frijoles Canyon watershed are:
   (1) frost action,
   (2) fire-associated ash layer formation,
   (3) post-burn needle cast,
   (4) burrowing activity of animals, and
   (5) type and length of hillslope.
2. The spring season is the time of the year when devegetated hillslopes are most susceptible to erosion.
3. Fire-induced erosion peaked during the second year following the La Mesa fire.
4. Post-burn runoff of the perennial Rito de los Frijoles is more flashy than under pre-burn conditions.
5. The landform components most affected by the La Mesa are the lower-elevation mesas (further depletion of the colluvial cover in an actively eroding environment) and the perennial Rito de los Frijoles channel in the lower portion of the Frijoles Canyon watershed (undercutting and widening of the incised channel).

Appendix I

Grain-Size Distributions

For All Study Basins Except

BMINT

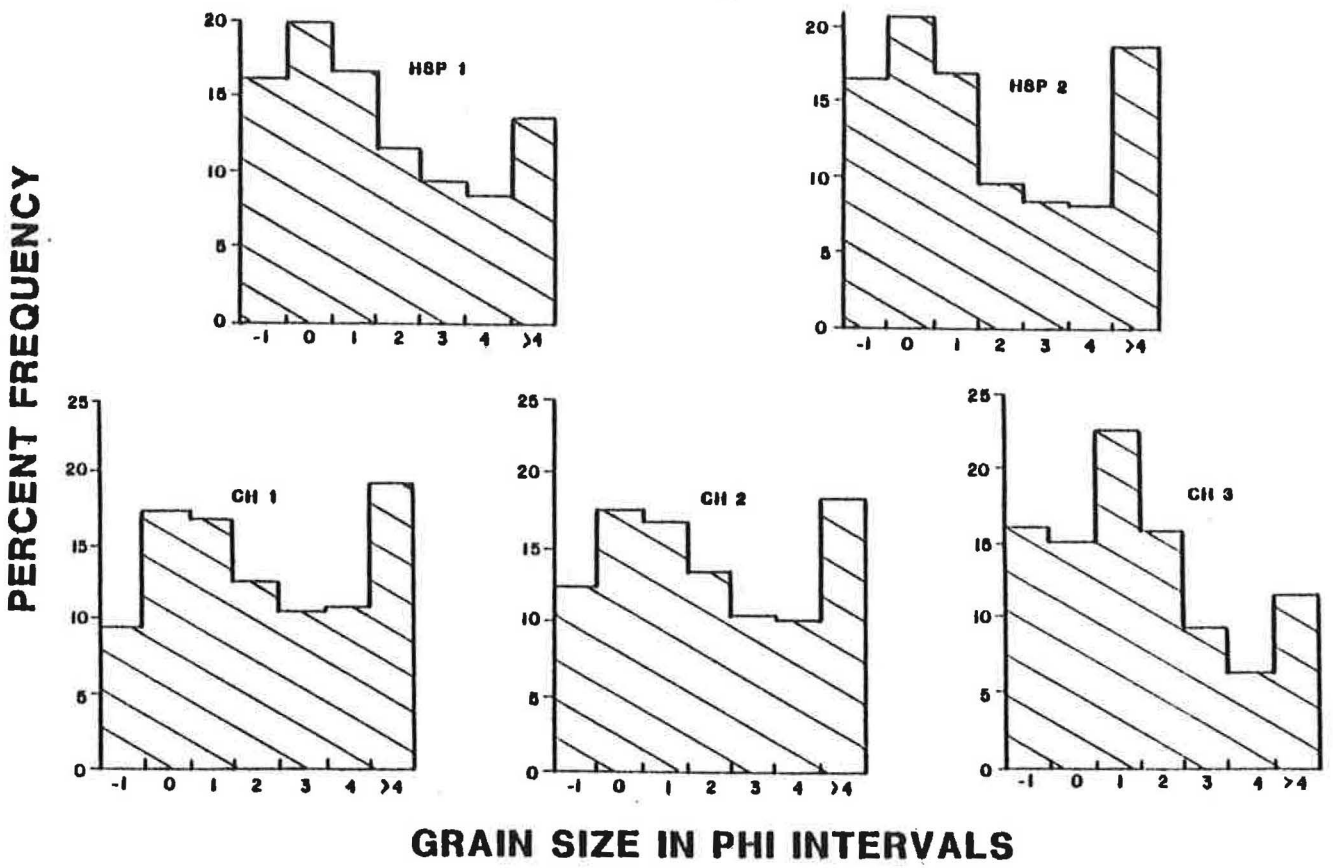


Figure IA: Grain-size Distributions of Hillslope and Channel Samples Taken from BMMOD.

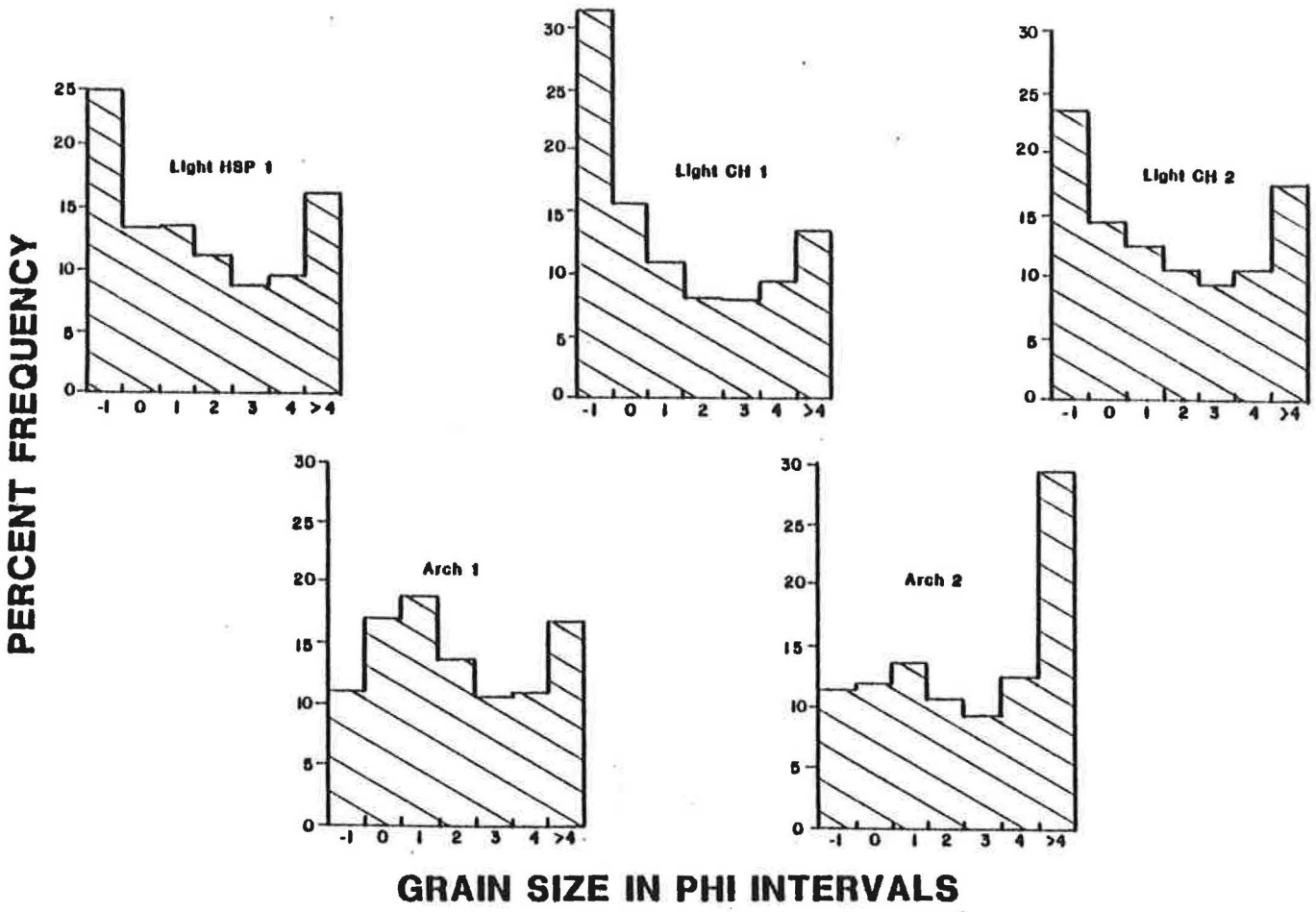


Figure IB: Grain-size Distributions of Hillslope and Channel Samples Taken from BMLIGHT and BMARCH.

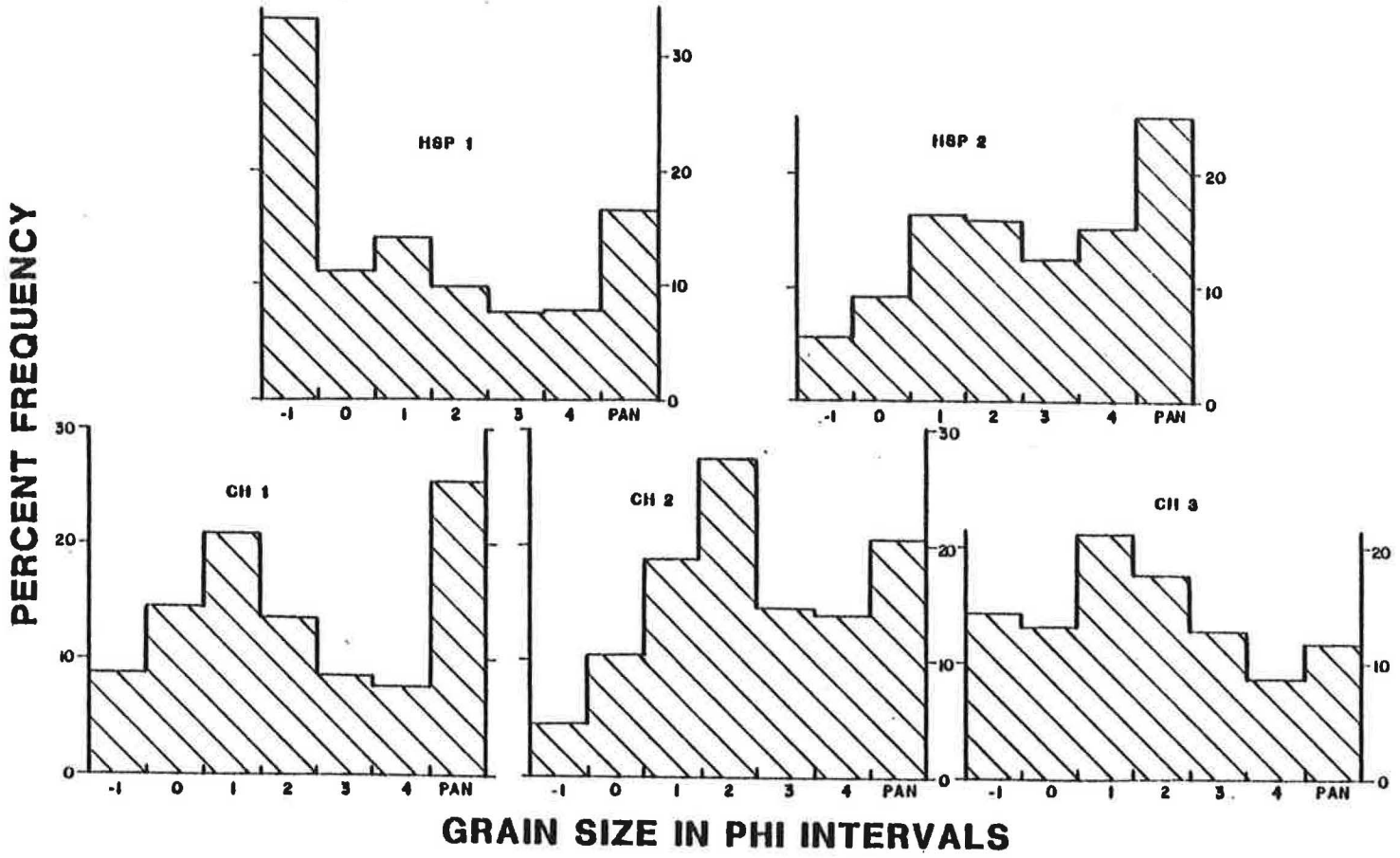


Figure IC: Grain-size Distribution of Hillslope and Channel Samples Taken from ASINT.

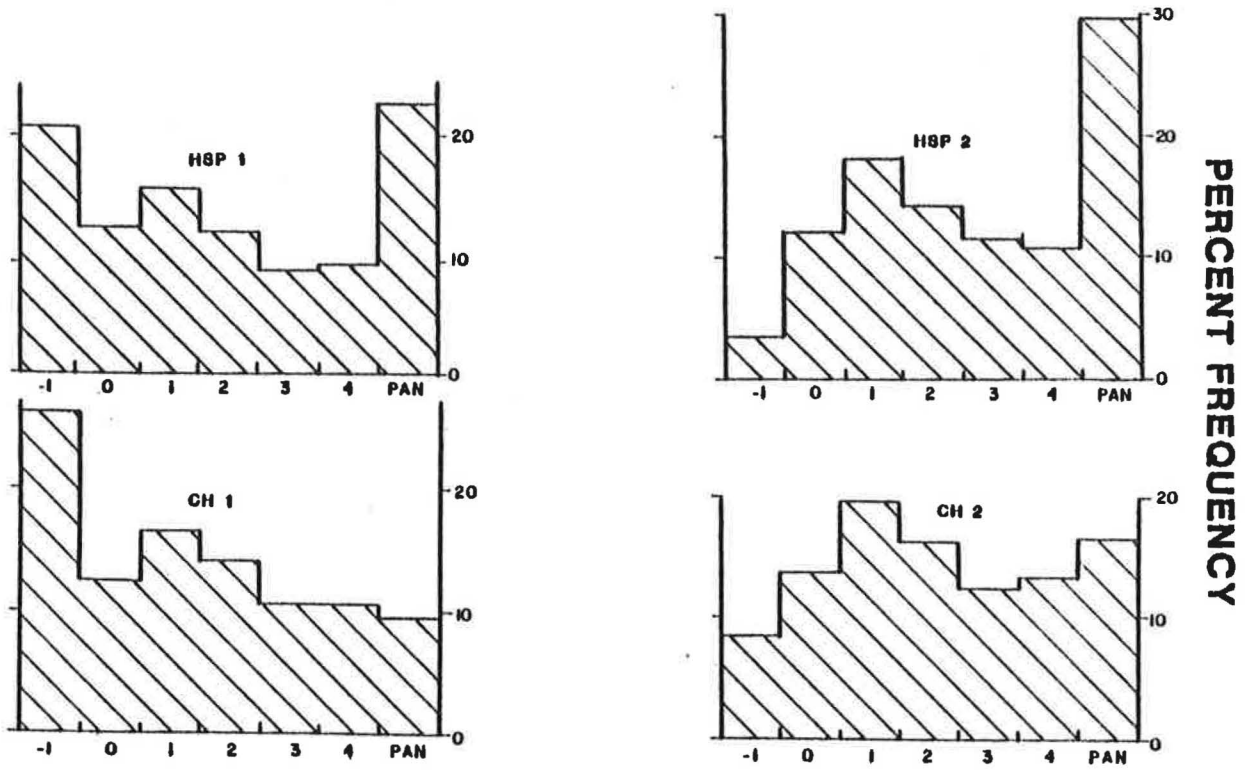


Figure ID: Grain-size Distribution of Hillslope and Channel Samples Taken from ASMOD.

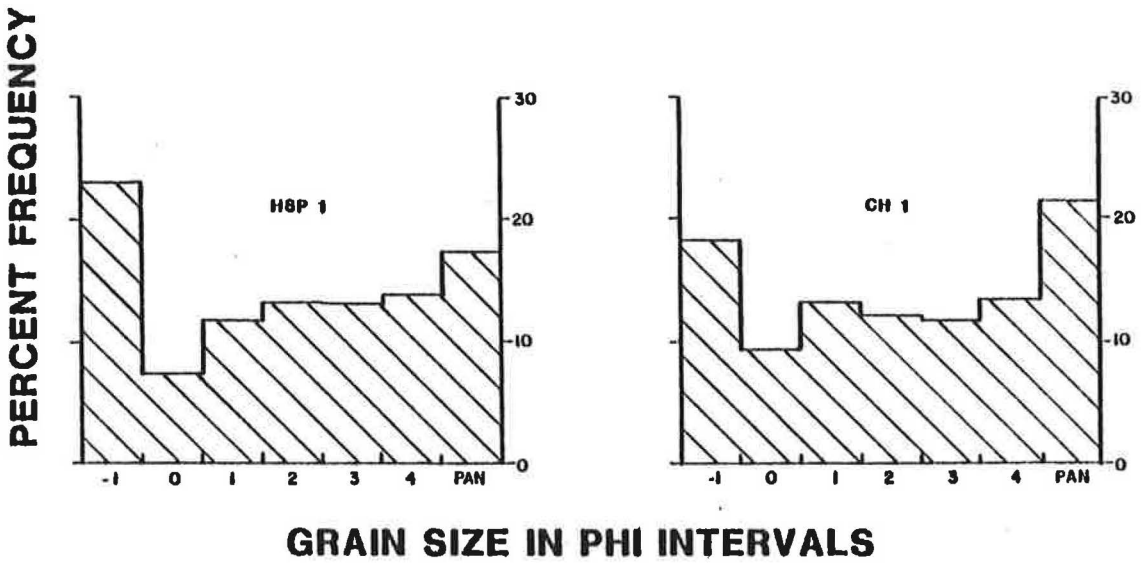


Figure IE: Grain-size Distribution for Hillslope and Channel Samples Taken from ASLIGHT.

Appendix II

Erosion-Pin Measurements

For All Sites

The data tabulated in this appendix are summaries of erosion-pin measurements for all study sites. The values tabulated are arrived at by reducing the erosion-pin data for each transect. For a given measurement date, the method of data reduction is as follows:

(1) The loss in ground-surface elevation at each pin is summed for a given transect ("Σ of Loss" in tables); the gain in ground-surface elevation over each washer is summed for a given transect ("Σ of Gain" in tables).

(2) The two summation values are arithmetically added for each transect to arrive at a net change in ground-surface elevation along a a given transect ("Net Δ" in tables). The Net Δ can be positive (net gain) or negative (net loss).

(3) The Net Δ is then divided by the number of pins along a given transect to arrive at an average change in ground-surface elevation (gain or loss) along a given transect ("Average Δ per transect" in tables).

(4) The change in ground-surface elevation from one measurement date to the next is arrived at by taking the average change for a given transect and subtracting the previous date's average change. For example, using the 12-77 and 4-78 average change values from the BMINT, transect A (Table IIA): (-1.8)-(-2.7) = +0.9. In this example, +0.9 represents a gain along transect A from 12-77 to 4-78 ("Δ between measurement" in tables).

(5) Each "Δ between measurement" value is then normalized by dividing each value by the number of months intervening between measurement dates ("numer of months" in tables).

(6) The final product is the average change in ground-surface elevation along a given transect, in millimeters per month ($\bar{\Delta}$/month).

Study Basin	Date	Change in Ground Surface Elevation (mm): Σ of Loss All Values Negative	Σ of Gain All Values Positive	Net Δ	Average Δ per Transect	Δ Betweem Measurement	Number of months	$\bar{\Delta}$ /month (mm)
BMINT	10-77	17.5	0	-17.5	-0.2	-0.2	1	-0.2
	12-77	332.5	94.5	-238	-2.7	-2.5	2	-1.2
Tran A	4-78	250	91	-159	-1.8	+0.9	4	+0.2
88 pins	5-78	398	129	-269	-3.1	-1.3	1	-1.3
Length =	6-78	457	148	-309	-3.5	-0.4	1	-0.4
52.7 m	7-78	501	186	-315	-3.6	-0.1	1	-0.1
	5-79	904	263	-641	-7.3	-3.7	10	-0.4
	6-79	1066	242	-824	-9.4	-2.1	1	-2.1
	7-79	1022	259	-763	-8.7	+0.7	1	+0.7
	9-79	1266	284	-982	-11.2	-2.5	2	-1.2
	10-79	1101	300	-801	-9.1	+2.1	1	+2.1
	4-80	1203	489	-714	-8.1	+1.0	6	+0.2
Tran B	10-77	1.5	0	-1.5	-0.1	-0.1	1	-0.1
42 pins	12-77	22.5	71	+48.5	+1.2	+1.3	2	+0.6
Length =	4-78	65.5	48	-17,5	-0.4	-1.6	4	-0.4
36.5 m	5-78	120.5	32.5	-88	-2.1	-1.7	1	-1.7
	6-78	132	50	-82	-2.0	+0.1	1	+0.1
	7-78	155	73	-82	-2.0	0.0	1	0.0
	5-79	354	94	-260	-6.2	-4.2	10	-0.4
	6-79	396	140	-256	-6.1	+0.1	1	+0.1
	7-79	475	67	-408	-9.7	-3.6	1	-3.6
	9-79	457	177	-280	-6.7	+3.0	2	+1.5
	10-79	439	148	-291	-6.9	-0.2	1	-0.2
	4-80	469	305	-164	-3.9	+3.0	6	+0.5

TABLE IIA: Summary of Erosion-Pin Data for the BMINT Basin.

Study Basin	Date	Change in Ground Surface Elevation (mm): Σ of Loss All Values Negative	Σ of Gain All Values Positive	Net Δ	Average Δ per Transect	Δ Between Measurement	Number of months	$\bar{\Delta}$ /month (mm)
BMINT	10-77	7.5	0	-7.5	-0.5	-0.5	1	-0.5
	12-77	29	2	-27	-1.7	-1.2	2	-0.6
Trans C	4-78	49.5	2	-47.5	-3.0	-1.3	4	-0.3
16 pins	5-78	72	0	-72	-4.5	-1.5	1	-1.5
Length =	6-78	69	3.5	-65.5	-4.1	+0.4	1	+0.4
10.8 m	7-78	116.5	2	-114.5	-7.2	-3.1	1	-3.1
	5-79	213	9	-204	-12.8	-5.6	10	-0.6
	6-79	237	19	-218	-13.6	-0.8	1	-0.8
	7-79	244	33	-211	-13.2	+0.4	1	+0.4
	9-79	258	66	-192	-12.0	+1.2	2	+0.6
	10-79	247	33	-219	-13.4	-1.4	1	-1.4
	4-80	234	103	-131	-8.2	+5.2	6	+0.9

Table IIA: (Cont'd) Summary of Erosion-Pin Data for the BMINT Basin.

Study Basin	Date	Change in Ground Surface Elevation (mm): Σ of Loss All Values Negative	Σ of Gain All Values Positive	Net Δ	Average Δ per Transect	Δ Between Measurement	Number of months	$\bar{\Delta}$ /month (mm)
BMMOD	10-77	10.5	0	-10.5	-0.8	-0.8	1	-0.8
Tran A	12-77	11.5	2	- 9.5	-0.7	+0.1	2	+0.0
13 pins	4-78	15	7	- 8	-0.6	+0.1	4	+0.0
Length =	5-78	25	2	-23	-1.8	-1.2	1	-1.2
16.7 m	6-78	30	7	-23	-1.8	0.0	1	0.0
	7-78	33	7	-26	-2.0	-0.2	1	-0.2
	5-79	73	19	-54	-4.2	-2.2	10	-0.2
	6-79	73	7	-66	-5.1	-1.1	1	-1.1
	7-79	60	14	-46	-3.5	+1.6	1	+1.6
	9-79	73	7	-66	-5.1	-1.6	2	-0.8
	10-79	72	8	-64	-4.9	+0.2	1	+0.2
	4-80	88	17	-71	-5.5	-0.6	6	-0.1
Tran B	10-77	9	0	- 9	-0.6	-0.6	1	-0.6
15 pins	12-77	9.5	23	+13.5	+1.0	+1.6	2	+0.8
Length =	4-78	21	12	- 9	-0.6	-1.6	4	-0.4
17.1 m	5-78	29.5	15	-14.5	-1.0	-0.4	1	+0.4
	6-78	36	8	-28	-1.9	-0.9	1	-0.9
	7-78	41	40	- 1	-0.1	+1.8	1	+1.8
	5-79	79	63	-16	-1.1	-1.0	10	-0.1
	6-79	83	22	-61	-4.1	-3.0	1	-3.0
	7-79	79	17	-62	-4.1	0.0	1	0.0
	9-79	83	24	-60	-4.0	+0.1	2	+0.0
	10-79	88	19	-69	-4.6	-0.6	1	-0.6
	4-80	90	81	- 9	-0.6	+4.0	6	+0.7

TABLE IIB Summary of Erosion-Pin Data for the BMMOD Basin.

Study Basin	Date	Change in Ground Surface Elevation (mm): Σ of Loss All Values Negative	Σ of Gain All Values Positive	Net Δ	Average Δ per Transect	Δ Between Measurement	Number of months	$\bar{\Delta}$ /month (mm)
BMMOD	10-77	6	0	-6	-0.4	-0.4	1	-0.4
Tran C	12-77	13	18	+5	-0.4	0.0	2	0.0
14 pins	4-78	15	46	+31	+2.2	+2.6	4	+0.6
	5-78	17.5	7.5	-10	-0.7	-3.9	1	-3.9
Length = 16.7 m	6-78	18	11	-7	-0.5	+0.2	1	+0.2
	7-78	46.5	34	-12.5	-0.9	-0.4	1	-0.4
	5-79	127	44	-83	-5.9	-5.0	10	-0.5
	6-79	126	33	-103	-7.4	-1.5	1	-1.5
	7-79	120	12	-108	-7.7	-0.3	1	-0.3
	9-79	127	9	-118	-8.4	-1.7	2	-0.8
	10-79	127	8	-119	-8.5	-0.1	1	-0.1
	4-80	163	85	-78	-5.6	+2.9	6	+0.5
Tran D	10-77	15	0	-0.5	-0.1	-0.1	1	-0.4
5 pins	12-77	3	4	+1	+0.2	+0.3	2	+0.2
	4-78	6	1	-5	-1.0	-0.6	9	-0.2
Length = 2.8 m	5-78	7	2	-5	-1.0	0.0	1	0.0
	6-78	7	0.5	-6.5	-1.3	-0.3	1	-0.3
	7-78	11	47	+36	+7.2	+8.5	1	+8.5
	5-79	29	76	+47	+9.4	-2.2	10	+0.2
	6-79	28	61	+33	+6.6	-2.8	1	-2.8
	7-79	33	69	+36	+7.2	+0.4	1	+0.4
	9-79	31	48	+17	+3.4	-3.8	2	-1.6
	10-79	32	47	+15	+3.0	-0.4	1	-0.4
	4-80	31	51	+20	+4.0	+1.0	6	-0.2

Table II B: (Cont'd) Summary of Erosion-Pin Data for the BMMOD Basin.

Study Basin	Date	Change in Ground Surface Elevation (mm): Σ of Loss All Values Negative	Σ of Gain All Values Positive	Net Δ	Average Δ per Transect	Δ Between Measurement	Number of months	Δ̄ /month (mm)
BM LIGHT								
	10-77	0	11.5	+11.5	+0.7	+0.7	1	+0.7
Tran A	12-77	13	0	-13	-0.8	-1.5	2	-0.8
16 pins	4-78	36	6	-26	-1.6	-0.8	4	-0.2
Length =	5-78	51	3	-48	-3.0	-1.4	1	-1.4
70.2 m	6-78	56.5	4.5	-52	-3.2	-0.2	1	-0.2
	7-78	67	0	-67	-4.2	-1.0	1	-1.0
	5-79	143	11	-132	-8.2	-4.0	10	-0.4
	6-79	154	11	-143	-8.9	-0.7	1	-0.7
	7-79	156	0	-156	-9.8	-0.9	1	-0.9
	9-79	156	10	-146	-9.1	-10.7	2	+0.4
	10-79	241	17	-224	-14.0	-4.9	1	-4.9
	4-80	144	72	-72	-4.5	+9.5	6	+1.6
Tran B	10-77	0	25	+25	+1.2	+1.2	1	+1.2
20 pints	12-77	36.5	20	-16.5	-0.8	-2.0	2	-1.0
	4-78	73.5	77.5	4	+0.2	+1.0	4	+0.2
Length =	5-78	109.5	37	-72.5	-3.6	-3.8	1	-3.8
24.1 m	6-78	128	52	-76	-3.8	-0.2	1	-0.2
	7-78	142	110	-32	-1.6	+2.2	1	+2.2
	5-79	335	143	-142	-7.1	-5.5	10	-0.6
	6-79	350	107	-243	-12.2	-5.1	1	-5.1
	7-79	353	77	-276	-13.8	-1.6	1	-1.6
	9-79	344	92	-252	-12.6	+1.2	2	+0.6
	10-79	348	97	-251	-12.6	0.0	1	0.0
	4-80	323	172	-151	-7.6	+5.0	6	+0.8

Table IIC: Summary of Erosion-Pin Data for the BMLIGHT Basin.

Study Basin	Date	Change in Ground Surface Elevation (mm): Σ of Loss All Values Negative	Σ of Gain All Values Positive	Net Δ	Average Δ per Transect	Δ Between Measurement	Number of months	$\bar{\Delta}$ /month (mm)
BM LIGHT								
	10-77	2	24	+22	+1.2	+1.2	1	+1.2
	12-77	27	26	-1	-0.0	-1.2	2	-0.6
Tran C	4-78	32	18	-14	-0.7	-0.7	4	-0.2
19 pins	5-78	57.5	18	-39.5	-2.1	-1.4	1	-1.4
Length =	6-78	77.5	16.5	-61	-3.2	-1.1	1	-1.1
21.6 m	7-78	84	23.5	-60.5	-3.2	-0.0	1	0.0
	5-79	239	32	-207	-10.9	-7.7	10	-0.8
	6-79	250	20	-230	-12.1	-1.2	1	-1.2
	7-79	279	16	-263	-13.8	-1.7	1	-1.7
	9-79	270	16	-254	-13.4	+0.4	2	+0.2
	10-79	264	7	-257	-13.5	-0.1	1	-0.1
	4-80	221	113	-108	-5.7	+7.8	6	+1.3

Table IIC: (Cont'd) Summary of Erosion-Pin Data for the BMLIGHT Basin.

Study Basin	Date	Change in Ground Surface Elevation (mm): Σ of Loss All Values Negative	Σ of Gain All Values Positive	Net Δ	Average Δ per Transect	Δ Between Measurement	Number of months	$\bar{\Delta}$ /month (mm)
BMARCH								
16 pins	5-78	22	1	-21	-1.3	-1.3	2	-0.6
	6-78	43	0	-43	-2.7	-1.4	1	-1.4
Length =	7-78	47	6.5	-40.5	-2.5	+0.1	1	+0.1
9.3 m	9-78	64	19	-45	-2.8	-0.3	2	-0.2
	11-78	57	25	-32	-2.0	+0.8	2	+0.4
	6-79	172	27	-145	-9.1	-7.1	7	-1.0
	9-79	170	51	-119	-8.5	+0.6	3	+0.2

Table IID: Summary of Erosion-Pin Data for the BMARCH Site.

Study Basin	Date	Change in Ground Surface Elevation (mm): Σ of Loss All Values Negative	Σ of Gain All Values Positive	Net Δ	Average Δ per Transect	Δ Between Measurement	Number of months	$\bar{\Delta}$ /month (mm)
ASINT								
	10-77	120.5	0	-120.5	-2.7	-2.7	1	-2.7
Tran A	4-78	187.5	99	-88.5	-2.0	+0.7	6	+0.1
45 pins	6-78	205	88.5	-116.5	-2.6	-0.6	2	-0.3
	7-78	225.5	120.5	-105	-2.3	+0.3	1	+0.3
Length =	5-79	368	214	-154	-3.4	-1.1	10	-0.1
34.6 m	6-79	372	100	-272	-6.0	-2.6	1	-2.6
	9-79	343	85	-258	-5.7	+0.3	3	+0.1
	11-79	396	119	-277	-6.2	-0.5	2	-0.2
	5-80	392	311	-81	-1.8	+4.4	6	+0.7
Tran B	10-77	37	0	-37	-1.1	-1.1	1	-1.1
34 pins	4-78	92.5	32.5	-60	-1.8	-0.7	6	+0.1
	6-78	100.5	28	-72.5	-2.1	-0.3	2	-0.1
	7-78	103.5	59.5	-44	-1.3	+0.8	1	+0.8
	5-79	223	104	-114	-3.4	-2.1	10	-0.2
	6-79	252	78	-174	-5.1	-1.7	1	-1.7
	9-79	242	144	-98	-2.9	+2.2	3	+0.7
	11-79	277	113	-169	-4.8	-1.9	2	-1.0
	5-80	292	277	-15	-0.4	+4.4	6	+0.7

Table IIE: Summary of Erosion-Pin Data for the ASINT Basin.

Study Basin	Date	Change in Ground Surface Elevation (mm) Σ of Loss All Values Negative	Σ of Gain All Values Positive	Net Δ	Average Δ per Transect	Δ Between Measurement	Number of months	$\bar{\Delta}$ /month (mm)
ASINT								
Tran C 8 pins	10-77	15	0	-15	-1.9	1.9	1	-1.9
	4-78	20.5	6	-14.5	-1.8	+0.1	6	+0.0
	6-78	26	0	-26	-3.2	-1.4	2	-0.7
Length = 4.1 m	7-78	25	11	-19	-1.8	+1.4	1	+1.4
	5-79	42	53	+11	+1.4	+3.2	10	+0.3
	6-79	36	31	-4	-0.5	-1.9	1	-1.9
	9-79	38	62	+24	+3.0	+3.5	3	+1.2
	11-79	40	64	+24	+3.0	0.0	2	0.0
	5-80	39	39	0.0	0.0	0.0	6	0.0

Table IIE: (Cont'd) Summary of Erosion-Pin Data for the ASINT Basin.

Study Basin	Date	Change in Ground Surface Elevation (mm): Σ of Loss All Values Negative	Σ of Gain All Values Positive	Net Δ	Average Δ per Transect	Δ Between Measurement	Number of months	$\bar{\Delta}$ /month (mm)
ASMOD								
	10-77	81	0	-81	-3.9	-3.9	1	-3.9
Tran A	4-78	110.5	0	-110.5	-5.3	-1.4	6	-0.2
21 pins	6-78	124	25	-99	-4.7	+0.6	2	+0.3
	7-78	131	43	-88	-4.2	+0.5	1	+0.3
Length =	5-79	195	43	-152	-7.2	-3.0	10	-0.3
16.9 m	6-79	214	19	-195	-9.3	-2.1	1	-2.1
	9-79	204	23	-181	-8.6	+0.7	3	+0.2
	5-80	244	118	-126	-6.0	+2.6	8	+0.3
Tran B	10-77	36	0	-36	-1.7	-1.7	1	-1.7
21 pins	4-78	32	28	-4	-0.2	+1.5	6	+0.2
	6-78	51	11	-40	-1.9	-1.7	2	-0.8
Length =	7-78	53	13.5	-39.5	-1.9	0.0	1	0.0
14.6 m	5-79	113	4	-119	-5.7	-3.8	10	-0.4
	6-79	125	0	-125	-6.0	-0.3	1	-0.3
	9-79	103	0	-103	-4.9	+1.1	3	+0.4
	5-80	117	19	-98	-4.7	+0.2	8	+0.0

Table IIF: Summary of Erosion-Pin Data for the ASMOD Basin.

Study Basin	Date	Change in Ground Surface Elevation (mm): Σ of Loss All Values Negative	Σ of Gain All Values Positive	Net Δ	Average Δ per Transect	Δ Betweem Measurement	Month	$\bar{\Delta}$ /month (mm)
ASLIGHT								
	4-78	86	135	+49	+2.3	+2.3	6	+0.4
Tran A	6-78	91	63	-28	-1.3	-4.6	2	-2.3
21 pins	7-78	100.5	61	-39.5	-1.9	-0.6	1	-0.6
	5-79	187	34	-153	-7.3	-5.4	10	-0.5
Length =	6-79	190	21	-169	-8.0	-2.7	1	-2.7
10.2 m	9-79	191	19	-172	-8.2	-0.2	3	-0.1
	11-79	187	57	-130	-6.2	+2.0	2	+1.0
	5-80	220	77	-143	-6.8	-0.6	6	-0.1
Tran B	4-78	46.5	2	-44.5	-3.2	-3.2	6	-0.5
14 pins	6-78	61	11	-50	-3.6	-0.4	2	-0.2
Length =	7-78	67	10	-57	-4.1	-0.5	1	-0.5
7.2 m	5-79	164	10	-154	-11.0	-6.9	10	-0.7
	6-79	185	8	-177	-12.6	-1.6	1	-1.6
	9-79	156	15	-141	-10.1	+2.5	3	+0.8
	11-79	158	0	-158	-11.3	-1.2	2	-0.6
	5-80	172	68	-109	-7.9	+3.9	6	+0.6

Table IIG: Summary of Erosion-Pin Data for the ASLIGHT Basin.

Appendix III

Erosion-Grid Measurements

For all Sites

The method of data reduction for the erosion-grid measurements (tabulated in this appendix) is the same as for the erosion-pin measurements. The only difference is that 25 (the number of measurement points within a grid station) is the divisor for the Net Δ (step 3, Appendix II).

Station	Date	Change in Ground Surface Elevation (mm): Σ of Loss All Values Negative	Σ of Gain All Values Positive	Net Δ	Average Δ per Grid Site	Δ Between Measurement	Month	Δ̄/month (mm)
(A)	1-78	27.5	57.5	+30.0	+1.2	+1.2	2	+0.6
BMINT	4-78	45.0	74.5	+29.5	+1.2	0.0	4	0.0
	5-78	32.0	79.5	+47.5	+1.9	+0.7	1	+0.7
1 m^2	6-78	54.0	81.5	+27.5	+1.1	-0.8	1	-0.8
	7-78	203.0	95.0	-108.0	-4.3	-5.4	1	-5.4
	9-78	200.0	95.5	-104.5	-4.2	+0.1	2	+0.0
	11-78	211.5	108.5	-103.0	-4.1	+0.1	2	+0.0
	5-79	302.0	379.5	+77.5	+3.1	+7.2	6	+1.2
	6-79	254.0	104.5	-149.5	-6.0	-9.1	1	-9.1
	7-79	274.0	105.5	-168.5	-6.7	-0.7	1	-0.7
	9-79	319.0	78.5	-240.5	-9.6	-2.9	2	-1.4
	10-79	297.0	86.5	-210.5	-8.4	+1.2	1	+1.2
	4-80	330.0	99.5	-230.5	-9.2	-0.8	6	-0.1
(B)	1-78	40.0	56.0	+16.0	+0.6	+0.6	2	+0.3
BMINT	4-78	42.0	54.0	+12.0	+0.5	-0.1	4	-0.0
	5-78	31.5	95.5	+64.0	+2.6	+2.1	1	+2.1
1 m^2	6-78	27.5	105.0	+77.5	+3.1	+0.5	1	+0.5
	7-78	86.0	100.0	+14.0	+0.6	-2.5	1	-2.5
	9-78	229.0	109.0	-120.0	-4.8	-5.4	2	-2.7
	11-78	259,5	131.0	-128.5	-5.1	-0.3	2	-0.2
	5-79	257.0	113.0	-144.0	-5.8	-0.7	6	-0.1
	6-79	414.5	154.5	-260.0	-10.4	-4.6	1	-4.6
	7-79	355.0	163.5	-191.5	-7.7	+2.7	1	+2.7
	9-79	395.5	152.5	-243.0	-9.7	-2.0	2	-1.0
	10-79	420.5	146.0	-274.5	-11.0	-1.3	1	-1.3
	4-80	408.0	120.0	-288.0	-11.5	-0.5	6	-0.1

Table IIIA: Summary of Erosion-Grid Data, Stations A and B, BMINT.

Station	Date	Change in Ground Surface Elevation (mm) Σ of Loss All Values Negative	Σ of Gain All Values Positive	Net Δ	Average Δ per Grid Site	Δ Between Measurement	Month	$\bar{\Delta}$/month (mm)
(C) BMMOD 1 m^2	1-78	30.0	96.0	+66.0	+2.6	+2.6	2	+1.3
	4-78	30.5	87.0	+56.5	+2.3	-0.3	4	-0.1
	5-78	23.0	95.0	+72.0	+2.9	+0.6	1	+0.6
	6-78	15.5	137.0	+121.5	+4.9	+2.0	1	+2.0
	7-78	19.0	118.0	+99.0	+4.0	-0.9	1	-0.9
	10-78	134.5	52.0	-82.5	-3.3	-7.3	3	-2.4
	11-78	70.0	61.0	-9.0	-0.4	+2.9	1	+2.4
	5-79	66.5	75.5	+9.0	+0.4	+0.8	6	+0.1
	6-79	108.0	56.5	-51.5	-2.1	-2.5	1	-2.5
	7-79	113.0	58.5	-54.5	-2.2	-0.1	1	-0.1
	9-79	115.0	84.0	-31.0	-1.2	+1.0	2	0.5
	10-79	175.5	51.0	-124.5	-5.0	-3.8	1	-3.8
	4-80	257.0	54.5	-202.5	-8.1	-3.1	6	-0.5
(D) BMLIGHT 1 m^2	1-78	54.0	29.0	-25.0	-1.0	-1.0	2	-0.5
	4-78	89.5	45.0	-44.5	-1.8	-0.8	4	-0.2
	5-78	53.0	86.0	+33.0	+1.3	+3.1	1	+3.1
	6-78	70.5	71.0	+0.5	+0.0	-1.3	1	-1.3
	7-78	56.0	93.0	+37.0	+1.5	+1.5	1	+1.5
	10-78	65.0	110.5	-45.5	+1.8	+0.3	3	+0.1
	11-78	171.0	50.0	-121.0	-4.8	-6.6	1	-6.6
	5-79	127.0	195.0	+68.0	+2.7	+7.5	6	+1.2
	6-79	58.0	216.5	+158.5	+6.3	+3.6	1	+3.6
	7-79	73.5	190.5	+117.0	+4.7	-1.6	1	-1.6
	10-79	77.0	187.0	+110.0	+4.4	-0.3	3	-0.1
	4-80	81.5	250.0	+168.5	+6.7	+2.3	6	+0.4

Table IIIB: Summary of Erosion-Grid Data for Stations C, BMMOD, and D, BMLIGHT.

References

Anderson, H.W., and Trobitz, H.E., 1941, Influence of watershed variables on a major flood: Journal of Forestry, v. 47, p. 347-356.

Brater, E.F., 1939, The unit hydrograph principle applied to small watersheds: American Society of Civil Engineering Proceedings, p. 1191-1215.

Campbell, I.A., 1974, Measurements of erosion on badlands surfaces: Zeitschrift für Geomorphologie, Supplement Band, 21, p. 122-137.

Campbell, R.E., Baker, M.B., Jr., Ffolliott, P.F., Larson, F.R., and Avery, C.C., 1977, Wildfire effects on a ponderosa pine ecosystem: An Arizona case study: U. S. Department of Agriculture, Forest Service Research Paper RM-191, 12 p.

Debano, L.F., Mann, L.D., and Hamilton, D.A., 1970, Translocation of hydrophobic substances into soil by burning organic litter: Soil Science Society of American Proceedings, v. 34. 130-133.

Dodge, R.E., 1902, Arroyo formation [abs.]; American Geologist, v. 29, 322 p.

Dryness, C.T., 1965, Erosion potential of forest watersheds, in Sopper, W.E., and Lull, H.W., eds. Forest Hydrology: New York, Pergamon Press, p. 599-611.

Dunford, E.G., 1954, Surface runoff and erosion from pine grasslands of the Colorado Front Range, Journal of Forestry, v. 52, p. 923-927.

Earth Environmental Consultants Incorporated, 1978, Soil survey of Bandelier National Monument: Research prepared for Office of Natural Science, Southwest Region, National Park Service, 34 p.

Eichelberger, J., and Heiken, F, undated, A trail guide to the lower Frijoles Canyon, unpublished report on file at the office of the Superintendent, Bandelier National Monument.

Gregory, K.J., and Walling, D.E., 1973, Drainage basin form and process, a geomorphological approach: New York, John Wiley and Sons, 455 p.

Foxx, T., and Potter, L.P., 1978, Fire ecology at Bandelier National Monument: Final report submitted to National Part Service, Southwest Region, U. S. Department of the Interior, 214 p.

Hack, J., and Goddlett, J.C., 1960, Geomorphology and forest ecology of a mountain region in the central Appalachians: U.S. Geological Survey Professional Paper 347, 66 p.

Harris, D.D., 1977, Hydrologic changes after logging in two small Oregon coastal watersheds: U. S. Geological Survey Water-Supply Paper, 31 p.

Heede, B.H., 1972, Flow and channel characteristics of two high mountain streams: U. S. Forest Service research paper Rm-96, 12 p.

_____, 1975, Mountain watersheds and dynamic equilibrium: in Watershed Management Procedings Symposium, American Society of Civil Engineering Irrigation and Drainage Division, Aug. 11-12, Logan Utah, p. 407-420.

_____, 1977 Influence of forest density on bedload movement in a small mountain stream: in Hydrology and Water Resources in Arizona and the Southwest, v. 7, p. 103-107.

Imeson, A.C., 1977, Splash erosion, animal activity and sediment supply in a small forested catchment: Earth Surface Processes, v. 2, p. 153-160.

Krammes, J.S., and Debano, L.F., 1965, Soil wettability: A neglected factor in watershed management: Water Resources Research, v. 1, p. 283-286.

Leopold, W.H., and Maddock, T., Jr., 1953, The hydraulic geometry of stream channels and some physiographic implications: U.S. Geological Survey Professional Paper 252, 56 p.

Leopold, L.B., Emmett, W.W., and Myrick, R.D., 1966, Channel and hillslope processes in a semiarid area, New Mexico: U. S. Geological Survey Professional Paper 352-6, 253 p.

Mackin, J.H., 1948, Concept of a graded river: Geological Society of America Bulletin, v. 59, p. 463-512.

Malde, H.E., 1973, Geologic bench marks by terrestrial photography: U.S. Geological Survey Journal of Research, v. 1, no. 2, p. 192-206.

Megahan, W.F., and Molitor, D.C., 1975, Erosional effects of wildfire and logging in Idaho: Watershed Management Symposium, p. 423-444.

Miller, J.P., 1958, High mountain streams: Effects of geology on channel characteristics and bed material: New Mexico State Bureau of Mines and Mineral Resources Memoir 4, 53 p.

Packer, P.E., and Williams, R.P., 1974, Logging and prescribed burning effects on the hydrologic and soil stability behavior of Larch/Dourlas fir forests in the Northern Rocky Mountains: Proceedings of Montana Tall Timbers Fire Ecology Conference and Fire and Land Management Symposium no. 14, p. 465-479.

Potter, L.D., and Foxx, T., 1979, Success of seeding native grasses after a holocaustic fire: Report submitted to the National Park Service, Southwest Region, U. S. Department of the Interior, 21 p.

Rich, J.L., 1911, Recent stream trenching in the semi-arid portion of southwestern New Mexico, a result of removal of vegetation cover: American Journal of Science, v. 32, p. 347-350.

Rich, L.R., 1962, Erosion and sediment movement following a wildfire in a ponderosa pine forest of central Arizona: U.S. Department of Agriculture Forest Service, Rocky Mountain Forest and Range Experiment Station Research Note 76, 12 p.

Savage, S.M., Osborn, J., Letey, J., and Henton, C., 1972, Substances contributing to fire-induced water repellency in soils: Soil Science Society of America Proceedings, v. 36, p. 674-678.

Schumm, S.A., 1968, Speculations concerning paleohydrologic controls of terrestrial sedimentation: Geological Society America Bulletin, v. 79, p. 1573-1588.

_____, 1977, The Fluvial System: New York, John Wiley and Sons, 338 p.

Smith, R.L., Bailey, R.A., and Ross, C.S., 1970, Geologic may of the Jemez Mountains, New Mexico: U. S. Geological Survey Map I-571, 1 sheet.

Storey, H.C., Hobba, R.L., and Rosa, J.M., 1964, Hydrology of forest lands and range lands, Sec. 22, in, Chow Ven-Ti, ed., Handbook of Applied Hydrology: New York, McGraw-Hill, p. 52.

Strahler, A.N., 1964, Quantitative geomorphology of drainage basins and channel networks, in Chow, Ven-Ti, ed., Handbook of Applied Hydrology: New York, McGraw-Hill, p. 4-39.

Strand, R.I., 1975, Bureau of Reclamation procedures for predicting sediment yield: Agriculture Research Service, ARS-S-40, p. 10-15.

Tarrant, R.F., 1956, Effect of slash burning on some physical soil properties: Forest Science, v. 2, p. 18-22.

U. S. Geological Survey, 1963-1969, Water Resources Data for New Mexico.

_____, 1977-1979, Water Resources Data for New Mexico.

White, W.D., and Wells, S.G., 1979, Forest-fire devegetation and drainage basin adjustments in mountainous terrain: in Adjustments of the Fluvial System, D. Rhodes, and E. Williams (eds.), Procedings of the tenth Annual Geomorphology Symposium Series, p. 199-223.

Zwolinski, M.J., 1971, Effects of fire on water infiltration rates in a ponderosa stand: in Hydrology and Water Resources in Arizona and Southwest, v. 1, p. 107-112.